Improving the Fire Behavior of Flexible Polyurethane Foams Using Eco-Friendly Fillers

eman ta zabal zazu

Universidad del País Vasco
Euskal Herriko Unibertsitatea

Sandra Gómez Fernández

Donostia-San Sebastián, 2018

GIPUZKOAKO INGENIARITZA ESKOLA
ESCUELA DE INGENIERÍA DE GIPUZKOA

Improving the fire behavior of flexible polyurethane foams using eco-friendly fillers

PhD Dissertation by
Sandra Gómez Fernández

Supervised by:
Arantxa Eceiza
María Angeles Corcuera

Donostia-San Sebastián, 2018

Acknowledgements

A mis directoras, Arantxa Eceiza y Marian Corcuera. Gracias por confiar en mí para desarrollar este trabajo, por vuestra paciencia y vuestro apoyo.

Gracias a la Universidad del País Vasco (UPV/EHU) y a las ayudas del Vicerrectorado de Investigación (Convocatoria de contratación para formación de personal investigador en la Universidad del País Vasco 2013, PIF//13/079) por financiar esta gran oportunidad profesional.

Quisiera agradecer también al Departamento de Ingeniería Química y del Medio Ambiente y a los Servicios Generales de Investigación (SGIker) de la UPV/EHU por el soporte técnico y por facilitarme el uso de las instalaciones y equipamiento necesario para llevar a cabo este trabajo. Gracias en especial al servicio de Macroconducta-Mesoestructura-Nanotecnología y en particular a Loli, por tu valiosa ayuda y asesoramiento tanto técnico como humano.

I would like to kindly acknowledge Dr. Bernhard Schartel his hospitality and generosity for offering me the most awesome internship ever in the *Division 7.5 Technische Eigenschaften von Polymerwekstoffen* at *Bundesanstalf für Materialforschung und -prüfung* (BAM). Burning down all the work of my own PhD studies is not a trifle. Thanks to Martin for sharing with me all his fire-related knowledge, and for his kindness and patience for being my babysitter. Thanks also to all the colleagues from BAM and to all the Berliner friends that made this internship an unforgettable experience. *Vielen Dank für diese wunderbare Erfahrung!*

Quería particularizar los agradecimientos pero me he dado cuenta de que necesitaría otra tesis para agradecer a todos los que me han acompañado durante esta etapa. Así que **GRACIAS** a todos los que habéis formado parte de mi vida y de este proyecto durante este periodo de tiempo.

A mis padres

¿Qué sería de la vida,
si no tuviéramos el valor
de intentar algo nuevo?
V. V. Gogh

Summary

The research included in this work is focused on the preparation and characterization of flexible polyurethane foams and on the modification and introduction of different eco-friendly fillers into polyurethane formulations.

The increase of the sustainability of polymeric materials is nowadays of especial interest owing to the increased environmental concern and the imminent depletion of fossil resources. In this work, the sustainability of the prepared materials is enhanced by using a renewable sourced polyol and selecting environmentally-friendly additives such as anionic clays (layered double hydroxides) and an industrial byproduct such as lignin, giving in this way added value to this abundant residue from pulp and paper industry.

These eco-friendly fillers were selected not only because of their sustainable nature, but also because of their chemical structure and morphology that makes them of special interest in another topic with increasing concern: the improvement of the fire behavior of polymeric materials.

In the last decades, the increased use of polymers has boosted the dangers related to the development of violent fire scenarios, forcing industries to improve the flame retardancy of polymeric materials by using different types of additives, such as halogenated compounds. These compounds reduce the flammability of polymeric materials with the drawback of increased toxicity and thus, increased death hazard while contributing also to the depletion of the ozone layer owing to the highly toxic halogenated fumes released during polymer and additive combustion.

For this reason, this work not only analyzes the effect on the properties of different eco-friendly additives in the properties of flexible polyurethane foams, but also explores their potential to be used as flame retardant agents.

Table of content

1. INTRODUCTION

2. MATERIALS AND CHARACTERIZATION TECHNIQUES

APPENDIX

“What is the most resilient parasite? A bacteria? A virus? An intestinal worm? An idea.

Resilient, highly contagious. Once an idea has taken hold of the brain it's almost impossible to eradicate. An idea that is fully formed, fully understood. That sticks; right in there somewhere.”

K. Sakura, Y. Taki, E. Thomas. T. Tull (Producers) and C. Nolan (Director). Inception. United States and United Kingdom: Warner Bros Pictures, 2010.

Chapter 1

1

Introduction

1. Introduction

1.1. Motivation

The use of polymers in daily life applications evolves increasingly each year as a consequence of their light weight, easy processing and tailorable properties. Nevertheless, their organic carbon and hydrogen based molecular structure makes most of polymeric materials intrinsically flammable (Arao, 2015), increasing with their use the hazard of violent fires in household scenarios and with this, the cases of deceased human have also increased in the recent years. According to United State's National Fire Protection Association (NFPA), 1320000 fires were reported in this country in 2016, taking with them 3390 human lives and leaving 14650 injured people (National Fire Protection Association, 2017a).

The main approach of improving the flame retardancy of polymers is the addition of flame retardant compounds to the formulation, which role is to interfere with the chemistry and/or the physics of the combustion process (Kiliaris and Papaspyrides, 2014). In the last decades, the use of halogen-based flame retardants was highly extended owing to their versatility and effectiveness in different types of polymeric matrices. However, several studies not only demonstrated the contribution of halogenated compounds to the destruction of the ozone layer, but also unmasked their toxicity towards human health, evidencing that most of the deaths during fires occurred as a consequence of the fatal side effects of poisoning through smoke inhalation rather than as a consequence of burning injuries (National Fire Protection Association, 2017b).

Therefore, the increasing environmental concern and the rising of more restrictive normative towards improving the fatal statistics, have forced the scientific community to find more safe and eco-friendly alternatives in order to replace the highly efficient halogen-based flame retardants. The replacement of such effective products is not straightforward, and it has resulted in a deeper understanding of the mechanism of action of the different types of flame retardant compounds, deriving also in the exploration of flame retardant systems with synergetic properties while detecting and avoiding antagonist combinations in different polymeric matrices (Lewin, 2001).

Polyurethanes constitute a broad part of the polymer market due to their versatility, low cost and customizable properties. Flexible polyurethane foams in particular are present not only in almost every home in form of mattresses and upholstered furniture, but also in automotive applications such as seating. Therefore, the improvement of their fire behavior is crucial towards decreasing fire deaths and to improve the safety in a society where the polymers are planned to be more and more present, expecting a growth of 4.8% in the polyurethane foam market by 2020 (Markets and Markets, 2016).

Hence, flexible polyurethane foams have been prepared and different eco-friendly alternatives to halogen-based flame retardants have been explored in this work, including additive compounds such as anionic clays (layered double hydroxides) and lignin as an industrial by-product, and also a phosphorus containing oligomeric diol as reactive compound.

1.2. Polyurethane generalities

Constituted by the Ancient Greek prefix poly- (*πολύς, polús*, which means many/much) and the word urethane which refers to a functional group in organic chemistry, the word **polyurethane** (PU) comprises a broad family of polymers formed by two main building blocks: isocyanate and alcohol. The addition reaction of a hydroxyl and isocyanate functional group (**Figure 1.1**) gives place to the formation of a urethane group. When their functionalities are above 1, a polyaddition reaction takes place resulting in the formation of several urethane groups, forming thus polyurethane.

Although no small molecules are lost in polyurethane formation, in the case of PUs this reaction can be considered a condensation polymerization owing to the rearrangement of the atoms constituting the functional groups of each monomer (one containing isocyanate and the other hydroxyl groups, usually alcohols or polyols with **functionality** $f > 1$) which react successively forming a growing chain of dimer, trimer, tetramer, etc. until a high conversion is reached.

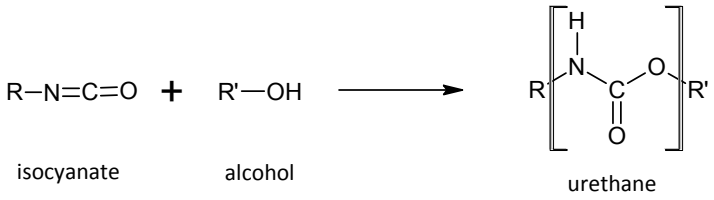

Figure 1.1. Addition reaction between isocyanate and hydroxyl group.

Since these building blocks can be of very different nature, the synthesis possibilities are endless depending on the selected raw materials. Their functionality, chemical structure, molecular weight and the use of additives among other parameters, determine the properties of the final material.

1.2.1. Isocyanate chemistry

Isocyanates constitute an important part of the polyurethane industry, including aliphatic, cyclic, aromatic and heterocyclic isocyanates. The most used commercially available isocyanates are the aliphatic hexamethylene diisocyanate (HDI), and the aromatic methylene diphenyl diisocyanate (MDI) and toluene diisocyanate (TDI), which are selected depending on the desired properties of the final material. Particularly, TDI is the most used in polyurethane foam industry due to its high reactivity and liquid form, which makes it easy to handle in the fast foaming reactions.

Isocyanates are characterized to react with hydrogen-active containing compounds (*e.g.* aldehyde, amine, hydroxyl groups, etc.) to form different functional groups, apart from the mentioned above urethane shown in **Figure 1.1**.

An important reaction in polyurethane foam industry involving H-active compounds is the reaction between isocyanate and water to form carbon dioxide (responsible to form foams' characteristic porous structure) and disubstituted urea. For the formation of a urea group, an unstable carbamic acid intermediate is formed in first place, decomposing readily into amine and carbon dioxide (**Figure 1.2a**).

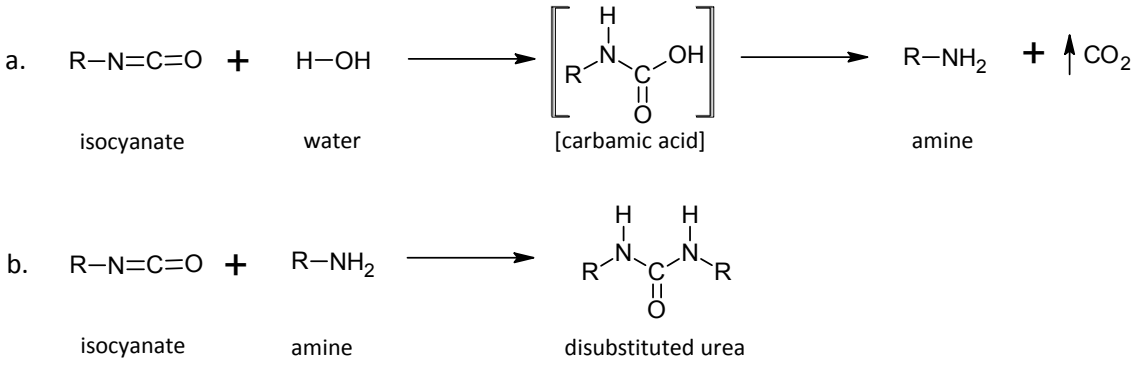

Figure 1.2. Reaction of isocyanate with water (a) and with amine (b).

This amine reacts with additional isocyanate forming finally disubstituted urea (**Figure 1.2b**). Therefore, the isocyanate not only reacts with hydroxyl groups and water, but also quickly reacts with amine to produce disubstituted urea.

Additionally, if added in excess, isocyanates can also react with urea containing active hydrogen (from N-H) capable of reacting with further isocyanate to produce biuret groups (**Figure 1.3a**). The same behavior is followed in presence of urethane groups, which active hydrogen can react with additional isocyanate forming allophanate groups (**Figure 1.3b**). Nevertheless, these reactions are less common since they need high temperatures or the presence of catalysts to take place (Szycher, 2013).

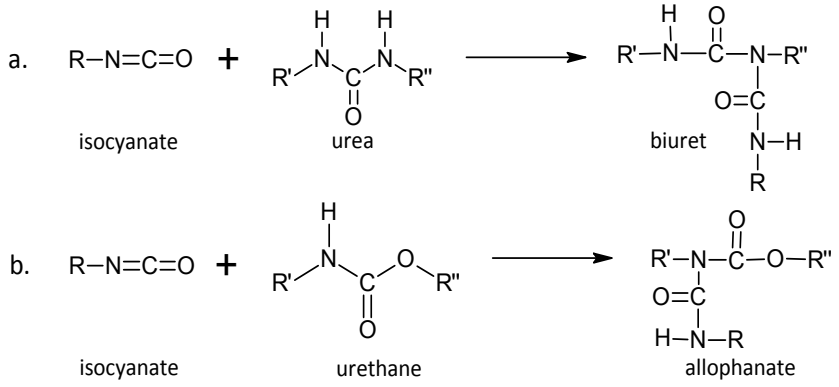

Figure 1.3. Reaction of isocyanate with urea (a) and urethane (b) groups.

Starting from either aliphatic or aromatic isocyanates, the induction of isocyanate trimerization (**Figure 1.4**) is common in polyisocyanurate foam preparation,

aiming to obtain materials with **higher thermal stability** and superior **fire performance** (Chattopadhyay and Webster, 2009). Slow dimerization is a reversible process that usually happens to isocyanates (both aliphatic and aromatic) that have been stored for a long time. On the other hand, trimerization is more usual in aromatic isocyanates, which formation is promoted by using tertiary amines or alkali salts of carboxylic acid as catalysts.

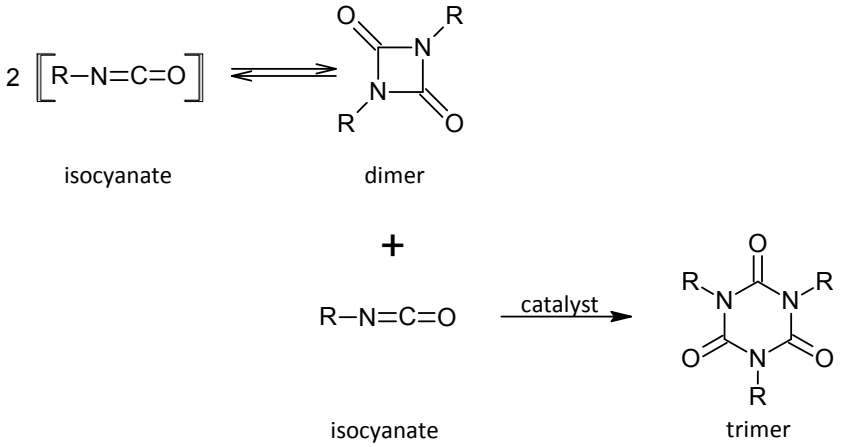

Figure 1.4. Dimerization and trimerization of isocyanate.

1.2.2. Types of polyurethanes

As mentioned above, only two reactants are needed to prepare polyurethanes: diisocyanate and polyol. However, polyurethanes encompass a large part of the polymeric materials owing to the wide variety of their raw materials available in the market. Many characteristics of the selected raw materials will have an impact on the final properties of the polyurethane.

Their **functionality** will determine the linearity or crosslinking degree of the material. From linear thermoplastic polyurethanes when bifunctional isocyanates and macrodiols are used, through elastomeric polyurethanes when using polyols with functionalities between 2 and 3 with a T_g below room temperature, to rigid thermoset materials with high crosslink density network when the functionalities of the isocyanate or polyol (or both) are above 3.

The crosslink density will also be affected by the **molecular weight** of the polyol. The lower the molecular weight, the closer will be located the crosslinking

points of the network, resulting in more compact and rigid materials, increasing properties such as modulus, tensile strength and glass transition temperature among many other features. It is common to include low molecular weight polyols in the formulation in order to tailor the crosslink density. Low molecular weight diols or diamines (f = 2) will act as **chain extenders** decreasing the crosslink density, whereas low molecular weight polyols ($f \geq 3$) will act as **crosslinking agents** increasing the compactness of the network.

Also, the **aromatic** or **aliphatic nature** of the selected isocyanate will have an effect on the properties. Aromatic compounds will hinder the mobility of the polymer chains resulting thus in stiffer and more brittle materials but with higher glass transition temperature. In case of the polyol, the presence of flexible groups in their structure such as ether will have the contrary effect increasing the flexibility and decreasing the glass transition temperature of the final material.

The polymer chains form primary structures that can be linear, branched or crosslinked. In case of polyurethanes, these chains are formed by covalent bonded **hard segments** (HS) constituted by the highly polar isocyanate groups and chain extenders, and by **soft segments** (SS) formed by the low polarity polyol chain. Urethane groups in the HS might form secondary structures owing to the **intermolecular forces** occurring as a consequence of the different polarity of the generated dipoles, deriving in weaker interactions such as hydrogen bonding and van der Waals forces. Thermodynamic incompatibilities in linear and low crosslink density polyurethanes can yield to HS and SS phase separation. The former contributes to increase the modulus and strength, whereas the latter provides flexibility to the material. These interactions act as physical crosslinks providing mechanical stability to the polymer network and can be broken by means of temperature or using an adequate solvent (Berezkin and Urick, 2013). The phase separation phenomenon is related to the structure of the material, which can yield to form **amorphous** disordered regions together with ordered **crystalline** regions when using low functionality polyols. This effect is more common in linear and low crosslink density polyurethanes, although it can also be found in highly crosslinked polyurethanes depending on the properties of the selected raw materials.

1.2.2.a. Thermoplastic polyurethanes

Thermoplastic polyurethanes (TPU) are block copolymers formed by three main precursors: diisocyanate, macrodiol and chain extender. Their versatility is attributed to their linear segmented structure, constituted by HS and SS. The former presents excellent mechanical properties and act as a reinforcement of the elastic SS. The later, in turn can be hardened by induced crystallization by the application of tensile or shear stress. The ratio between segments can be calculated according to **Equation 1.1:**

$$HS\ (\%) = \frac{wt_{diisoc} + wt_{ce}}{wt_{macrodiol}} \cdot 100 \qquad \textbf{Eq. 1.1.}$$

where *HS (%)* is the weight percent of hard segment, wt_{diisoc} is the diisocyanate weight (g), wt_{ce} the chain extender weight (g) and $wt_{macrodiol}$ the macrodiol weight (g).

TPU synthesis can be carried out in one or two steps. In **one step** synthesis, all the components of the formulation are added simultaneously, resulting to be an economic method to produce TPU but with the disadvantage that the structure of the polyurethane cannot be controlled during the synthesis. In **two step** synthesis (**Figure 1.5**), a prepolymerization takes place firstly through the condensation reaction of the macrodiol and the diisocyanate, adding the chain extender in a second step to obtain the final polyurethane. In this way, a narrower molecular weight distribution and higher control over the structure of the final polymer can be achieved.

TPU behave like crosslinked elastomers at room temperature, with the benefit that they can be melted and conformed by means of different processing techniques such as injection, extrusion or compression molding. Their characteristic properties are high toughness, high tensile and tear strength, high resistance to abrasion and to oxidizing atmospheres, high flexibility at low temperatures and even recyclability. Additionally, they can be sterilized and welded. These properties make TPU attractive for applications such as biomedical devices, coatings for electrical cables, textile fibers, textile coatings, furnishing, sports equipment, machinery joints and bearings, etc.

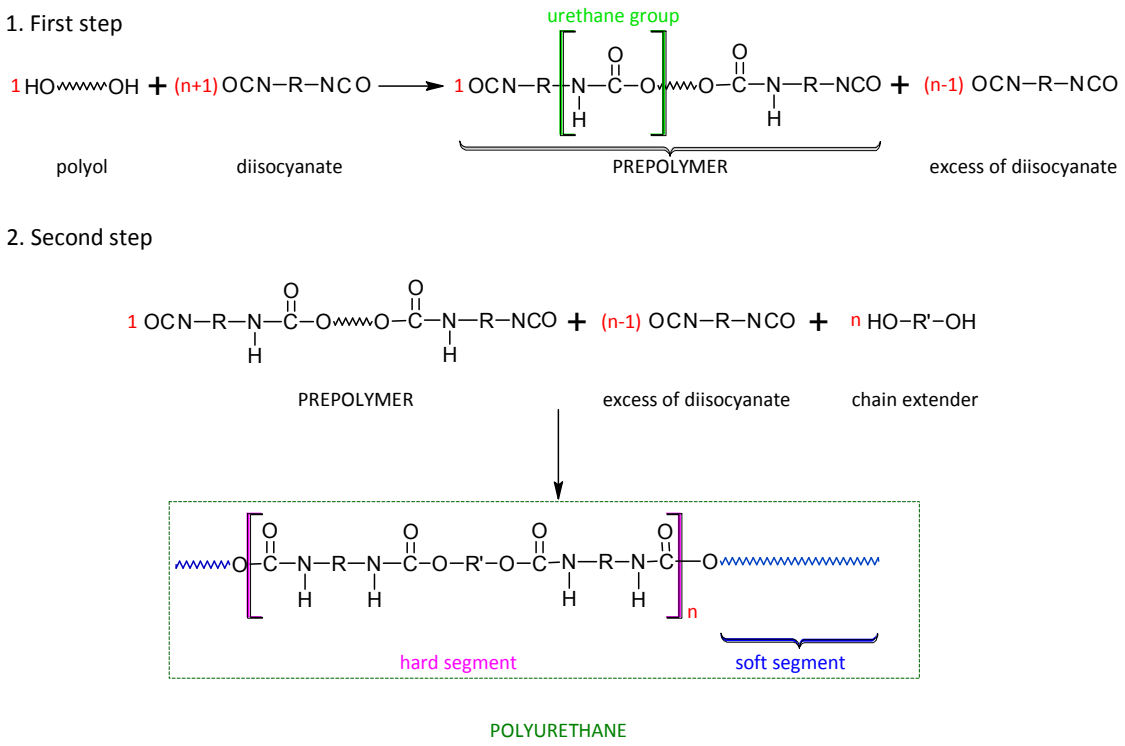

Figure 1.5. Two step condensation reaction: prepolymerization and polymerization.

1.2.2.b. Thermoset polyurethanes

Thermoset polyurethanes (TSPU) are obtained when the functionality of the used isocyanate and/or polyol is above 2, so that crosslinking points can be generated in the condensation reaction resulting in the synthesis of a three-dimensional network. This type of structure is covalently bonded, decomposing without melting, so TSPU cannot be thermally conformed and thus, they cannot be recycled and have to be shaped before curing. Their main advantage over TPU is that TSPU present higher durability, higher abrasion and chemical resistance and increased thermal stability.

A wide variety of TSPU can be obtained for different applications: solid pieces for automotive or aeronautic industry, coatings or varnishing in flooring applications, rigid, semi-rigid or flexible foams for insulation applications in construction, comfort and furnishing, respectively. These different products can be prepared depending on the selected raw materials (isocyanate and/or polyol with $f > 2$), being the foams those with a more extended use in the industry. Depending on the specifications and requirements of the final application, other components need to be added into the

formulation in order to achieve the desired properties, such as catalysts, stabilizers, colorants, flame retardants, etc.

1.3. Polyurethane foams

Polyurethane foams (PUF) consist on biphasic structures formed by the generation of gas cells in a polyurethane matrix. Two different processes take place in the foam reaction in order to obtain this kind of structure: the polycondensation reaction (or gelling reaction) between the polyol and the isocyanate, and the blowing reaction where bubbles are formed and grow by the reaction between water and isocyanate or by using low boiling point liquids that lead to a porous structure. The achievement of a sophisticated balance between these two processes will be decisive to prepare quality polyurethane foams.

Depending on whether the cells are closed (*i.e.* the gas is trapped) or not, the foam will be endowed with totally different features despite their similar appearance. This characteristic is commonly known as the open cell content of the foam and can vary from nearly 0 to almost 100%.

Polyurethane foams are among thermoset polyurethanes, those with the highest industrial output. From flexible (FPUF) to rigid foams (RPUF), their properties can be tailored by controlling their crosslinking density. Their versatility, easy production, low density and low cost make polyurethane foams present in many daily life applications.

The FPUFs are produced by selecting polyols with low functionalities whereas RPUF can be prepared by using high functionality polyols and/or isocyanates. Notwithstanding, the chemical structure of the raw materials, the use of additives and so on, will also have an effect on their final properties. Water blown polyurethane foams, similarly to TPU and TSPUs, can also present phase segregation between hard and soft segments owing to the urea linkages present in the HS as a product of the blowing reaction. Therefore, PUF are not exclusively formed by urethane bonding but

also by urea linkages: the SS (rich in polyol) and the HS (rich in urea) are covalently bonded by urethane linkages. These urea linkages are responsible of strong intermolecular interactions that give place also to HS and SS phase separation, a decisive process in the cell opening stage.

Flexible polyurethane foams present an irregular cellular structure with interconnected cells (**Figure 1.6b**), so that the air inside the material can flow along the pores when the material is subjected to deformation. Flexible foams with nearly 100% open cells are known as **reticulated foams (Figure 1.6a)** and despite not having load resistance capability, they can act as dust barriers. This ability to circulate fluid (gas or sometimes liquid too) along the polyurethane pores is responsible of bad acoustic or thermal insulation and can be adjusted by the use of different surfactants and catalysts that enhance or impede the wall opening process. Nevertheless, the **low resistance to compression** and the **viscoelastic properties** due to their low crosslinking density makes them ideal for **comfort applications** such as bedding, furnishing, upholstery, seat padding, etc. In these applications the resilience (energy storage per volume unit when they are elastically deformed under compressive stress) is one of the most significant properties, and its value will limit their final application.

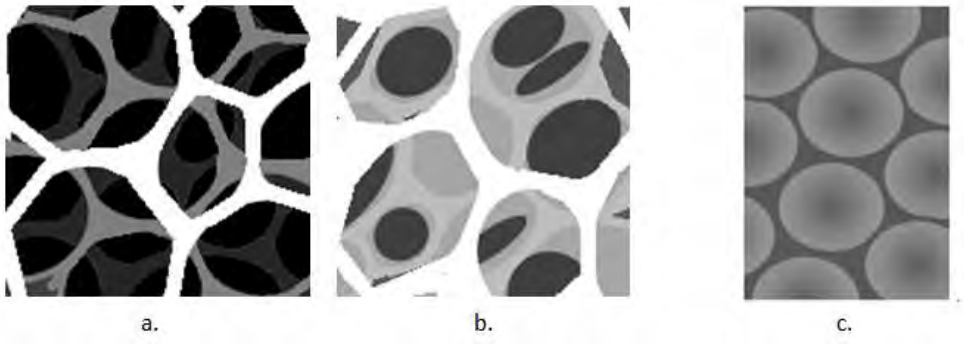

Figure 1.6. Representation of the cell morphology with decreasing open cell content: reticulated (a), flexible (b) and rigid (c) foams.

On the other side, the structure of **rigid polyurethane foams** present individual and isolated cells with homogeneous size (**Figure 1.6c**) that cover completely the gas bubble preventing thus its circulation through the cell walls. This characteristic provides the RPUF with **low thermal conductivity**, low water and vapor absorption

that prevents the growth of mold and mildew in the material. Additionally, the highly crosslinked molecular chains endow RPUF with high resistance to compression. This type of foams is therefore widely used in acoustic and thermal insulation applications in construction, as well as sandwich core panels in refrigeration equipment. During RPUF preparation the viscosity of the reactive mixture increases in such a way that allows the adhesion of the foam to a wide variety of surfaces.

Between flexible and rigid, **semi-rigid polyurethane foams** can also be prepared. Their properties are near to those from FPUF, but they provide higher modulus and elasticity resulting in improved impact absorption properties.

1.3.1. Chemistry of polyurethane foams

Apart from the polyol and the isocyanate, polyurethane foams require the use of other compounds in order to achieve the desired cellular structure. Usually, these additives are previously mixed with the polyol (also known as the **part B** of the formulation) and then the isocyanate (**part A**) is added to this mixture. Few seconds after adding the isocyanate while mixing vigorously, the mixture begins to grow thanks to the increasing size of the bubbles and the cellular structure sets as a result of the condensation reaction between the polyol and the isocyanate. This foam preparation method is known as **one shot method**, where all the reactants are mixed together to produce the foam, although other methods such as prepolymer preparation methods are also typical. As mentioned before, in this process **two main reactions** take place during polyurethane foam formation: blowing and gelling reaction.

In water blown foams the **blowing reaction** takes place when the isocyanate reacts with water (**Figure 1.2a**) resulting in the formation of amine and carbon dioxide bubbles. The formed amine will further react with isocyanate forming urea linkages (**Figure 1.2b**). Simultaneously, the **gelling reaction** *i.e.* the condensation reaction between the polyol and the isocyanate, takes place (**Figure 1.1**) releasing heat and increasing the viscosity of the reactive mixture as a consequence of the increased polymerization conversion while bubble growth takes place. This conjunction of

processes gives place to the achievement of a **gel point** where the cellular structure is finally set until complete conversion is achieved.

These two reactions should be in delicate balance for setting the cellular structure in the right moment in order to avoid the formation of defects in the structure, especially in flexible polyurethane foams. If the **blowing takes place faster than the gelling reaction**, the viscosity of the reactive mixture will be too low and the liquid will be drained resulting in the formation of splits in the foam or in the worst case it will result in the **collapse** of the porous structure. On the other hand, if **gelling reaction takes place faster than blowing**, the polymer will have gelled too early and the cell struts will not be capable to break the walls by draining due to the high viscosity of the mixture. This effect will result in a high proportion of closed cells with warm gas trapped inside, which volume will decrease while cooling, resulting in the **shrinkage** of the cellular structure (Defonseka, 2013).

Different stages take place in the formation of FPUF, which monitoring is critical in order to obtain reproducible foams at industrial scale.

- **Creaming:** when mixing the raw materials, bubbles are mechanically formed due to the vigorous stirring and the nucleating effect of the surfactant. These bubbles act as nucleation sites for the gas produced in the blowing reaction that will increase their size. The time between the incorporation of the part A to the formulation and the beginning of the bubble growth due to gas generation is known as the **cream time**. It is easily detectable because the reactive mixture changes from translucent to white color and usually happens between the first 6 and 15 seconds after mixing part A and B.

- **Growth:** with the continuous production of blowing agent, the foam keeps growing while the viscosity increases in the liquid phase. The time between mixing part A and B and the moment when the expansion of the foam stops is known as **rise time** and usually takes between 100 and 200 seconds to finish.

- **Gelling and curing:** the viscosity of the reactive mixture increases while foam grows due to increased crosslinking density. When the surface of the foam changes

from a low viscosity liquid to a string forming liquid, the **gel time** has been reached. Then, when the foam evolves from a high viscosity liquid and stops to be sticky, the **tack-free time** has been reached. Nonetheless, this tack-free time does not guarantee the complete cure of the foam, so the foams are usually left curing for 24 hours.

A wide range of catalysts and surfactants are used in the formulation of FPUF in order to achieve the perfect balance between these reactions and will affect the timing of these stages in order to obtain good flexible foams where the open cells predominate over closed ones.

1.3.2. Reactants used in polyurethane foam preparation

The main raw materials to produce polyurethanes are isocyanates and polyols. Regarding the production of polyurethane foams, other raw materials are needed such as blowing agents, catalysts and surfactants.

1.3.2.a. Isocyanates

An indispensable requirement in the preparation of polyurethane foams is the selection of raw materials with high reactivity. For this reason, aromatic isocyanates are mainly used in the preparation of polyurethane foams due to their high reactivity. Among these, the most popular are toluene diisocyanate (TDI) and polymeric methylene diphenyl diisocyanate (pMDI).

TDI is commercialized as a mixture of 2,4- and 2,6- isomers in 80/20 and 65/35 weight ratios (**Figure 1.7a**), being the first the most used for flexible polyurethane foam preparation. In this work, all the flexible polyurethane foams were formulated with 80/20 TDI.

Methylene diphenyl diisocyanate (MDI, **Figure 1.7b**) is widely used in the synthesis of thermoplastic and elastomeric polyurethanes. However, as regards to polyurethane foams, it is its polymeric form (pMDI, **Figure 1.7c**) which is used in the preparation of **rigid foams** as a consequence of its higher viscosity and functionality.

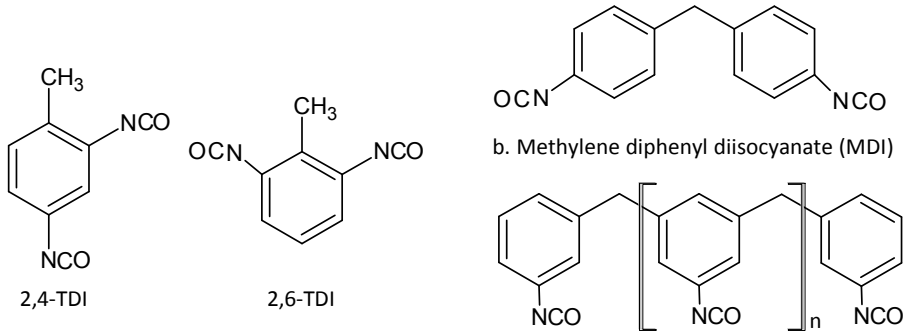

Figure 1.7. Chemical structures of the most used aromatic isocyanates in polyurethane production.

The **isocyanate index** (I.I.) is an important parameter in polyurethane foam formulation, which determines the isocyanate excess, expressed as a percentage, used in the formulation with respect to the required stoichiometric equivalent ratio. Increasing I.I. will favor side reactions producing biuret, allophanate and isocyanurate groups, providing in this way higher reactivity to the system.

1.3.2.b. Polyols

Polyols are usually liquid oligomers or macromolecules with at least two hydroxyl groups. The other functional groups contained in their structure will determine the type of polyol and will have an influence in the final properties of the polyurethane, being **polyester** and **polyether type polyols** the most used in polyurethane industry. Although the first polyurethane foams were prepared with polyester polyols, nowadays polyether polyols are the most used in foam industry (between 80 and 90% of the polyurethane foam market) due to several advantages over polyesters, such as lower viscosity, low cost, higher resistance and durability but with the disadvantage of being more susceptible to oxidation (Ashida, 2007).

The selection of polyols with low functionality (*f = 2-3*) and high molecular weight (between 2000-10000 g mol^{-1}) will result in the production of flexible polyurethane whereas the use of polyols with higher functionality (*f = 3-8*) and with molecular weights below 1000 g mol^{-1} will result in the formation of highly crosslinked

polyurethanes. Polyols are also characterized by their **hydroxyl number** (I_{OH}), which determines the number of reactive hydroxyl groups per gram of polyol.

Recently, the increasing environmental concern has focused the scientific attention on using vegetable oil derived polyols, thus reducing the exploitation of fossil resources. However, these vegetable oils require several purification and transformation stages until obtaining a polyol with similar characteristics to those derived from fossil ones. Vegetable oils are constituted by triglycerides that are obtained from the condensation of glycerol and three fatty acids (**Figure 1.8a**), which chemical structure R', R'' and R''' will be determined by the type of oil. Among the increasing variety of vegetable oil derived polyols, castor oil (**Figure 1.8c**) is a polyester based polyol derived from ricinoleic acid (**Figure 1.8b**) containing secondary OH groups. The castor oil based renewable polyol Lupranol Balance® 50 (LB50, **Figure 1.8d**) has been used in **Chapters 3, 4 and 5** in the production of foams as a replacement of fossil polyether polyol.

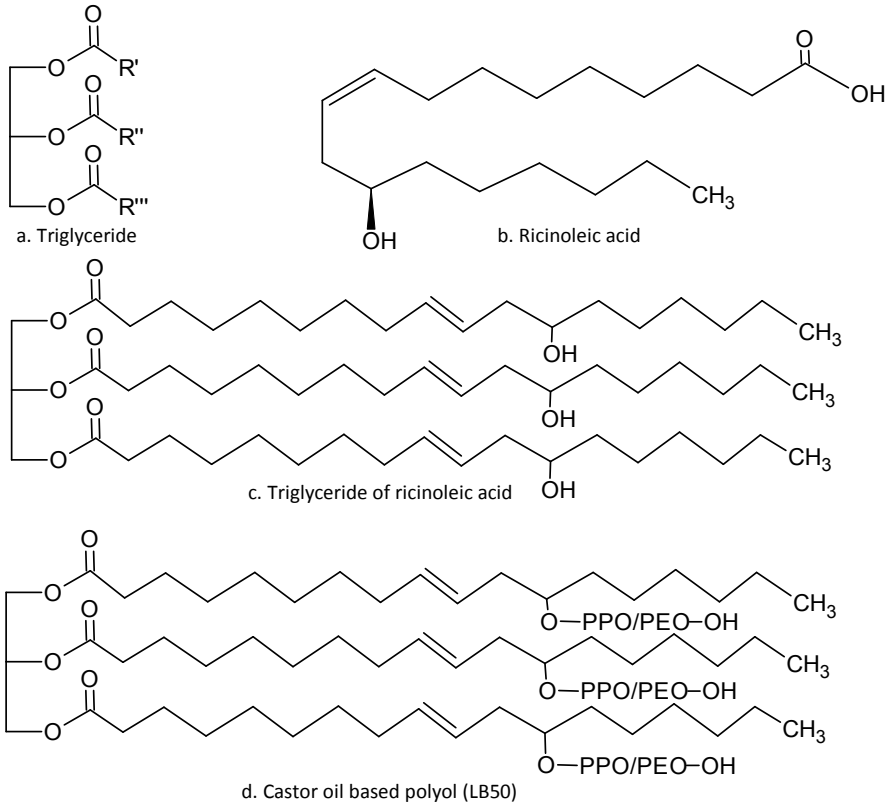

Figure 1.8. Chemical structures of a general triglyceride (a), ricinoleic acid (b), triglyceride derived from ricinoleic acid (c) and a castor oil based polyol (d).

1.3.2.c. Blowing agents

Blowing agents are essential in the production of polyurethane foams, since are responsible of the gas generation that will produce the characteristic cellular structure of the foam. There are chemical and physical blowing agents depending on whether the gas is formed by chemical reaction or by physical state change. These two types of blowing agents can be used all alone or in combination depending on the desired final properties of the material.

Water is the most commonly used **chemical blowing agent**, being the most popular in flexible polyurethane foam production (water blown foams), and the one that has been selected to prepare FPUF in this work. It reacts with isocyanate (**Figure 1.2a**) producing carbon dioxide and disubstituted urea. However, the use of water together with high isocyanate index (I.I.) values has to be carefully handled due to high exothermic reaction with potential risk of fire.

Among **physical blowing agents** low boiling organic liquids are commonly used. They are mixed in the formulation as liquids and change to gas phase as a consequence of the increasing temperature owing to the exothermic polymeric reaction between polyol and isocyanate. When used in combination with water, they are also known as **auxiliary blowing agents**. These low boiling point compounds are commonly halogenated and are selected in order to decrease the thermal conductivity in rigid foams, but they are on the spotlight due to their contribution to ozone layer depletion, with increasing use restrictions. Liquid carbon dioxide is an alternative for halogenated physical blowing agents but it does not contribute to decrease the thermal conductivity.

1.3.2.d. Catalysts

In order to achieve the delicate balance between the blowing and the gelling reaction, different catalysts are often used in polyurethane foam formulation, being the amine and the organometallic type catalysts those with the highest industrial output.

Amine catalysts affect mainly the reactivity of the blowing reaction, but depending on their chemical structure will also have an effect on the gelling reaction (**Figure 1.9**). In flexible polyurethane foams in particular, the most used amine catalyst are tertiary amines (such as **triethylenediamine**), but there also exist delayed action amines for applications such as molded foams where the blowing reaction needs to be delayed in order to have enough time to fill the mold with the reactive mixture. These delayed action amines are amines reacted with a carboxylic acid forming amine salts. These amine salts have no catalytic effect and are mixed with amine excess. This excess of amine will give rise to the beginning of blowing reaction slowly, resulting in heat generation that will dissociate the salt forming amine that will accelerate the blowing reaction.

In relation to **organometallic catalysts**, they participate in the polymerization between polyol and isocyanate (**Figure 1.9**), reason why they are also known as gelling catalysts. They are constituted mainly by metal carboxylates which are susceptible to hydrolization, so special care has to be taken when formulating with water as blowing agent, because it will decrease the activity of the organometallic catalyst. Organotin compounds are the most used in the production of flexible polyurethane foams due to their low cost, being Sn(II) less stable in presence of water than Sn(IV). **Stannous octoate** is the most popular among flexible polyurethane foams whereas **dibutyltin dilaurate** is mostly used in rigid foam formulations.

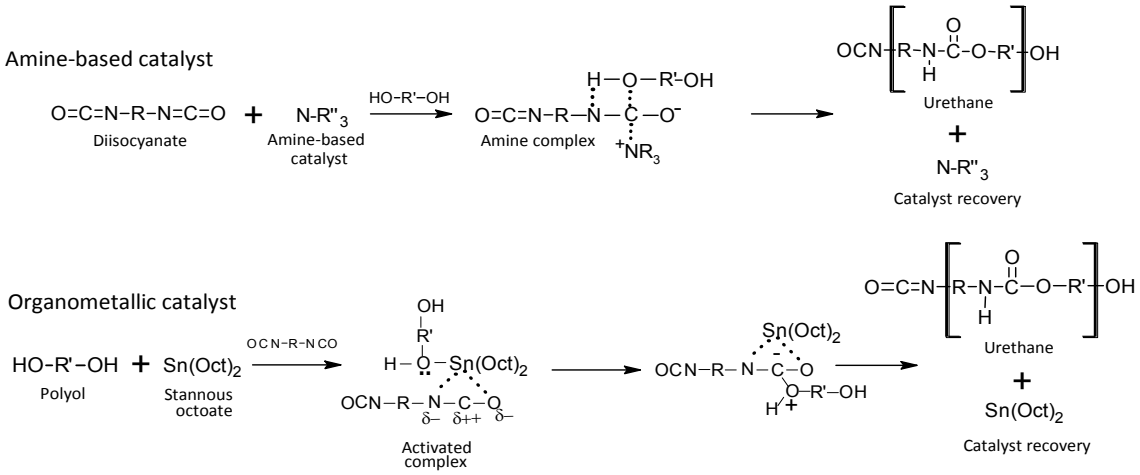

Figure 1.9. Chemical reactions of amine-based and organometallic catalysts during polyurethane foam formation.

1.3.2.e. Surfactants

Surfactans are usually polysiloxane based block copolymers that modify the compatibility between the urea aggregates and reactive mixture, controlling thus the beginning of the phase separation during the foaming process and therefore, controlling also the cell-opening stage. In flexible polyurethane foams, the surfactant decrease the compatibility of the urea aggregate and the medium, promoting the cell opening to an early stage of the polymerization resulting in the formation of flexible foams with high open cell content.

Surfactants also promote the emulsification of raw materials, the nucleation of bubbles avoiding their coalescence and also contribute to stabilize the growth of the foamed structure. They also improve the uniformity of cell size, as well as the visual appearance of the foam while facilitate the adjustment of the density of the foam.

1.3.2.f. Other additives

In the formulation of flexible polyurethane foams other additives such as **colorants** for improving their visual appearance, **mold release agents** to avoid the adhesion of the foam piece to the mold or **fillers** that provide specific properties such as increased density, mechanical strength, hardness or chemical resistance, are widely used in industry. However, the additives that provide the polyurethane foams with **flame retardant** characteristics are of high importance. Flame retardants (FRs) contribute to decrease different characteristics such as ignitability, flame propagation or heat release during the combustion of the material decreasing thus the hazard in case of fire.

But, **how important is it to improve the flame retardant performance of polyurethane foams?** The **organic** nature and **low density** of polyurethane foams make them easily flammable, what in conjunction with their widespread use in daily life applications and the increasingly restrictive standards make the improvement of their fire behavior a necessity of special interest.

1.4. Flame retardancy of polyurethanes

Every year several lives are lost as a consequence of domestic fires, not only because of burning injuries, but in most of the cases owing to smoke inhalation. Polyurethane foams constitute an important fire hazard in domestic scenarios due to their widespread use and their organic nature. Their rapid ignition can be the cause of violent domestic or industrial fires because of their own combustion and also as a consequence of the flame propagation to adjacent objects that are located close to the burning polyurethane.

In order to achieve a better understanding of the fire behavior of polyurethanes, it is also necessary to take a glance at their thermal degradation mechanism.

1.4.1. Thermal degradation of polyurethanes

Thermal degradation of PU is a complex process that takes place in different stages. The covalent bonds present in PU structure break by radical or small molecule formation when subjected to thermal excitation, releasing volatile compounds especially in the early stages of decomposition. This process is known as depolymerization or chain scission. Upon degradation under inert atmosphere, this depolymerization occurs in two differentiated stages: firstly, the **cleavage of the weakest bond** (**urea** and **urethane**, contained in the HS) takes place resulting in the formation of isocyanate, amines and alcohols, followed by the slower **degradation of the SS** producing volatile fragments. The decomposition ends with the formation of carbonaceous residue (char) and/or inorganic residue if heteroatoms are present in the polyurethane formulation (Chattopadhyay and Webster, 2009). Under oxidative atmosphere, these processes are usually merged and shifted to lower temperatures (Krämer et al., 2010). However, the temperatures at which these processes take place will not only depend on the atmosphere, but also on the chemical structure of the polyurethane and the additives if they have been introduced in the formulation.

The decomposition stages can take place following three different routes or by

a combination of them: random chain scission, chain end scission, chain disassemble and crosslinking (Beyler and Hirschler, 2002), which will depend on the characteristics of the selected raw materials.

Different parameters affect the decomposition of PUs, such as the HS and SS structure and molar ratio, the interactions between hard domains, the oxygen content in the polymer structure, molecular weight of the polyol and the crosslinking degree of the material.

1.4.2. Flammability of polymers

The combustion of polyurethane foams is not only related to a violent process and rapid flame propagation due to their low density and big volume, but it is also related to the release of toxic fumes that can be fatal when inhaled.

The polyurethane decomposes quickly upon exposure to heat producing volatile molecules and radicals that diffuse into the polymer-air interface forming a flammable mixture with oxygen in the flame zone when mixed with air. In this point, it is worth noting that the surface of the substrate suffers a thermo-oxidative decomposition as a consequence of the oxygen present in air, while the material underneath present a pyrolytic decomposition process due to the absence of oxygen inside the bulk material (Cullis, 1987).

When the concentration of the volatiles produced during decomposition and the temperature crosses the flammability limit, ignition occurs (*i.e.* the material starts to burn) releasing heat and more volatiles that fuel the flame. The heat produced during burning feds back the pyrolysis process in the condensed phase increasing the decomposition of the substrate, sustaining in this way the combustion of the material.

Therefore, three basic elements are needed to develop a fire (also known as the **combustion triangle**): fuel, oxygen and heat (**Figure 1.10**). The **fuel** refers to the burning material, which as mentioned before, produces volatile and flammable compounds. Also, a **heat source** is needed (not necessarily a flame) that irradiates high enough heat that triggers the ignition of the flammable volatiles.

Finally, **oxygen** is also essential to sustain combustion. Air is composed by 21% of oxygen by volume whereas most of the fires need just a concentration of 16% to be supported (Zlochower and Green, 2009), and acts as an oxidizing agent in the surface of the substrate reacting with the burning volatiles.

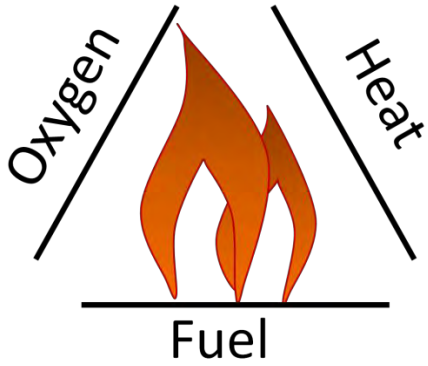

Figure 1.10. Combustion triangle showing the main elements needed to ignite a fire: fuel, heat and oxygen.

In order to improve the flame retardancy of flexible polyurethane foams, these elements have to be evaluated in each situation to determine the most suitable approach to improve the flame retardant behavior. Different types of flame retardant additives exist, acting in different ways depending on their chemical structure.

1.4.3. Classical flame retardants

The aim of adding flame retardants (FRs) in polymer formulations is to decrease their combustibility. FRs can be classified depending on whether they are attached or not into the chemical structure of the polymer. Therefore, if the FR has been covalently bonded to the polymeric matrix they are known as **reactive FRs**, and if they are just physically mixed in the matrix, they are known as **additive FRs**. Up to now, the most used type of flame retardants have been **halogenated compounds**. Their high efficiency in improving the fire behavior of different polymers and their low cost have made them widely used in the industry. However, increasing environmental concern in relation to the ozone layer depletion due to the use of this kind of compounds, and the demonstrated toxicity of the produced fumes (Darnerud, 2003) containing hydrogen halides that can be fatal when inhaled, are the main reasons of their restricted use.

Pentabromodiphenyl ether (pBDE) was widely used in the FPUF industry until 2004, however due to suspects of its hazards towards human health and environment its use was restricted. These suspects and increasing research in the toxicity of halogenated compounds put also the most commonly used halogenated flame retardants in flexible polyurethane industry in the spotlight. These flame retardants included brominated and chlorinated compounds such as 2-ethylhexyl-2,3,4,5-tetra**bromo**benzoate (TBB), bis(2-ethylhexyl)-2,3,4,5-tetra**bromo**phthalate (TBPH), tris(2-**chloro**ethyl) phosphate (TCEP) and tris(2-**chloro**-1-methylethyl) phosphate (TCPP) among others (United States Environmental Protection Agency, 2015). Several governmental and industrial bodies like United States Environmental Protection Agency have developed intensive research in the field of hazard detection towards finding safer and eco-friendly flame retardants.

The mechanism of action of such FRs is based on the radical production in the gas phase during combustion by free radical mechanism (**Figure 1.11**).

a. Free radical formation during polymer combustion

$$H\cdot + O_2 \longrightarrow OH\cdot + O\cdot$$
$$\cdot O\cdot + H_2 \longrightarrow OH\cdot + H\cdot$$

b. Halogenated FR (RX) cleavage

$$RX \longrightarrow R\cdot + X\cdot$$

c. Hydrogen halide (HX) formation by reaction with polymer chain (RH)

$$X\cdot + RH \longrightarrow R\cdot + HX$$

d. H· and OH· radical removal in the gas phase

$$HX + H\cdot \longrightarrow H_2 + X\cdot$$
$$HX + OH\cdot \longrightarrow H_2O + X\cdot$$

Figure 1.11. Free radical mechanism taking place in the gas phase during combustion (Hull et al., 2014).

During combustion, the cleavage of the polymeric chain gives place to the formation of H· and OH· radicals (**Figure 1.11a**). When halogenated FRs are present in

the formulation, they interfere with radical production in the gas phase, removing the high energy OH· and H· radicals that trigger ignition at high concentrations. This interference takes place owing to the breakage of the halogenated FR (**Figure 1.11b**) that forms halogen radicals, which react with the polymeric chain producing hydrogen halides (HX) (**Figure 1.11c**) that will further contribute to H· and OH· removal (**Figure 1.11d**). Nevertheless, the reduction of H· and OH· radicals increases the production of harmful products of incomplete combustion such as **carbon monoxide** or **hydrogen cyanide** (Hull et al., 2014).

1.4.4. Alternatives to halogenated flame retardants

Different approaches to improve the flame retardancy of polyurethanes have been explored in the last years in order to find an effective replacement for halogenated compounds. Some of the alternative FRs are effective by their own, but in many cases they have to be combined with other FR compounds in order to get a significant improvement of the flame retardant properties. Nevertheless, the FR combinations must be carefully selected and their effect thoroughly studied since some of them might have antagonist effect depending on the chemical nature of the substrate.

The main alternatives to halogenated flame retardants in FPUF are phosphorus and/or nitrogen containing compounds, metal hydroxides, layered silicates, intumescent systems and recently nanofillers have grabbed the attention of the scientific community.

1.4.4.a. Phosphorus and/or nitrogen containing compounds

Phosphorus is a well known environmentally friendly alternative for halogenated FRs owing to their low toxic fume and low smoke production during combustion. Phosphorus containing compounds exist in inorganic and organic form, and act mainly in the condensed phase contributing to increase the char formation through dehydration of the polymeric chain owing to the acid nature of phosphorus.

However, they also affect the gas phase due to PO· and/or PO_2· radical formation (Livermore, 2000).

Ammonium polyphosphate (APP) is an effective FR inorganic salt for polyurethanes, but high loads are needed to get a significant improvement in FR properties with the consequent decrease in mechanical performance. In order to avoid this deterioration, the encapsulation of APP with melamine derivatives became popular due the increased FR response while improving the compatibility with the polyurethane matrix (Allan et al., 2014; Jin et al., 2014). Organophosphorus compounds such as **phosphine derivatives** (Zhang et al., 2018), **phosphonium salts** (Sivriev et al., 1982), **phosphonates** (Jimenez et al., 2015), **phosphites** and **phosphates** (Yang et al., 2015) are the most used alternatives for halogenated compounds in FPUF (Chattopadhyay and Webster, 2009) with better compatibility than APP since they can be chemically attached to the polymer backbone. In this sense, phosphorus containing low molecular weight polyols can be incorporated as reactive compounds into the chemical structure of polyurethanes.

Nitrogen containing flame retardants are also known for their environmentally friendly character and for their low toxicity (Horacek and Grabner, 1996). They are also available in form of organic and inorganic compounds and act in both the condensed and gas phase by the formation of crosslinked structures that promote char in the first case, and acting as flammable gas dilutor by releasing ammonia. The most common nitrogen containing flame retardants used in polyurethane market are **melamine derivatives** such as **melamine polyphosphate** (Liu et al., 2017) which demonstrate that the combination of both **nitrogen and phosphorus** provide a synergetic flame retardant effect in both condensed and gas phase.

1.4.4.b. Metal hydroxides

Metal hydroxides, particularly aluminium hydroxide ($Al(OH)_3$, also known as alumina trihydrate, ATH) and magnesium hydroxide ($Mg(OH)_2$) are the most used flame retardants in industry owing to their low cost and low toxicity (Brown, 1998). Nevertheless, for a good flame retardant performance high loads are needed in polymers (up to 60% by weight) assuming a significant loss in mechanical properties.

Their flame retardant mechanism relies on their endothermic decomposition at high temperatures (200 °C in case of ATH, and 300 °C in case of $Mg(OH)_2$), releasing water that cool down the flame zone and dilute volatile gases (**Figure 1.12**). Depending on the processing temperature of the polymer ATH or $Mg(OH)_2$ will be selected, relegating the use of $Mg(OH)_2$ to polymers with higher processing temperatures.

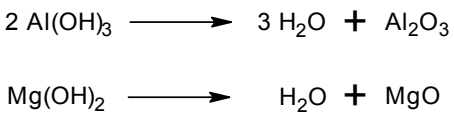

Figure 1.12. Decomposition of aluminium and magnesium hydroxides.

1.4.4.c. Intumescent systems

Intumescent flame retardants produce upon exposure to flame thermally stable foamed char, which is accumulated in the surface and acts as a heat and oxygen shield for the underlying substrate. Therefore, in the condensed phase they limit the pyrolysis of the polymer decreasing also the release of volatile moieties to the gas phase. Additionally the foam shield prevents the molten polymer from dripping, decreasing the hazard of flame propagation to adjacent objects (Camino, 1998).

This family of FRs is widely used as coating in a broad range of materials, not only in polymers but also in wood and even in steel. They are known as **intumescent systems** because three different agents are needed in order to obtain the characteristic intumescent expanding effect: an **acid source** (or dehydrating agent), a **charring agent** and a **blowing agent**. The acid will act as a catalyst of the charring agent, producing a shield of char that will be expanded as a consequence of the release of gases of the blowing agent. The most common intumescent FRs used in polyurethanes include the mixture of melamine polyphosphate (acting the melamine as blowing agent and the phosphate as an acid source) and pentaerythritol as char forming agent (Sun et al., 2013).

1.4.4.d. Nanoparticles

Nanoparticles can increase the thermal stability of polymeric materials while enhancing the mechanical properties due to their small size and interactions with the matrix, such as van der Waals, electrostatic interactions, etc. Nevertheless, nanoparticles do not provide a good flame retardant performance neither self-extinguishing properties on their own. They need to be combined with effective flame retardants in order to enhance its performance on the material (Arao, 2015).

Nanoclays are layered silicates at nanoscale size, existing in a broad range of types depending on their chemical composition and stacked structure. Montmorillonite (Ubowska, 2014), bentonite (Franchini et al., 2008), sepiolite (Pappalardo et al., 2016) and layered double hydroxides are among layered clays the most used ones in polymeric formulations and demonstrated to increase tensile strength and thermal stability in a variety of polymeric matrices (Hapuarachchi and Peijs, 2010). Their dispersion in the matrix is crucial in order to obtain the best properties: depending on the dispersion technique, their interaction with the matrix and so on, the layered silicates can be in exfoliated, intercalated or stacked form in the polymers. Their layered structure, delay the release of volatiles to the flame zone (Chattopadhyay and Webster, 2009), being also of special interest their use in intumescent systems since they contribute to reinforce the char residue (Wu et al., 2014). In addition, they offer the possibility of replacing the interlayer ions contributing to improve their dispersion or even the flame retardant behavior of the polymeric matrix.

Other nanoentities such as single and multiwalled carbon nanotubes, graphene and graphene oxide are also used in the same way than nanoclays, aiming to improve thermal stability and mechanical properties while enhancing the flame retardant effect of other flame retardant additives. However, in most of the cases these carbonaceous nanoentities need to be functionalized in order to improve their compatibility with the polymeric matrix and thus achieve a good dispersion, being sometimes functionalized with phosphorus containing molecules pursuing to enhance the charring of the polymer when exposed to fire (Ma et al., 2008).

1.4.5. Proposed eco-friendly alternatives

In this work, different eco-friendly fillers have been proposed in order to study their effect on the properties of flexible polyurethane foams. Aiming to improve thermal stability and their potential as flame retardant agents, **layered double hydroxides** and **lignin** have been selected for being based on natural resources in both cases, and also to give added value to an industrial byproduct like lignin.

1.4.5.a. Layered double hydroxides

Layered double hydroxides (LDH) belong to the group of anionic clays, also known as hydrotalcite-like compounds, which can be natural or synthetic. Their structure consists on $Mg(OH)_2$ octahedra (namely brucite) that share their edges to form sheets stacked through hydrogen bonding. The stacking can follow hexagonal or rhombohedral symmetry, being the latter the stacking configuration of the natural hydrotalcite, which consists on a hydroxycarbonate of magnesium and aluminium. Its first formula, $Mg_6Al_2(OH)_{16}CO_3{\cdot}4H_2O$ was given by Manasse (Manasse, 1915). The general formula of hydrotalcite-like compounds is $\mathbf{[M^{2+}_{(1-x)}M^{3+}_x(OH)_2]^{x+}(A^{n-}_{x/n})^{x-}{\cdot}mH_2O}$, which is constituted by the mixture of divalent (Ca^{2+}, Mg^{2+}, Mn^{2+}, Fe^{2+}, Zn^{2+}, etc.) and trivalent (Al^{3+}, Fe^{3+}, Ni^{3+}, etc.) metal ions with similar sizes with values of x ranging $0.20 < x < 0.33$ (Evans and Slade, 2006). The water content (m) can be varied over a wide range of values. The trivalent cation is present in the structure as a partial substitution of the divalent one in the brucite-like structure, causing an imbalance on the charge neutrality of the clay, thus leaving the hydroxide sheets positively charged. This positive surcharge is compensated by the presence of anions in the interlayer space, usually CO_3^{2-}, OH^-, Cl^- or NO_3^-, being the carbonate the most common and the one with higher affinity among the clay sheets. These negative ions are exchangeable for a broad range of inorganic and organic anions, providing to these clays the flexibility of being used in several applications, such as catalyst or as catalyst support (Eshaq and Elmetwally, 2016), adsorbent in wastewater (Abou-El-Sherbini et al., 2015), drug carrier in medicine (R.R. Cunha et al., 2016), and even as flame retardant (Elbasuney, 2015) among other uses (Li and Duan, 2006).

LDH can have a flame retarding effect due to the coexistence along the interlayer space of anions, water of crystallization and OH^- from the sheets, acting as combustible compound diluters due to the generation of non-combustible gases (usually CO_2 and H_2O) (Cavani et al., 1991) and through the local cooling of the flaming material by the release of hydroxyl groups and interlayer water (Kiliaris and Papaspyrides, 2010).

Hydrotalcite-like compounds can be synthesized from different routes such as co-precipitation, urea hydrolysis, hydrothermal treatment, ion exchange or calcination-rehydration process. After calcination, a mixture of the corresponding metal oxides is obtained allowing the regeneration of the brucite-like structure in contact with water due to their memory effect properties. If the desirable intercalating anion is diluted in this water under the adequate conditions of pH and temperature, the reconstruction can be performed together with the intercalation of the selected anion. Thus, the addition of phosphorus containing anions in the rehydration process of LDH can contribute to the reduction of the flame spread through the catalytic effect of the phosphorus in the oxidation of polymeric chains, leading to the formation of a protective carbonaceous layer which can prevent the feeding of the flame (Lu and Hamerton, 2002).

1.4.5.b. Lignin

Wood is mainly composed by cellulose, hemicellulose and lignin, apart from extractives and other inorganic compounds. Lignin acts as a binder of the cellulose fibers in the cell walls of vascular plants, providing structural stability as well as performing a protective function as an antimicrobial agent (Barakat et al., 2010). Its aromatic and heterogeneous structure gives place to an amorphous macromolecule that is considered the second most abundant biopolymer on earth only after cellulose, being the main source of aromatic compounds. Lignin structure is composed by the bonding of three main monomers (**Figure 1.13**).

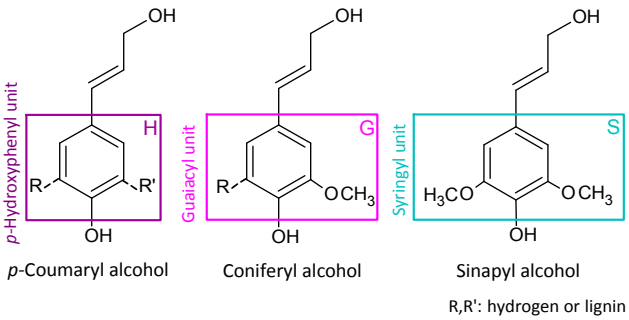

Figure 1.13. Main structural units of lignin structure: p-hydroxyphenyl, guaiacyl and syringyl units.

These monomers are known as monolignols and consist on phenylpropane units with different substitutions (p-hydroxyphenyl (H), guaiacyl (G) and syringyl (S) units) derived from coumaryl, coniferyl and sinapyl alcohol, respectively (Gosselink et al., 2004). The prevalence of one unit or another will depend on the vegetable species of origin; for instance, G units are predominant in softwood lignin, a mixture of G and S units in hardwood and finally H units are more abundant in lignin derived from annual plants. These monomers are connected by different C-C and ether linkages, such as β-β, β-1, 4-O-5 and β-O-4, being the latter the most common, especially in softwood lignin (Laurichesse and Avérous, 2014).

These linkages hamper the isolation of lignin without its fractionation. Nowadays different processes are used for the extraction of lignin, such as enzymatic acidolysis, ionic liquid pretreatment, organosolv, kraft and lignosulfonate processes, being the last two the most used and developed at industrial scale (Li et al., 2015).

The kraft pulping method is used for the conversion of wood (both softwood and hardwood) into pulp for the further production of paper. In this process, the wood is cooked in digesters where a great part of the lignin contained in wood is degraded into different molecular weight fragments. These fragments are dissolved in an aqueous solution of sodium hydroxide and sodium sulfide together with carbohydrates obtained from hemicelluloses and inorganic salts, forming the so called black liquor. An appropriate treatment and purification of this black liquor gives rise to the isolation of kraft lignin. The integration of wood-related industrial processes with biorefineries, would provide added value to byproducts such as lignin and would provide a great source of renewable materials and energy.

Nevertheless, the heterogeneous composition makes difficult to obtain large lignin batches with a homogeneous quality for chemical and materials production. For this reason, softwood kraft lignin, which is characterized for being more reactive and for having a more homogeneous structure than hardwood lignin (Gellerstedt, 2015), is the perfect candidate for large scale production. Even though most of this lignin is commonly burned as internal production of energy for the pulping process, nowadays more and more quantities are commercialized for its use as additive, dispersant or dye (Holladay et al., 2007).

Research is nowadays focused on taking advantage of lignin in high added value applications such as the obtaining of fine chemicals (Bouxin et al., 2015), carbon fiber production (Kadla et al., 2002) and materials containing lignin not only as an additive (Morandim-Giannetti et al., 2012), but also as a part of the formulation (Zhang et al., 2013). The use of lignin in polyurethane chemistry is promising since lignin provides the hydroxyl groups needed for urethane linkage formation. In this way, several approaches have been developed in order to obtain polyurethanes containing lignin as an additive or as a replacement of the main reactive materials by using oxypropylated or liquefied lignin as a promising eco-friendly alternative for fossil sourced polyols (Cateto et al., 2009). Lignin modification with functional groups containing phosphorus and/or nitrogen has also been considered an effective way to its incorporation into polyurethane formulations. In addition, the functionalization with isocyanate groups can also contribute to increase its reactivity in order to achieve a better dispersion of lignin in the polyurethane.

1.5. Bench scale characterization techniques and standards

Different techniques can be used in order to characterize the flame retardancy of polymeric materials. Nevertheless, it is worth noting that these techniques are intended for laboratory-scale purposes and that the obtained results cannot be extrapolated to real life cases, since many different and sometimes unexpected parameters are involved in a real fire scenario that cannot be taken into account in laboratory tests.

1.5.1. Thermogravimetric analysis

Thermogravimetric analysis (TGA) is a powerful tool to characterize the thermal stability of materials by their mass loss at a controlled temperature program under different atmospheres. Different types of analysis can be performed, such as **dynamic analysis** by using a ramp of temperature (usually up to high temperatures, between 800 and 1000 °C) or **isothermal analysis** at constant temperature. Each mass loss corresponds to one or various overlapped decomposition processes. It is a useful and quick method to detect the presence of additives and contaminants in materials by selective decomposition.

In case of polymers, in general at low temperatures the loss of low boiling volatile compounds takes place. Increasing the temperature low molecular weight fractions and trapped water between the polymeric chains are released and at higher temperatures, the thermal or thermo-oxidative decomposition of the polymer takes place, depending whether the essay is performed under inert (nitrogen or argon) or oxidative (air or pure oxygen) atmosphere. When performed under inert atmosphere, the pyrolysis of the sample occurs, leaving char or inorganic residue. If oxidative decomposition takes place, the remaining residue will be constituted by oxides.

A more thorough analysis can be performed if TGA is combined with techniques such as mass spectrometry (TGA-MS) or Fourier transform infrared spectroscopy (TGA-FTIR) in order to characterize the volatile gases released during decomposition.

1.5.2. Limiting oxygen index

The limiting oxygen index (LOI) is a simple method used to determine and compare the ignitability and the burning behavior of materials. This technique gives a measure of the minimum oxygen concentration in mixture with nitrogen needed to initiate and support combustion. The LOI index is given as a percentage in **Equation 1.2**, being $[O_2]$ the minimum oxygen concentration needed for self-sustained burning and $[N_2]$ the nitrogen concentration during the essay. When LOI index of a material is below 21 (below the 21% concentration of oxygen in air), the material will support

sustained combustion. Increasing LOI index indicates that the material will not sustain combustion under air atmosphere, *i.e.* it can take fire but the material will cease the flame once the pilot flame has been removed. The results obtained in this test are merely comparative and are influenced by sample geometry, size and orientation, as well as temperature of the chamber, viscosity and dripping of the molten polymer, formation of char shield during combustion, etc. The LOI value of neat polyurethane foams is below 21, meaning that they are easily ignitable in an open-air situation (air atmosphere) (Mark et al., 1975).

$$\text{LOI (\%)} = \frac{[O_2]}{[O_2]+[N_2]} \cdot 100 \qquad \textbf{Eq. 1.2.}$$

The standard ISO 4589-2 (2006) gathers the conditions needed to perform this test to plastic materials. A candle like sample is supported in a vertical glass chamber with an oxygen/nitrogen atmosphere with a certain oxygen concentration. The gas ratio is varied in order to record the minimum concentration of oxygen that will support combustion.

1.5.3. UL 94 horizontal burning test

The UL 94 (Test for flammability of plastic materials for parts in devices and appliances) is a test method developed by Underwriter Laboratories, Inc in order to study the burning behavior at bench scale of plastic materials for parts in devices and appliances. In the particular case of flexible polyurethane foams, the ISO 9772 (2012) standard covers the determination of horizontal burning of small specimens and can be followed in order to perform comparative tests.

In this standard, the conditions for measuring the flame spread along the length of a rectangular foam sample are collected, such as the orientation of the burner, the height of the flame, the distance from the flame to the sample, the heat capacity of the flame and the distance from the sample to a cotton gauze placed below in order to study the dripping of the polymer, among many other parameters. It is important to have timing devices for measuring the flame spread along specified distances (at 25, 60 and 125 mm measured from one side) previously marked on the sample.

1.5.4. Cone calorimetry

Cone calorimetry test is a useful tool to determine the heat and the smoke released by a material subjected to well-defined flaming conditions, such as a determined external heat flux. This heat flux can be varied up to 100 kW m^{-2}, but usually this test is performed under 35 or 50 kW m^{-2} (being 50 kW m^{-2} the closest to developing fire conditions). The higher the applied heat flux, the higher the reproducibility of the test and the closest to real fire conditions (Schartel and Hull, 2007).

The ISO 5660-1 (2015) specifies a method for determining the heat release rate of a specimen in horizontal orientation to determined levels of radiant heat flux and ignited with an external pilot flame. The heat release rate is determined by the measurement of the oxygen consumption during combustion and the flow rate in the gas phase.

The cone calorimetric test can be of special interest under vertical orientation since the dripping characteristics of the materials cannot be taken into account in horizontal. Vertical orientation enhances the dripping effect and the heat feedback from the pool of burning melt, since the high velocity layer of melting decomposition products are immediately removed from the burning sample forming a pool fire, overlapping in this way the foam collapse stage with the fire pool stage.

Combustion of flexible polyurethane foams is affected by their physical behavior and governed by their low density. For these reasons, these materials present practically immediate time to ignition and immediate fire growth (Krämer et al., 2010), and burn practically completely leaving almost no char.

1.6. General objectives

The general objectives of this work are:

- Incorporate layered double hydroxides to flexible polyurethane foams. For this purpose, the layered double hydroxides have been modified with different phosphorus containing molecules.
- Substitute part of the polyol of the flexible polyurethane foam formulation with a phosphorus containing oligomeric diol. Also, study the effect on the properties of the foam due to the combination of phosphorus containing oligomeric diol and layered double hydroxides.
- Introduce kraft lignin and functionalized kraft lignin in flexible polyurethane foam formulations.
- Study the effect in the fire behavior of the combined use of layered double hydroxides, lignin and phosphorus containing oligomeric diol in flexible polyurethane foams by means of standardized techniques.

1.7. References

Abou-El-Sherbini, K.S., Kenawy, I.M.M., Hafez, M.A.H., Lotfy, H.R., Abdelbary, Z.M.E.A., 2015. Synthesis of novel carbonate/chloride bearing 3(Mg + Zn)/(Al + Fe) layered double hydroxides for the removal of anionic hazards. J. Environ. Chem. Eng. 3, 2707–2721.

Allan, D., Daly, J.H., Liggat, J.J., 2014. Thermal volatilisation analysis of a TDI-based flexible polyurethane foam containing ammonium polyphosphate. Polym. Degrad. Stab. 102, 170–179.

Arao, Y., 2015. Flame retardancy of polymer nanocomposites, in: Visakh, P.M., Arao, Y. (Eds.), Flame Retardants: Polymer Blends, Composites and Nanocomposites. Springer Cham, Heidelberg, pp. 15–44.

Ashida, K., 2007. Fundamentals, in: Polyurethane and Related Foams: Chemistry and

Technology. CRC Press, Boca Ratón, pp. 11–64.

Barakat, A., Bagniewska-Zadworna, A., Frost, C.J., Carlson, J.E., 2010. Phylogeny and expression profiling of CAD and CAD-like genes in hybrid Populus (P. deltoides x P. nigra): Evidence from herbivore damage for subfunctionalization and functional divergence. BMC Plant Biol. 10, 100–110.

Berezkin, Y., Urick, M., 2013. Modern polyurethanes: overview of structure property relationship, in: Patil, A., Ferritto, M.S. (Eds.), Polymers for Personal Care and Cosmetics. American Chemical Society, Washington, DC, pp. 65–81.

Beyler, C.L., Hirschler, M.M., 2002. Thermal decomposition of polymers, in: Hurley, M.J., Gottuk, D.T., Hall Jr., J.R., Harada, K., Kuligowski, E.D., Puchovsky, M., Torero, J.L., Watts Jr, J.M., Wieczorek, C.J. (Eds.), SFPE Handbook of Fire Protection Engineering 2. Springer-Verlag, New York, pp. 110–131.

Bouxin, F.P., McVeigh, A., Tran, F., Westwood, N.J., Jarvis, M.C., Jackson, S.D., 2015. Catalytic depolymerisation of isolated lignins to fine chemicals using a Pt/alumina catalyst: Part 1 - Impact of the lignin structure. Green Chem. 17, 1235–1242.

Brown, S.C., 1998. Flame retardants: inorganic oxide and hydroxide systems, in: Pritchard, G. (Ed.), Plastics Additives. An A-Z Reference. Springer, Bristol, pp. 287–296.

Camino, G., 1998. Flame retardants: intumescent systems, in: Pritchard, G. (Ed.), Plastics Additives. An A-Z Reference. Springer Science+Business Media, LLC, Bristol, pp. 297–306.

Cateto, C.A., Barreiro, M.F., Rodrigues, A.E., Belgacem, M.N., 2009. Optimization study of lignin oxypropylation in view of the preparation of polyurethane rigid foams. Ind. Eng. Chem. Res. 48, 2583–2589.

Cavani, F., Trifirò, F., Vaccari, A., 1991. Hydrotalcite-type anionic clays: Preparation, properties and applications. Catal. Today 11, 173–301.

Chattopadhyay, D.K., Webster, D.C., 2009. Thermal stability and flame retardancy of polyurethanes. Prog. Polym. Sci. 34, 1068–1133.

Cullis, C.F., 1987. The role of pyrolysis in polymer and flame retardance combustion. J. Anal. Appl. Pyrolysis 11, 451–463.

Darnerud, P.O., 2003. Toxic effects of brominated flame retardants in man and in wildlife. Environ. Int. 29, 841–853.

Defonseka, C., 2013. Polyurethane raw materials, in: Practical Guide to Flexible Polyurethane Foams. Smithers Rapra Technology Ltd, Shawbury, pp. 41–54.

Elbasuney, S., 2015. Surface engineering of layered double hydroxide (LDH) nanoparticles for polymer flame retardancy. Powder Technol. 277, 63–73.

Eshaq, G., Elmetwally, A.E., 2016. (Mg–Zn) – Al layered double hydroxide as a regenerable catalyst for the catalytic glycolysis of polyethylene terephthalate. J. Mol. Liq. 214, 1–6.

Evans, D.G., Slade, C.T., 2006. Structural aspects of layered double hydroxides. Struct. Bond. 119, 1–87.

Franchini, M.C., Fabbri, P., Frache, A., Ori, G., Messori, M., Siligardi, C., Ricci, A., 2008. Bentonite-based organoclays as innovative flame retardants agents for SBS copolymer. J. Nanosci. Nanotechnol. 8, 6316–6324.

Gellerstedt, G., 2015. Softwood kraft lignin: Raw material for the future. Ind. Crops Prod. 77, 845–854.

Gosselink, R.J.A., Abächerli, A., Semke, H., Malherbe, R., Käuper, P., Nadif, A., Van Dam, J.E.G., 2004. Analytical protocols for characterisation of sulphur-free lignin. Ind. Crops Prod. 19, 271–281.

Hapuarachchi, T.D., Peijs, T., 2010. Multiwalled carbon nanotubes and sepiolite nanoclays as flame retardants for polylactide and its natural fibre reinforced composites. Compos. Part A 41, 954–963.

Holladay, J.E., White, J.F., Bozell, J.J., Johnson, D., 2007. Top value-added chemicals from biomass volume II - Results of screening for potential candidates from biorefinery lignin. Pacific Northwest Natl. Lab. II, 87.

Horacek, H., Grabner, R., 1996. Advantages of flame retardants based on nitrogen compounds. Polym. Degrad. Stab. 54, 205–215.

Hull, T.R., Law, R.J., Bergman, A., 2014. Environmental drivers for replacement of halogenated flame retardants, in: Polymer Green Flame Retardants. Elsevier B.V., Amsterdam, pp. 120–165.

ISO 4589-2, 2006. Plastics - Determination of burning behaviour by oxygen index - Part 2: Ambient-temperature test.

ISO 5660-1, 2015. Reaction-to-fire tests - Heat release, smoke production and mass loss rate - Part 1: Heat release rate (cone calorimeter method) and smoke production rate (dynamic measurement).

ISO 9772, 2012. Cellular plastics - Determination of horizontal burning characteristics of small specimens subjected to a small flame.

Jimenez, M., Lesaffre, N., Bellayer, S., Dupretz, R., Vandenbossche, M., Duquesne, S., Bourbigot, S., 2015. Novel flame retardant flexible polyurethane foam: plasma induced graft-polymerization of phosphonates. RSC Adv. 5, 63853–63865.

Jin, J., Dong, Q., Shu, Z., Wang, W., He, K., 2014. Flame retardant properties of polyurethane/expandable graphite composites. Procedia Eng. 71, 304–309.

Kadla, J.F., Kubo, S., Venditti, R.A., Gilbert, R.D., Compere, A.L., Griffith, W., 2002. Lignin-based carbon fibers for composite fiber applications. Carbon N. Y. 40, 2913–2920.

Kiliaris, P., Papaspyrides, C.D., 2014. Polymers on Fire, in: Papaspyrides, C.D., Kiliaris, P. (Eds.), Polymer Green Flame Retardants. Elsevier B.V., Amsterdam, pp. 1–43.

Kiliaris, P., Papaspyrides, C.D., 2010. Polymer/layered silicate (clay) nanocomposites: An overview of flame retardancy. Prog. Polym. Sci. 35, 902–958.

Krämer, R.H., Zammarano, M., Linteris, G.T., Gedde, U.W., Gilman, J.W., 2010. Heat release and structural collapse of flexible polyurethane foam. Polym. Degrad. Stab. 95, 1115–1122.

Laurichesse, S., Avérous, L., 2014. Chemical modification of lignins: Towards biobased polymers. Prog. Polym. Sci. 39, 1266–1290.

Lewin, M., 2001. Synergism and catalysis in flame retardancy of polymers. Polym. Adv. Technol. 222, 215–222.

Li, C., Zhao, X., Wang, A., Huber, G.W., Zhang, T., 2015. Catalytic transformation of lignin for the production of chemicals and fuels. Chem. Rev. 115, 11559–11624.

Li, F., Duan, X., 2006. Applications of layered double hydroxides. Struct. Bond. 119, 193–223.

Liu, S.-H., Kuan, C.-F., Kuan, H.-C., Shen, M.-Y., Yang, J.-M., Chiang, C.-L., 2017. Preparation and flame retardancy of polyurethane composites containing microencapsulated melamine polyphosphate. Polymers (Basel). 9, 407–421.

Livermore, L., 2000. Kinetic study of the combustion of organophosphorus compounds. Proc. Combust. Inst. 28, 1749–1756.

Lu, S., Hamerton, I., 2002. Recent developments in the chemistry of halogen-free flame retardant polymers. Prog. Polym. Sci. 27, 1661–1712.

Ma, B.H., Tong, L., Xu, Z., Fang, Z., 2008. Functionalizing carbon nanotubes by grafting on intumescent flame retardant: Nanocomposite synthesis, morphology, rheology, and flammability. Adv. Funct. Mater. 18, 414–421.

Manasse, E., 1915. Idrotalcite e piroaurite. Atti Soc. Toscana Sci. Nat. 24, 92.

Mark, H.F., Atlas, S.M., Shalaby, S.W., Pearce, E.M., 1975. Combustion of polymers and its retardation, in: Lewin, M., Atlas, S.M., Pearce, E.M. (Eds.), Flame-Retardant Polymeric Materials. Plenum Press, New York, pp. 1–15.

Markets and Markets, 2016. Polyurethane foam market by type (flexible, rigid, and spray foam), end-use industry (bedding & furniture, building & construction, electronics, automotive, footwear, packaging), and region - global forecast to 2021.

Morandim-Giannetti, A.A., Agnelli, J.A.M., Lanças, B.Z., Magnabosco, R., Casarin, S.A.,

Bettini, S.H.P., 2012. Lignin as additive in polypropylene/coir composites: Thermal, mechanical and morphological properties. Carbohydr. Polym. 87, 2563–2568.

National Fire Protection Association, 2017a. Fires in the United States during 2016. Washington, DC.

National Fire Protection Association, 2017b. A reporter's guide to fire and the NFPA - The consequences of fire. Washington, DC.

Pappalardo, S., Russo, P., Acierno, D., Rabe, S., Schartel, B., 2016. The synergistic effect of organically modified sepiolite in intumescent flame retardant polypropylene. Eur. Polym. J. 76, 196–207.

R.R. Cunha, V., A. Guilherme, V., de Paula, E., R. de Araujo, D., O. Silva, R., V.R. Medeiros, J., R.S.A. Leite, J., A.D. Petersen, P., Foldvari, M., M. Petrilli, H., R.L. Constantino, V., 2016. Delivery system for mefenamic acid based on the nanocarrier layered double hydroxide: Physicochemical characterization and evaluation of anti-inflammatory and antinociceptive potential. Mater. Sci. Eng. C 58, 629–638.

Schartel, B., Hull, T.R., 2007. Development of fire-retarded materials - Interpretation of cone calorimeter data. Fire Mater. 31, 327–354.

Sivriev, H., Borissov, G., Walczyk, W., 1982. Synthesis and studies of phosphorus-containing polyurethane foams based on tetrakis(hydroxymethyl)phosphonium chloride derivatives. J. Appl. Polym. Sci. 27, 4137–4147.

Sun, L., Qu, Y., Li, S., 2013. Co-microencapsulate of ammonium polyphosphate and pentaerythritol in intumescent flame-retardant coatings. J. Therm. Anal. Calorim. 111, 1099–1106.

Szycher, M., 2013. Isocyanate chemistry, in: Szycher's Handbook of Polyurethanes. CRC Press, Boca Ratón, pp. 87–134.

Ubowska, A., 2014. Montmorillonite as a polyurethane foams flame retardant. Arch. Combust. 30, 459–462.

United States Environmental Protection Agency, (EPA), 2015. Flame retardants used in flexible polyurethane foam: An alternatives assessment update.

Wu, H., Krifa, M., Koo, J.H., 2014. Flame retardant polyamide 6/nanoclay/intumescent nanocomposite fibers through electrospinning. Text. Res. J. 84, 1106–1118.

Yang, R., Hu, W., Xu, L., Song, Y., Li, J., 2015. Synthesis, mechanical properties and fire behaviors of rigid polyurethane foam with a reactive flame retardant containing phosphazene and phosphate. Polym. Degrad. Stab. 122, 102–109.

Zhang, K., Hong, Y., Wang, N., 2018. Flame retardant polyurethane foam prepared from compatible blends of soybean oil-based polyol and phosphorus containing polyol. J. Appl. Polym. Sci. 45779, 1–10.

Zhang, W., Ma, Y., Wang, C., Li, S., Zhang, M., Chu, F., 2013. Preparation and properties of lignin-phenol-formaldehyde resins based on different biorefinery residues of agricultural biomass. Ind. Crops Prod. 43, 326–333.

Zlochower, I.A., Green, G.M., 2009. The limiting oxygen concentration and flammability limits of gases and gas mixtures. J. Loss Prev. Process Ind. 22, 499–505.

“If my answers frighten you then you should cease asking scary questions.”

L. Bender (Producer) and Q. Tarantino (Director). Pulp Fiction. United States: Miramax, 1994.

Chapter 2

2

Materials and characterization techniques

2. Materials and characterization techniques

2.1. Introduction

This chapter describes the reactants that will be used in the following chapters for the modification of layered double hydroxides, functionalization of lignin and for the preparation of polyurethane foams, in addition to the experimental techniques that will be used to characterize the prepared materials.

2.2. Materials

The preparation of flexible polyurethane foams (FPUF) in this work was carried out using different polyether polyols. In **Chapter 3**, **4 and 5**, the foams were prepared using a castor oil based polyether polyol, Lupranol Balance® 50, **LB50** (BASF) with a functionality of 2.7. In **Chapter 6**, due to the lack of commercial availability of LB50, the foams were prepared using a trifunctional fossil derived polyether type polyol Alcupol® F-4811, **ALC** (Repsol). Additionally, in **Chapters 4** and **6**, an oligomeric phosphonate diol (Exolit® OP 560, **E560**, Clariant) was used as a reactive flame retardant replacing partially the polyether polyol in order to improve the fire behavior of the foams. The phosphorus content of E560 (13.91%) was determined by inductively coupled plasma optical emission spectrometry (ICP-OES).

The main characteristics of the polyols are shown in **Table 2.1**. The hydroxyl index (I_{OH}) was determined by titration following the acetylation procedure (test A) from ASTM E1755-01 (2015) standard, the equivalent weight (*Eq wt*) was calculated according to **Equation 2.1**, where *56.1* is the molecular weight of potassium hydroxide (KOH, g mol^{-1}), I_{OH} the hydroxyl index (mg KOH g^{-1}) and the *acid number* (mg KOH g^{-1}) is the residual acidic material in the polyol.

$$\text{Eq wt}\ \left(\text{g eq}^{-1}\right) = \frac{56.1 \cdot 1000}{I_{OH} \cdot \text{acid number}} \qquad \textbf{Eq. 2.1}$$

The viscosity at 25 °C was determined by rheological measurements and the functionality and the acid number values were provided by the manufacturers. The weight average molecular weight ($\bar{M}_w$) referred to polystyrene standards and

polydispersity index (PD) of the LB50 and ALC polyols were determined by gel permeation chromatography (GPC).

Table 2.1. Main characteristics of the polyols used in the preparation of flexible polyurethane foams.

Polyol	*f*	I_{OH} (mg KOH g^{-1})	Acid number (mg KOH g^{-1})	Eq wt (g eq^{-1})	Viscosity at 25 °C (mPa s)	$\bar{M}_w$ (g mol^{-1})	PD
LB50	2.7	50.3	≤ 0.06	1113.9	837	4636	1.1
ALC	3.0	49.7	≤ 0.10	1126.5	603	4915	1.0
E560	2.0	489.0	≤ 2.00	114.3	302	-	-

The preparation of flexible polyurethane foams was carried out using a highly reactive isocyanate, *i.e.* toluene diisocyanate, **TDI** (Desmodur T 80 from Covestro) constituted by a mixture of 2,4- and 2,6-toluene diisocyanate isomers in a 80/20 ratio and containing a 48.2% NCO. TDI was selected due to its high reactivity, low price and its suitability for slabstock foam manufacture at industrial scale compared to other commodity isocyanates. The isocyanate index was maintained at 110 and 120 depending on the prepared system and the used fillers. This parameter will be specified in each chapter. Increasing isocyanate index provides higher reactivity to the system together with higher stiffness and greater support to the cellular structure.

Different additives were used in order to enhance the foaming process. Tegoamin® B 75 (Evonik) was selected as amine-type catalyst, which consisted of a mixture of triethylenediamine and bis(2-dimethylaminoethyl) ether that boosted both blowing and gelling reactions. On the other hand, Kosmos® 29 (Evonik), constituted by stannous octoate, was selected as organometallic catalyst to enhance the gelling reaction. Aiming to improve the mixture and provide more stability to the cellular structure during the foaming process, a silicone based surfactant was used, Tegostab® B 4900 (Evonik).

Synthetic hydrotalcite, ($Mg_6Al_2(OH)_{16}{\cdot}4H_2O$, **LDH-$CO_3$**) from Sigma-Aldrich, a synthetic carbonate intercalated anionic clay (layered double hydroxide), was selected for its modification with phosphorus containing anions and their further introduction in flexible polyurethane foams. An inorganic phosphorus containing compound (potassium phosphate monobasic, **KH_2PO_4**, ≥99%) and a organophosphorus compound (bis(2-ethylhexyl) hydrogen phosphate, **HDEHP**, ≥97%) were used as intercalation

agents and were purchased from Sigma-Aldrich. Ammonia (NH_3, 30% v/v) and sodium hydroxide (NaOH, 1M), also from Sigma-Aldrich, were used in order to adjust the pH of the rehydration media for the intercalation of KH_2PO_4 and HDEHP, respectively. The obtained modified LDHs were labeled as **LDH-HPO_4** and **LDH-DEHP**.

Southern pine kraft lignin, **k-lignin** (Domtar's BioChoice™ from UPM Biochemicals) was selected as a potential charring agent for flexible polyurethane foams. In order to characterize this lignin by GPC and carbon-13 nuclear magnetic resonance (^{13}C NMR), it had to be derivatized (*i.e.* acetylated, **ac-lignin**) using acetic anhydride (Panreac) and pyridine (Panreac). Ethanol (Panreac), high permeation liquid chromatography (HPLC) grade chloroform (Lab-Scan Analytical Sciences) and diethyl ether (Panreac) were used for washing the ac-lignin after the acetylation process, which is described in detail in **Chapter 5**. Furtherly, k-lignin was functionalized with isocyanate groups (**k-IPDI**) aiming to increase its reactivity towards the polyurethane matrix. This procedure was carried out using isophorone diisocyanate, **IPDI** (Desmodur®I, Covestro) with a NCO content of 37.8%. HPLC grade tetrahydrofuran, THF (Macron Fine Chemicals) was used as reaction medium for the NCO functionalization and dibutyltin dilaurate, **DBTDL** (Sigma-Aldrich) was used as selective catalyst to enhance reaction of the hydroxyl groups from k-lignin with the secondary NCO groups of IPDI. Finally, HPLC grade toluene (Lab-Scan Analytical Sciences) was used to wash the functionalized lignin.

2.3. Physico-chemical characterization

2.3.1. Fourier transform infrared spectroscopy

Fourier transform infrared spectroscopy (FTIR) is a technique that provides molecular structural information. The technique consists on the irradiation of a sample with an infrared beam. Part of this radiation is absorbed and the other is transmitted through the sample giving place to the formation of a signal in the IR detector. This signal is transformed to an interpretable patron, which is considered to be the fingerprint of each sample.

Infrared spectra of layered double hydroxides, lignin and flexible polyurethane foams were obtained by using a Nicolet Nexus equipment. In case of powder samples (LDHs and lignin), KBr platelets were prepared by grinding in a mortar 0.5% by weight of sample with KBr and drying the mixture under an infrared light lamp in order to avoid interferences with moisture. In case of FPUFs and liquid raw materials such as polyols, an attenuated total reflectance accessory was used (ATR Golden Gate). When using KBr platelets, the spectra were recorded from 4000 to 400 cm^{-1} performing 32 scans and when using the ATR accessory, the spectra were recorded from 4000 to 600 cm^{-1}, with an accumulation of 64 scans. In both cases, the scans were recorder with 4 cm^{-1} resolution.

2.3.2. Ultraviolet-visible spectroscopy

Part of the characterization of lignin consisted on the determination of acid soluble lignin (ASL), which was quantified by ultraviolet-visible (UV-vis) spectroscopy (Dence, 1992). This technique is a kind of photon emission spectroscopy where electromagnetic radiation from the visible, near ultraviolet and near infrared region is used. This radiation is absorbed by the molecules resulting in electronic transitions that can be quantified. Functional groups that absorb this kind of radiation *e.g.* double bonds (C=C, C=O, N=N, etc.) or aromatic rings among others, are known as **chromophores**.

Owing to the abundant presence of double bonds in lignin, ASL was determined in a UV-3600/3100 equipment from Shimadzu at 25 °C by placing a sample of soluble lignin in a quartz absorption cell with a 10 mm light path. The absorbance was measured at 205 nm using a 3% H_2SO_4 solution as a blank and the sample was diluted with the H_2SO_4 solution until obtaining absorbance values ranging between 0.2 and 0.7. Beer's Law was used in order to calculate the acid soluble lignin content (**Equation 2.2**), where b = 1 cm; a = 110 L g^{-1} cm^{-1}, V_D was the volume of the diluted sample and V_O the volume of the original sample.

$$\text{ASL (g L}^{-1}) = \frac{\text{A (Absorbance)}}{\text{b(light path, cm)}\cdot\text{a}\left(\text{absorptivity, L g}^{-1}\text{ cm}^{-1}\right)} \cdot \frac{V_D}{V_O} \qquad \textbf{Eq. 2.2}$$

2.3.3. Gel permeation chromatography

GPC is a type of size exclusion chromatography (SEC), where the molecules are separated in accordance to their hydrodynamic volume as a consequence of the different pore sizes present in the columns of the equipment, without interacting physically or chemically with the sample molecules. The lower the size of the molecules, the higher the amount of pores they will be able to pass through. This means that the small molecules spend more time in going across the columns, taking more time to reach the detector. The large molecules will not be retained in the pores, reaching the detector in less time.

The average molecular weight ($\bar{M}_w$) and polydispersity (PD) of the polyols and derivatized (acetylated) lignin were calculated by means of GPC, using a Thermo Scientific UltiMate 3000 equipped with four Phenogel GPC columns from Phenomenex (particle size of 5 μm and porosity of 10^5, 10^3, 100 and 50 Å) and a RefractoMax 521 refractive index detector.

The analyses were carried out at 30 °C with a flow rate of 1 mL min^{-1} using THF as mobile phase. A THF solution with a concentration of 1% by weight of sample was prepared and a volume of 20 μL was injected, after filtering the solution with 0.20 μm pore sized nylon filters. The $\bar{M}_w$ values were referred to monodisperse polystyrene standards.

2.3.4. High performance liquid chromatography

High performance liquid chromatography (HPLC) is a type of column chromatography that separates the components of a mixture by means of the interactions of the components of the mobile phase with the column (stationary phase). The analytes are retained in the column according to their chemical nature and depending on their interactions (physical or chemical) with the stationary phase. The time for an analyte to pass through the column is known as retention time and it is characteristic for a compound in a given determined mobile and stationary phase.

The presence of sugar impurities in lignin was determined by HPLC using a Jasco LC Net II/ADC with a ROA Organic Acid column from Phenomenex, equipped with a refractive index detector and a photodiode array detector. 0.005 N H_2SO_4 was used as mobile phase, performing the assay with a flow rate of 0.35 mL min^{-1} at 40 °C. High purity standards of d-(+)-glucose, d-(+)-xylose, and d-(-)-arabinose (Fluka) were used for calibration (Gordobil et al., 2014). The analysis was performed twice.

2.3.5. Atomic absorption spectroscopy

The detection and quantification of different chemical elements in LDH and lignin was performed by elemental analysis. The atomic absorption spectroscopy (AAS) is an elemental analysis technique that provides quantitative information about the concentration of different elements in a sample, using specific wavelengths of light that are absorbed by each element, corresponding to the energy needed to move electrons to a higher energy level. For this purpose, the sample is atomized or aerosolized (converted into desolvated atoms in vapor state) with a flame or in a graphite furnace, and irradiated with different electromagnetic beams originated from different element lamps. The light absorbed by the sample will determine the amount of different elements present in the sample.

In this case, the carbon, hydrogen and nitrogen elemental content in pristine and modified layered double hydroxides, as well as sulfur in unmodified and functionalized lignin, was determined using a Eurovector EA 3000 atomic absorption spectrometer heated up to 980 °C with a constant flow of helium stream.

2.3.6. Inductively coupled plasma optical emission spectrometry

Inductively coupled plasma optical emission spectrometry (ICP-OES) is a technique derived from AAS in which the different atoms present in a sample are excited by plasma energy. When the excited atoms return to their low energy state, they release radiation that corresponds to different photon wavelengths. The photon ray wavelength will determine the type of element present in the sample, and its

intensity will determine its amount. This technique offers the possibility to analyze a greater variety of elements than AAS.

This technique was used in order to determine the content of aluminum, magnesium and phosphorus in LDH and the content of sodium in lignin. For this purpose, a Mettler Toledo Optima 8300 equipment was used, dissolving the samples in concentrated nitric acid and then diluting them with deionized water, adapting the dilution protocol proposed by Song et al. (2013).

2.3.7. Nuclear magnetic resonance

Nuclear magnetic resonance (NMR) spectroscopy consists on the application of an electromagnetic field to a sample in order to orientate the atomic nuclei giving place to local magnetic fields in their surroundings. In this work, proton, carbon and phosphorus NMR were performed in order to characterize the chemical structure of lignin. The frequencies at which resonance occur in these nuclei will change depending on their surrounding chemical environment, making these fields highly characteristic of each compound.

The determination of aromatic and aliphatic hydroxyl groups in lignin was performed by proton-1 NMR (^{1}H NMR), performing the test to acetylated lignin (ac-lignin). The ^{1}H NMR spectra were recorded using the zg from Bruker library at 500.13 MHz. A time domain of 64 k, and a spectral width of 10000 Hz were used. The interpulse delay was set to 2 s, the acquisition time to 1.5 s and the number of scans to 32.

The results obtained by ^{1}H NMR were confirmed by ^{13}C NMR. This technique was used to distinguish between primary, secondary and phenolic OH groups (OH(I), OH(II) and OH(Φ), respectively). The liquid ^{13}C NMR spectra were recorder on a Bruker Advance 500 spectrometer, equipped with a BBO probe with gradient in Z axis. A decoupled sequence zgdg from Bruker library was used at 125.77 MHz. A time domain of 64 k, and a spectral width of 31000 Hz were used. The interpulse delay was set to 2 s and the acquisition time to 1.5 s. For each spectrum 32000 scans were accumulated.

Additionally, k-IPDI was qualitatively characterized by solid state ^{13}C cross-polarization magic angle spinning (CP/MAS) NMR, performing directly the test over dried k-lignin and k-IPDI. The spectra were recorded on a Bruker 400 AVANCE III WB spectrometer 9.40T, using a 4 mm DVT-MAS probe at a spinning rate of 10 kHz. The standard cross-polarization pulse sequence (100.6 MHz), a time domain of 2 k, a spectral width of 29 kHz, a contact time of 1.5 ms and an interpulse delay of 5 s were used.

In order to perform a more thorough characterization of the type of hydroxyl groups present in lignin, phosphorus-31 NMR (^{31}P NMR) was performed by phosphytilation of lignin. ^{31}P NMR presents the advantage of discerning the aliphatic and the different kinds of phenolic OH units such as condensed phenolic, guaiacyl, syringyl and p-hydroxyphenil units. The ^{31}P NMR spectrum was also recorded in a Bruker 500 spectrometer using the zgdc from Bruker library at 202.46 MHz. A time domain of 16 k and a spectral width of 50000 Hz with an interpulse delay of 2 s, an adquistion time of 1.5 s and 64 scans were performed.

2.3.8. Rheological measurements

Rheology studies the flow and deformation of fluids under the application of shear stress. The viscosity gives a measure of the internal resistance of a fluid subjected to external stress. In this work, the viscosity of the mixtures of polyol and additives was measured in flow mode, recording the viscosity values at 25 °C within a shear rate range from 10 to 100 s^{-1} using a Thermo Haake Viscotester iQ equipped with P35/Ti plate-plate geometry.

2.4. Morphological characterization

2.4.1. X-ray diffraction

The effective intercalation of the different anions along the LDH clay sheets and the microstructure of the LDH nanocomposite foam samples were studied by X-ray diffraction (XRD). This technique allows the study of the crystallographic nature of a

sample at atomic or molecular level, allowing the measurement of the orientation of a single crystal, the average spacing between layers or rows of atoms that form the crystalline structure and the shape and size of small crystalline regions in a sample. This technique relies on the diffraction of X-rays into different specific directions by crystalline ordered atom regions.

The basal spacing of the LDHs and the microstructure of the nanocomposite foam samples were studied by XRD using a Philips X-Pert automatic diffractometer operating at 40 kV and 40 mA with CuKα radiation (λ = 1.5418 Å). Data were collected at room temperature from 2θ values ranging from 2 to 70° in steps of 0.026° and time per step of 67.32 s. The basal space of the LDH samples and the interlayer space inside the polyurethane matrix was determined from the (003) reflection position following Bragg's law (Bragg, 1929) (**Equation 2.3**), where *d* is the interplanar spacing between planes (Å), θ is the X-ray diffraction angle (°), *n* is an integer number and *λ* is the wavelength of the X-rays (Å). Additionally, the crystallite size was calculated by the Scherrer equation (Jenkins and De Vries, 1970) (**Equation 2.4**), where *D* is the mean size of the ordered domains (Å), *K* is the Scherrer constant or shape factor, *λ* is the wavelength of the X-rays (Å), β is the peak width at half maximum intensity of the diffraction peak of the sample (rad) and θ is the X-ray diffraction angle (°).

$$2 \cdot d \cdot \sin\theta = n \cdot \lambda \qquad \textbf{Eq. 2.3}$$

$$D = \frac{K \cdot \lambda}{\beta \cdot \cos\theta} \qquad \textbf{Eq. 2.4}$$

2.4.2. Optical microscopy

Optical microscopy (OM) is a traditional tool that allows the observation of a sample by magnifying the image by means of a lens and visible light. OM was used in order to determine the average size of the cells constituting the structure of the foams, using a Nikon optical microscope Eclipse E600, measuring on the surface perpendicular to foam growth the average cell diameter of at least 50 cells for each sample. The average strut width of the foams was measured following the same procedure.

2.4.3. Scanning electron microscopy

The scanning electron microscope (SEM) is a type of microscope that produces magnified images of the surface of a sample by scanning it with a beam of focused electrons. The electron beam interacts with the atoms of the surface producing signals that provide information about the topography of the surface and also about its composition when coupled with energy dispersive X-ray spectroscopy (SEM-EDX).

In this work, the surface morphology of clays, lignin particles and the structure of flexible polyurethane foams were characterized by SEM images, which were obtained with a JEOL JSM-7000F microscope operating at 10 kV and a surrounding beam current of 10 pA. Secondary electron images were taken. Samples, stored in a desiccator, were placed over a double sided carbon based conductive tape and were then coated with a 10 nm chromium layer.

2.4.4. Transmission electron microscopy

Transmission electron microscopy (TEM) is based on the same principles than OM, with the advantage of a higher image resolution provided by using a beam of accelerated electrons instead of visible light. This electron beam is irradiated over a thin sample and transmitted through it, obtaining an image of the sample according to the transmitted and dispersed electrons.

The dispersion of the clays through the flexible polyurethane foam nanocomposite matrix was analyzed by TEM. The images were obtained on a TECNAI G2 20 TWIN transmission electron microscope operating at an accelerating voltage of 200 keV in a bright field image mode. The foam samples were filled and embedded in epoxy resin and were allowed to cure at room temperature for 48 h. Thin sections of samples (100 nm) were cut using a Diatome diamond knife at -90 °C on a Leica EMUC6 ultramicrotome equipped with a FC6 cryochamber and then were placed in 300 mesh copper grids.

2.4.5. Open cell content

The open cell content of the foams was measured by using a porosity tester (MicroFlo, IES). The test was carried out at 20 °C measuring the air passing through the cellular structure of the foam, parallel to grow direction. Four specimens were tested for each sample, and the average open cell content was reported.

2.5. Mechanical characterization

2.5.1. Resilience

Resilience (R) measures the capacity of foam to absorb elastic energy and to recover its original shape after being deformed. Therefore, this parameter gives an insight into the support of the foams which unique structure, made of flexible struts, membranes and voids, allow them to support large deformations and recover their original shape once the stress has been removed with different recovery rates depending on the characteristics of the material.

The resilience of the prepared foams was calculated following the ASTM D 3574 (2011) test H standard, using a Qualitest Ball Rebound Tester in the operating mode 3. The average value of 9 measurements was reported for each sample in the foam rise direction.

2.5.2. Compression

The specific elastic modulus, compressive stress at 10% of deformation and the energy storage of the foams were determined from the stress-strain curves using a MTS equipment with a 10 kN load cell and equipped with compression plates. Four specimens of each foam sample with 50 × 50 × 25 mm^3 dimensions were tested at a crosshead rate of 5 mm min^{-1} until a deformation of 70%. The elastic modulus was calculated as the slope of the initial linear behavior and the energy storage as the area below the stress-strain curves until 50% of strain.

2.5.3. Compression force deflection

The compression force deflection (CFD) value of the foams gives a measure of their firmness and support, being one of the most important parameters of flexible foams. CFD was measured in the foam rise direction according to the ASTM D 3574 (2011) test C standard, using a MTS equipment with a load cell of 10 kN equipped with compression plates. At least four specimens per sample with dimensions of 50 × 50 × 25 mm^3 were tested, covering the entire sample surface area with the compression plates. Two fast pre-compressions were previously performed until a deformation of 75% at a crosshead rate of 250 mm min^{-1}. After 5 min of resting without contact with the upper compression plate, the measurement of CFD was conducted at 50 mm min^{-1} until 50% of deformation, recording the stress value after 60 s of compression.

2.5.4. Compression set

Compression set test was carried out according to the ASTM D 3574 (2011) Test D standard. The specimens (with dimensions of 50 x 50 x 25 mm^3) were compressed to a constant deflection of 50% for 22 h at 70 °C. After this process, the samples were left recovering for 30 min at 25 °C and then the final thickness was measured. Three specimens per sample were tested. The compression set value as a percentage of the original thickness, C_t was given according to the **Equation 2.5**, where t_0 is the original thickness of the specimen and t_f is the thickness of the specimen after recovery.

$$C_t = \frac{t_o - t_f}{t_o} \cdot 100 \qquad \textbf{Eq. 2.5}$$

2.6. Thermal characterization

2.6.1. Differential scanning calorimetry

Differential scanning calorimetry (DSC) is a technique that allows the study of thermal transitions of materials by measuring the heat required to maintain both sample and reference at the same temperature. These transitions can be solid-solid

(such as glass transition temperature, T_g), solid-liquid (melting temperature, T_m and melting enthalpy, ΔH_m) and other different phase transitions as well as polymerization reactions and degradations.

The glass transition temperature of raw lignin (k-lignin) and isocyanate modified lignin (k-IPDI) was determined using a Mettler Toledo DSC 822e equipment. Around 5 mg of previously dried lignin (24 h at 50 °C) were weighed and a scan from −60 to 200 °C was performed at a heating rate of 10 °C min^{-1}, with a nitrogen flow of 10 mL min^{-1}. In case of polyurethane foams, the DSC analyses were conducted in a Mettler Toledo DSC3+ equipment, from −120 to 200 °C at a heating rate of 30 °C min^{-1} under a nitrogen flow of 10 mL min^{-1}. Two scans were performed in samples of approximately 5 mg in order to remove the thermal history of the samples.

2.6.2. Dynamic mechanical analysis

Dynamic mechanical analysis (DMA) studies the rheological behavior of solid materials under sinusoidal stress or deformation. In this way, the viscoelastic behavior of polymers can be studied as a function of temperature measuring the delay (phase difference) between the applied stress or strain and the response of the material. The storage modulus (E') and the loss modulus (E'') can be measured as well as the loss factor (the tangent of phase angle). The maximum of the loss factor as a function of temperature was associated to the T_g of the material (Saba et al., 2016).

Dynamic thermomechanical behavior of flexible polyurethane foams was studied by this technique using an Eplexor 100 N equipment from Gabo. The assays were carried out under compression with a static strain of 0.03% and operating frequency of 1 Hz, between −100 and 200 °C and a heating rate of 2 °C min^{-1}.

2.6.3. Thermogravimetric analysis

The thermal degradation of LDH, lignin and flexible polyurethane foams was studied by thermogravimetric analysis (TGA) in a Mettler Toledo equipment

(TGA/SDTA 851) performing the test under nitrogen atmosphere with a flowing rate of 10 mL min^{-1}, from 25 to 700 °C at a heating rate of 10 °C min^{-1}. Samples with weight ranging between 8 and 10 mg were tested.

In case of the flexible polyurethane foams prepared in **Chapter 6**, the thermal degradation was studied using a TGA Q500 (TA Instruments) in a temperature range from 25 to 800 °C at a heating rate of 10 °C min^{-1} under nitrogen atmosphere (30 mL min^{-1}). The sample weight was also around 10 mg.

2.6.4. Pyrolysis combustion flow calorimetry

Pyrolysis combustion flow calorimetry (PCFC) measures the heat of combustion of pyrolysis products of a sample, by subjecting it to a controlled pyrolysis under nitrogen stream and oxidizing at high temperature the volatiles produced in the pyrolysis. These volatiles are mixed with excess oxygen and oxidized at high temperature measuring the heat of combustion by oxygen consumption calorimetry. The advantage of PCFC over other techniques that measure fire-related properties is its ability to operate with milligram scale samples. Nevertheless, this tool does not recreate the conditions of real fire scenarios, so its use is limited to be a preliminary assess.

The heat release rate of the samples at microscale was studied by this technique using a Fire Testing Technology FAA Microcalorimeter, from a load temperature of 100 °C to a maximum temperature of 750 °C, at a heating rate of 1 °C s^{-1}, a combustor temperature of 900 °C and a nitrogen/oxygen ratio of 80/20. Three measurements per sample were carried out. After sample testing, micrographs of the remaining residue of some samples were taken using a Leitz Aristomet optical microscope (Leica Microsystems) with 200x magnification.

2.6.5. Limiting oxygen index

As described in **Section 1.5.2.**, the limiting oxygen index (LOI) allows comparing the ignitability and the burning behavior of materials. LOI measurements were performed using a FTA Flammability Unit (Stanton Redcroft), according to ISO 4589-2 (2006) standard. The specimen size was 150 x 10 x 10 mm^3 and they were previously conditioned in a climatic chamber for at least 48 h at 23 °C and a relative humidity of 50%.

2.6.6. UL 94 horizontal burning test

UL 94 horizontal burning test (UL 94-HB) was carried out in order to determine the propagation rate of the flame in the foam samples according to ISO 9772 (2012) standard. Briefly, prior to testing the samples were conditioned in a climatic chamber at 23 °C and 50% relative humidity during 48 h. Ten specimens per sample were prepared with 150 x 50 x 13 mm^3 size, they were marked along their length at 25, 60 and 125 mm and placed horizontally on a metallic grid. The samples were burnt during 60 s with a methane burner coupled to a winged top, whose methane flow and oxygen input were calibrated until obtaining a blue flame with a height of 38 mm. The burner was placed 13 mm below the corner of the sample closest to the 25 mm mark. A cotton indicator (also conditioned) was placed 175 mm below the grid in order to determine the dripping behavior of the foams, and the flame spread rate was measured over a 100 mm span using a stopwatch.

2.6.7. Cone calorimetry

Cone calorimetry (CC) tests were carried out using a Fire Testing Technology cone calorimeter according to ISO 5660-1 (2015) standard. Two specimens were tested for each sample in horizontal and in vertical orientation, obtaining results reproducible to within 5 and 10%, respectively. In case of vertical testing, the samples were hold in a wire cage and were ignited applying a pilot methane flame to the bottom corner closest to the cone. The specimens were cut with 100 x 100 x 50 mm^3 size and were

conditioned in a climatic chamber for 48 h at 23 °C and a relative humidity of 50%. During the test, the specimens were exposed to an external heat flux of 50 kW m^{-2} at a distance of 25 mm from the cone. 60 s of baseline was recorded prior to sample testing.

In order to determine the layer thickness and viscosity of the liquid pyrolysis products during burning, 100 x 100 x 50 mm^3 foam samples were ignited in horizontal position under the cone with a heat flux of 50 kW m^{-2}, and were quenched by using liquid nitrogen 20 s after ignition. Aiming to facilitate the flame extinction and liquid nitrogen handling, a distance of 60 mm was left between the cone and the sample.

The viscosity of the molten polymer in the surface of the quenched samples was determined with a Thermo Haake Viscotester iQ using a P35/Ti parallel plate geometry with shear rate values ranging from 10 to 100 s^{-1} at room temperature. The melt thickness of the molten polymer layer was determined by optical microscopy using a Nikon Eclipse E600 performing 20 measurements of the layer thickness and the average value was reported.

2.7. References

ASTM D 3574, 2011. Standard test methods for flexible cellular materials - Slab, bonded and molded urethane foams.

ASTM E1755-01, 2015. Standard test method for ash in biomass.

Bragg, W.L., 1929. The diffraction of short electromagnetic waves by a crystal. Scientia 23, 153–162.

Dence, C.W., 1992. The determination of lignin, in: Lin, S.Y., Dence, C.W. (Eds.), Methods in Lignin Chemistry. Springer-Verlag, Berlin, pp. 33–61.

Gordobil, O., Egüés, I., Llano-Ponte, R., Labidi, J., 2014. Physicochemical properties of PLA lignin blends. Polym. Degrad. Stab. 108, 330–338.

ISO 4589-2, 2006. Plastics - Determination of burning behaviour by oxygen index - Part

2: Ambient-temperature test.

ISO 5660-1, 2015. Reaction-to-fire tests - Heat release, smoke production and mass loss rate - Part 1: Heat release rate (cone calorimeter method) and smoke production rate (dynamic measurement).

ISO 9772, 2012. Cellular plastics - Determination of horizontal burning characteristics of small specimens subjected to a small flame.

Jenkins, R., De Vries, J.L., 1970. Line broadening, in: Worked Examples in X-Ray Analysis. Springer, New York, pp. 132–135.

Saba, N., Jawaid, M., Alothman, O.Y., Paridah, M.T., 2016. A review on dynamic mechanical properties of natural fibre reinforced polymer composites. Constr. Build. Mater. 106, 149–159.

Song, Q., Liu, W., Bohn, C.D., Harper, R.N., Scott, S.A., Dennis, J.S., 2013. A high performance oxygen storage material for chemical looping processes with CO_2 capture. Energy Environ. Sci. 6, 288–298.

“A minute of perfection was worth the effort. A moment was the most you could ever expect from perfection.”

C. Palahniuk. Fight Club. United States: W. W. Norton & Company, 1996.

Chapter 3

3

Flexible polyurethane foams with modified layered double hydroxides

3. Flexible polyurethane foams with modified layered double hydroxides

3.1. Introduction

The aim of this chapter is to functionalize a carbonate intercalated layered double hydroxide (synthetic hydrotalcite) with organic and inorganic phosphorus containing compounds for introducing them in the formulation of flexible polyurethane foams. Thus, the effect of the different intercalating compounds on the dispersion degree through the matrix and their impact on the properties of flexible polyurethane foams is studied.

A commercial carbonate intercalated Mg/Al LDH with a 3R (3 layer polytype with rhombohedral symmetry) stacking, is calcined for subsequent rehydration and reconstruction of the LDH structure with inorganic and organic phosphorus containing anions (hydrogen phosphate, HPO_4^{-2} and bis(2-ethylhexyl) phosphate, $DEHP^-$) in order to determine their effect when incorporated into flexible polyurethane foams. The dispersion of different amount of unmodified and modified LDHs (1, 3 and 5 parts per hundred of polyol, pphp) is carried out into a castor oil based polyether polyol (LB50), prior to the preparation of different flexible polyurethane foam nanocomposite systems.

The effect of the addition of LDH on the properties of the FPUF matrix is analyzed by Fourier transform infrared spectroscopy, X-ray diffraction, density and average cell size measurements, compression and ball rebound tests and scanning and transmission electron microscopy. The impact on thermal behavior is also studied by means of thermogravimetric analysis and pyrolysis flow combustion calorimetry. The characterization is carried out following the protocols described in **Chapter 2**.

3.2. Experimental procedure

3.2.1. Materials

The modification of synthetic hydrotalcite (LDH-CO_3) was carried out with phosphorus containing inorganic and organic reagents (KH_2PO_4 and HDEHP, respectively). The flexible polyurethane foam samples with different unmodified and

modified LDH content were synthesized using the materials described also in **Chapter 2** (**Section 2.2**), using as A-side formulation toluene diisocyanate, TDI (Desmodur T 80, Covestro). The B-side formulation was constituted by LB50 and the foaming additives detailed in **Chapter 2** (**Section 2.2**) such as deionized water, Tegoamin® B 75, Kosmos® 29 and Tegostab® B 4900.

3.2.2. Intercalation of LDH

The modification of LDH-CO_3 was accomplished following the rehydration process (Miyata, 1980), in basic medium for both organic and inorganic phosphate based intercalation agents. The procedure was performed as follows: firstly, the LDH-CO_3 was calcined in a muffle furnace at 500 °C for 5 h in order to remove the water, hydroxyl groups and carbonate anions accommodated between the hydrotalcite layers. In this calcination process, the layered structure is destroyed achieving a mixture of aluminium and magnesium oxides (cLDH-CO_3) which in contact with water restores the original brucite-like layer arrangement due to its structural memory effect (He et al., 2006). The rehydration media were prepared dissolving the intercalation agents (KH_2PO_4 and HDEHP) in deionized water to obtain a 250 mL solution for each one, considering their purity and adding an excess of 50% for the ionic reconstruction regarding the synthetic hydrotalcite formula, ensuring in this way the presence of a divalent anion for two aluminium atoms when using HPO_4^{-2}, and an intercalated monovalent anion for each aluminium atom when $DEHP^-$ was used. The pH of the corresponding solutions was adjusted to 9 with ammonia in case of KH_2PO_4 in order to enhance the dissociation of phosphorus as a divalent anion, HPO_4^{-2} (O'Neil, 2001) and to 10 in case of HDEHP with NaOH, forming a sodium salt in presence of the $DEHP^-$ monovalent anion (Wang et al., 2009). These solutions were decarbonated with nitrogen during 20 min for minimizing the contamination with atmospheric CO_2 before adding the calcined LDH. The time for the regeneration process was selected depending on the size of the intercalating anion, obtaining after the rehydration process LDH-HPO_4 and LDH-DEHP.

LDH-HPO_4 was obtained refluxing cLDH-CO_3 for 24 h at 80 °C under nitrogen with vigorous stirring (600 rpm). In case of LDH-DEHP, cLDH-CO_3 was refluxed in the same conditions but for 48 h, allowing the bigger organic molecules more time to accommodate between the interlayer galleries. **Figure 3.1** shows a brief scheme of the regeneration procedure.

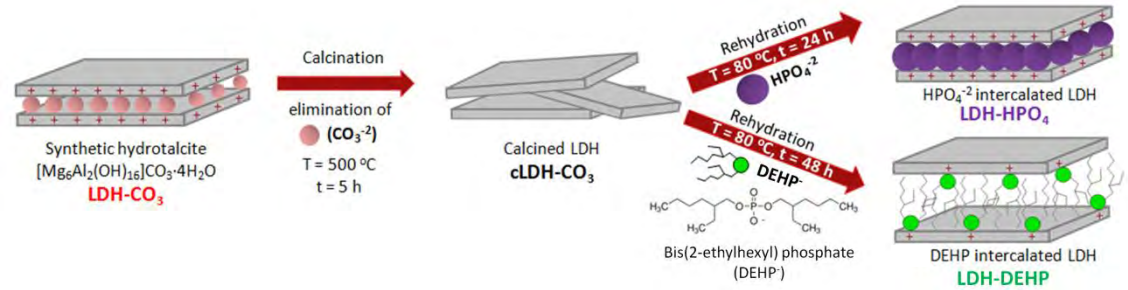

Figure 3.1. Schematic representation of calcination-rehydration process intercalating different anions such as hydrogen phosphate HPO_4^{-2} and bis(2-ethylhexyl) phosphate ($DEHP^-$).

In both cases, the slurry was then centrifuged at 4500 rpm for 5 min and washed with deionized water. This procedure was repeated four times to remove the excess of intercalation agent. Finally, the filtrate was dried under vacuum at 60 °C during 48 h and the resulting powder was ground in a mortar, sieved with a 0.5 mm mesh and stored in a desiccator into polyethylene containers.

3.2.3. Preparation of flexible polyurethane foam nanocomposites

The preparation of polyurethane foam nanocomposites was carried out by *in situ* polymerization process, drying firstly pristine and modified layered double hydroxides in an oven at 110 °C overnight for moisture removal and dispersing them afterwards into the polyol. Different quantities of LDH (1, 3 and 5 pphp) were incorporated into LB50 and were mixed at 12000 rpm in a rotor-stator mixer (Polytron® PT 2500 E from Kinematika) during 2 min. Thereafter the mixture was sonicated with a Bioblock Scientific ultrasonic probe (VibraCell® 75043) in pulses of 4 s during 15 min at 20 kHz and amplitude of 20%. The polyurethane foam nanocomposites were synthesized following the formulation specified in **Table 3.1** and the procedure depicted in **Figure 3.2** with an isocyanate index of 120. Briefly, the

water, the amine and the surfactant were incorporated to the LDH-polyol mixture after the dispersion was achieved and mixed at 2000 rpm during 60 s and then the organometallic catalyst was added and homogenized for 30 s.

Table 3.1. Flexible polyurethane foam formulation.

Component	LB50	Deionized water	Tegoamin® B 75	Kosmos® 29	Tegostab® 4900	TDI (I.I.)
wt (pphp)	100	0.5	0.3	0.4	1.1	120

Subsequently the A-side, *i.e.* the isocyanate, was added to the mixture and after stirring during few seconds the mixture was poured into a 150 × 135 × 90 mm^3 open mold and polymerized under free rise conditions, allowing them to cure at room temperature for 48 h. Reference sample was also synthesized and denoted as PUF-REF and nanocomposite foams were named PUF-$LCO_3$1, PUF-$LCO_3$3 and PUF-$LCO_3$5 (with 1, 3 and 5 pphp of LDH-CO_3); PUF-$LHPO_4$1, PUF-$LHPO_4$3 and PUF-$LHPO_4$5 (with 1, 3 and 5 pphp of LDH-HPO_4) and finally PUF-LDEHP1, PUF-LDEHP3 and PUF-LDEHP5 (with 1, 3 and 5 pphp of LDH-DEHP). Foams with 5 pphp of LDH presented lower growth than reference and foam nanocomposites filled with 1 and 3 pphp. This effect was attributed to the higher LDH content, which led to a higher viscosity of the reactive mixture and larger number of nucleation sites, thus giving place to foams with higher density.

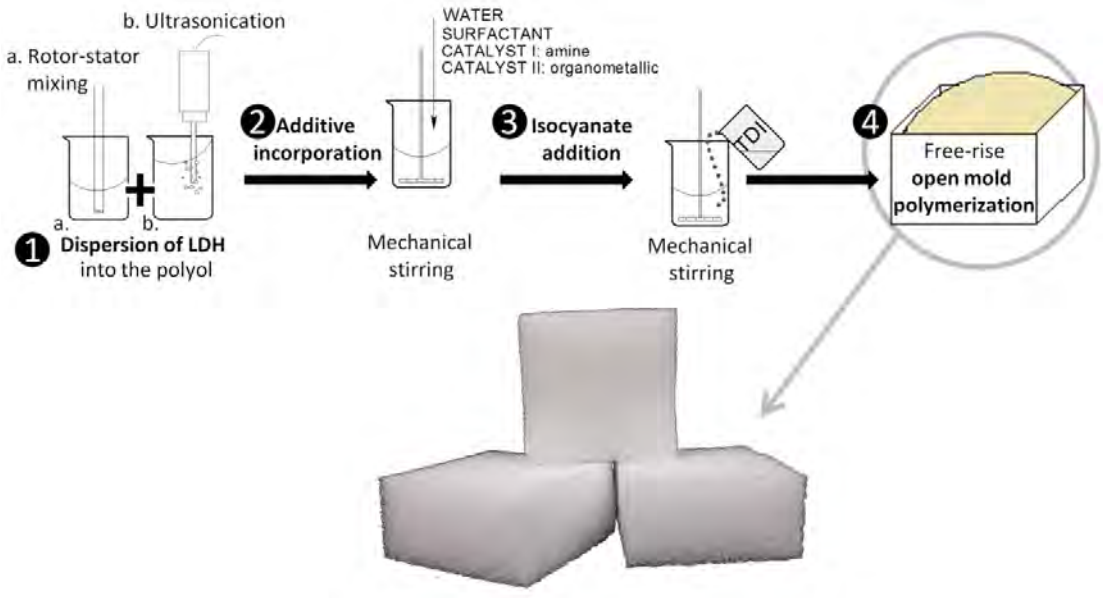

Figure 3.2. Followed procedure for flexible polyurethane foam preparation.

3.3. Results and discussion

3.3.1. Characterization of LDH

3.3.1.a. Fourier transform infrared spectroscopy

Modified and unmodified LDH samples were characterized by FTIR for determining the presence of the intercalating anions. **Figure 3.3** shows the spectra of LDH-CO_3, cLDH-CO_3, LDH-HPO_4 and LDH-DEHP. Peaks at 1371, 874 and 672 cm^{-1}, characteristic of carbonate intercalated layered double hydroxides, were attributed to the asymmetric stretching (v_3 mode), non-planar bending (v_2 mode) and angular bending (v_4 mode) vibrations of carbonate anions, respectively (Hernandez-Moreno et al., 1985; Cavani et al., 1991). These peaks appeared with lower intensity in all the modified LDH samples and its presence was attributed to the contamination with atmospheric CO_2 during rehydration, filtration or drying process of the anionic clays. Nevertheless, the intensity of all three modes of vibration of CO_3^{-2} anion in cLDH-CO_3, especially the intensity of the peak centered at 1371 cm^{-1}, decreased drastically after calcination confirming thus the withdrawal of a great part of carbonate anions.

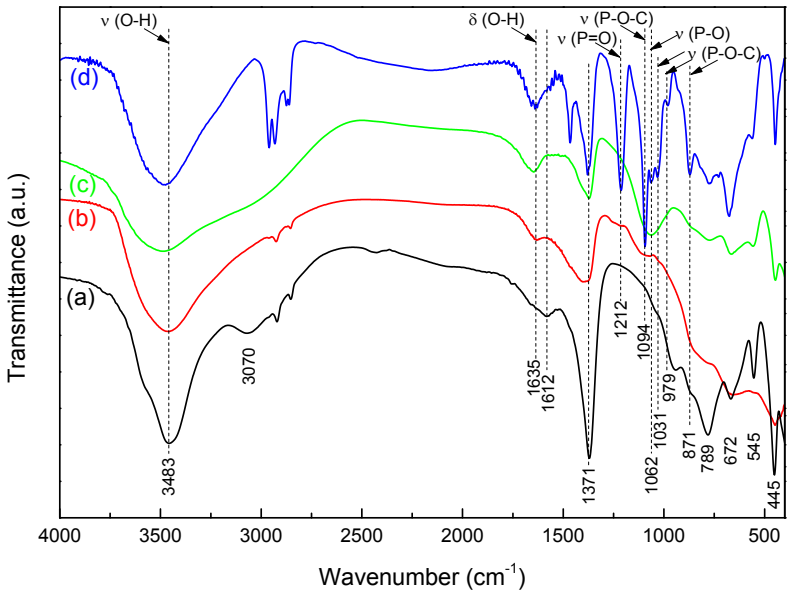

Figure 3.3. FTIR spectra of (a) LDH-CO_3, (b) cLDH-CO_3, (c) LDH-HPO_4 and (d) LDH-DEHP.

The broad peak around 3500 cm^{-1} corresponded to the –OH stretching vibration of both metal hydroxide sheets and interlayer water, which also presented a peak at 1612 cm^{-1} associated to H_2O bending vibration. In case of both modified LDH, the peak

corresponding to –OH bending of water was shifted to 1635 cm^{-1} since this vibration was affected by the interlayer water surrounding anions (Kloprogge and Frost, 2001). The shoulder appearing at 3070 cm^{-1} in the spectrum of LDH-CO_3 was attributable to the formation of hydrogen bonds between water and carbonate anions inside the layers (Cavani et al., 1991). Peaks appearing below 800 cm^{-1} (at 789, 545 and 445 cm^{-1}) corresponded to metal hydroxide sheet (M–OH) lattice vibrations, which disappeared in cLDH-CO_3 verifying the reconstruction of the brucite-like layered structure after the rehydration process. The characteristic peak of P–O stretching was shown in LDH-HPO_4 spectrum at 1062 cm^{-1}, which confirmed the presence of HPO_4^{-2}.

The LDH modified with organic phosphorus showed narrow peaks below 3000 cm^{-1} corresponding to CH_3– and –CH_2– symmetric and asymmetric stretching vibrations, evidencing the presence of a hydrocarbonaceous compound. The absence of a shoulder between 3000 and 3100 cm^{-1} denoted the lack of interaction between water and CO_3^{-2} suggesting that the hydrocarbon tail had filled the interlayer space (Costa et al., 2008). The presence of phosphorus was confirmed in LDH-DEHP by strong peaks at 1212 cm^{-1} (P=O stretching) and between 1094 and 979 cm^{-1} (P–O–C asymmetric stretching) and less intense peak at 871 cm^{-1} (P–O–C symmetric stretching).

3.3.1.b. X-ray diffraction

One of the most substantial approaches for characterizing the hydrotalcite-like compounds is the X-ray diffraction technique, which allows determining if a given anion has been successfully intercalated or whether they are just adsorbed on the surface of the clay. These compounds are characterized for having several orders of diffraction in the XRD patterns which intensity is related to the crystallinity of the sample and where the most intense reflection, *i.e.* the (003) reflection, is taken as reference since it corresponds to the basal space between adjacent layers (Evans and Slade, 2006).

Figure 3.4 shows the diffraction patterns of the pristine and modified LDH, as well as that of the calcined LDH. The *d*-values of (003) and (110) reflections are provided in **Table 3.2**, which allowed to calculate *c* and *a* cell lattice parameters,

respectively assuming a hexagonal unit cell structure (Millange et al., 2000). The former is defined as $c = 3 \cdot d_{003}$ and its value corresponds to three times the distance from the centre of one layer to the adjacent one, being highly dependent of the nature of the metal cations and also of the interlayer anions. The latter corresponds to the distance between two adjacent metal ions by means of the calculation of the *a* cell lattice parameter, defined as $a = 2 \cdot d_{110}$.

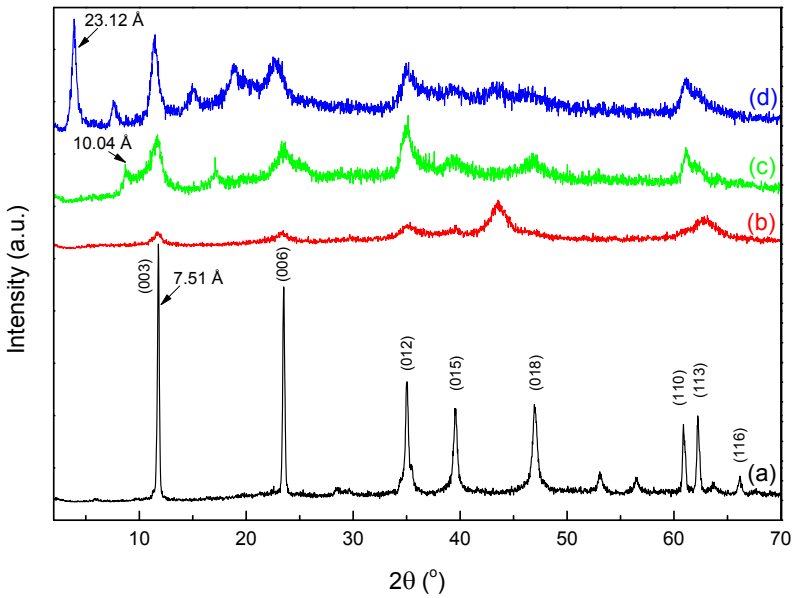

Figure 3.4. XRD patterns of (a) LDH-CO_3, (b) cLDH-CO_3, (c) LDH-HPO_4, and (d) LDH-DEHP.

The pristine LDH showed a pattern with narrow and intense reflections evidencing its crystallinity, which decreased in the calcined and the two modified LDH. The XRD pattern of cLDH-CO_3 confirmed the FTIR results, suggesting that not all the LDH-CO_3 structure was destroyed during calcination, thus still remained some crystalline LDH structure with CO_3^{-2} intercalated within the layers. The two modified LDH showed a decrease in crystallinity evidenced by the intensity diminution and broadening of the reflections, which might be influenced by the regeneration process in basic pH that induced the formation of more amorphous LDH (He et al., 2006).

Additionally, LDH-HPO4 and LDH-DEHP exhibited a shift of (003) reflections to lower 2ϑ angles (from 11.77 to 8.80 and 3.82° respectively), attributed to an increase in the basal space between the layers (10.04 Å for LDH-HPO4 and 23.12 Å for LDH-DEHP with respect to 7.51 Å of LDH-CO3), hence confirming the intercalation of the

phosphate containing anions in accordance to the values obtained elsewhere (Wang et al., 2009).

Table 3.2. *2θ* values of (003) and (110) reflections and their corresponding basal spacing (d_{003}) and adjacent cation distance (d_{110}) as well as *a* and *c* lattice cell parameters for neat and modified LDH.

Sample	$2\theta_{003}$ (°)	$2\theta_{110}$ (°)	d_{003}[a] (Å)	d_{110}[a] (Å)	a[b] (Å)	c[b] (Å)	Crystallite size[c] (nm)
LDH-CO_3	11.77	60.89	7.51	1.52	3.04	22.54	~80
LDH-HPO_4	8.80	61.03	10.04	1.52	3.04	30.13	~5
LDH-DEHP	3.82	61.10	23.12	1.52	3.03	69.37	~10

[a]Basal spacing calculated with Bragg's law.

[b]Cell lattice parameters calculated by $a = 2 \cdot d(110)$ and $c = 3 \cdot d(003)$.

[c]Crystallite size in c direction, calculated from the (003) reflection using the Debye-Scherrer equation.

Nevertheless, still prevailed in the same *2θ* values, those (003) reflections corresponding to the original LDH at 11.77°, denoting thereby the coexistence between carbonate-intercalated LDH and phosphate containing anions. The distance between adjacent cations, *a*, remained constant in all samples (around 3 Å) being consistent with those values found by Cavani et al. (1991) and Zhao et al. (2002) and which are characteristic from Mg-based LDH. The crystallite size in the stacking direction (*c* direction) was estimated by the Debye-Scherrer equation measuring the full width at half-maximum of the (003) reflection, showing that modified LDH by calcination rehydration process presented a smaller average crystallite size than the original LDH, corresponding to their loss of crystallinity. Therefore, LDH-CO_3 resulted to be the most crystalline sample, while the less crystalline structure corresponded to LDH-HPO_4.

3.3.1.c. Chemical composition

Table 3.3 shows the chemical composition of LDH. The Mg/Al molar ratio of the pristine LDH is 2.16. The molecular formula given by Sigma-Aldrich is that of the natural hydrotalcite $Mg_6Al_2(OH)_{16}(CO_3)\cdot 4H_2O$. Theoretically the molecular formula of hydrotalcite is given as $Mg_{(1-x)}Al_x(OH)_2(CO_3)_{x/2}\cdot mH_2O$ where *x* is comprised between 0.20 and 0.33 (Li and Duan, 2006), which are the limiting values for avoiding the formation of single hydroxides and therefore for ensuring the brucite-like structure. Regarding the results obtained by elemental analysis (**Table 3.3**), the approximate formula for the unmodified LDH would be **(1)**.

$Mg_{0.68}Al_{0.32}(OH)_2(CO_3)_{0.16}\cdot 0.37H_2O$ **(1)**

The Mg/Al molar ratio increased from nearly 2.16 in case of pristine LDH to nearly 2.39 and 2.57 for LDH-HPO_4 and LDH-DEHP respectively, due to the strong dependence on pH of the reconstruction process (Xu and Lu, 2005). The more atoms of aluminium are available for each magnesium atom, the higher charge density is going to be available in the hydroxide layer and thus, more anions will be needed to be intercalated to keep the electroneutrality. The presence of a monovalent anion for each aluminium atom or a divalent anion for every two aluminium atoms preserves the charge equilibrium in the clay, balancing the positive charges of the metal hydroxide layers with the intercalating anions. The P/Al molar ratio was lower than 0.5 in LDH-HPO_4 and much lower than 1 in LDH-DEHP implying, as confirmed by FTIR and XRD, the coexistence of phosphate-containing molecules with other anions, such as CO_3^{-2}.

Table 3.3. Chemical compositions[a] of pristine and modified LDH.

Composition (wt. %)	Sample		
	LDH-CO_3	LDH-HPO_4	LDH-DEHP
Mg	20.78	20.05	14.75
Al	10.69	9.33	6.37
P	-	3.30	1.08
C	5.33	1.15	25.26
H	3.90	3.76	3.62
N	0.07	0.08	0.07
Mg/Al (molar ratio)	2.16	2.39	2.57
P/Al (molar ratio)	-	0.31	0.15

[a]Al, Mg and P content determined by ICP-OES, C, H and N by elemental analysis.

The low ratio in LDH-DEHP denoted that low quantities of the organophosphorus compound were intercalated probably due to its higher size. Also, a smaller Mg/Al ratio could accelerate the rate of stacking of layers (Zhao et al., 2002) in accordance to the average crystallite size obtained by XRD, which happened to be higher as Mg/Al ratio decreased. In case of modified LDH, the approximate chemical formula would be, for LDH-HPO_4 **(2)** and LDH-DEHP **(3)** respectively:

$Mg_{0.70}Al_{0.30}(OH)_2(HPO_4)_{0.09}(CO_3)_{0.06}\cdot 0.55H_2O$ **(2)**

$Mg_{0.72}Al_{0.28}(OH)_2(DEHP)_{0.02}(CO_3)_{0.13}\cdot 0.39H_2O$ **(3)**

3.3.1.d. Morphology

The hydrotalcite-like compounds are characterized by being constituted by hexagonal-shaped particles with dimensions within 100 nm and few microns (Xu and Lu, 2005) that form aggregates with dimensions ranging from 2 to 20 µm (Wypych and Satyanarayana, 2004) due to their strong electrostatic attraction between layers. **Figure 3.5** shows that the hexagonal shape was not lost in modified LDH, but the surface appeared to be more irregular, especially in the case of LDH-HPO_4, which also featured particle aggregation. This stacking was a consequence of the high surface energy of the modified clay (Jiang, 2010). Additionally, Zhou et al. (2012) found that when the LDH layers had low crystallinity, the interlayer anions were accumulated in the borders of the crystal domains causing high charge density and thus, higher particle agglomeration.

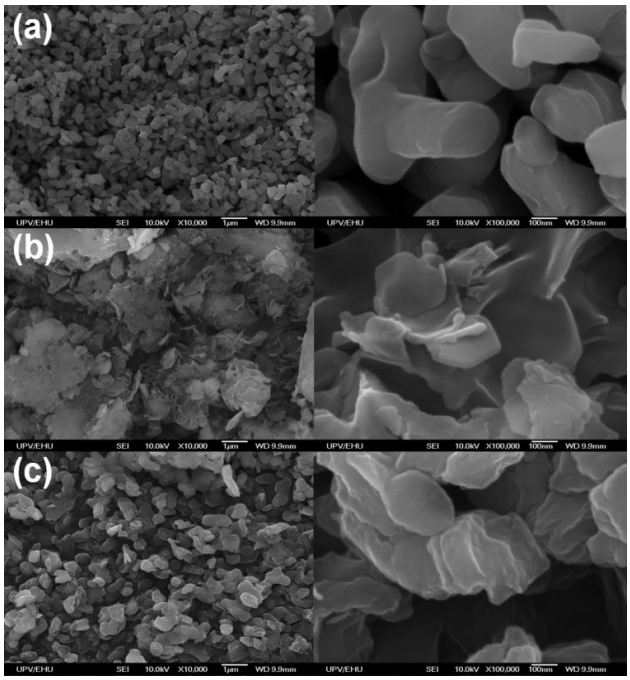

Figure 3.5. SEM images of (a) LDH-CO_3, (b) LDH-HPO_4 and (c) LDH-DEHP. Magnification ×10000 (left) and ×100000 (right).

The superficial irregularities also corresponded to the loss of crystallinity associated with the decrease in the intensity of XRD reflections. Their lateral dimensions between 200 and 300 nm resulted to be smaller, thus having a higher aspect ratio than those found in the literature with $DEHP^-$ as intercalating anion (Costa

et al., 2008), but the three LDH samples showed quite similar aggregate morphology and size than those found in different works obtained by other procedures such as hydrothermal precipitation (Chubar et al., 2013). SEM micrograph of LDH-DEHP showed particles with softer edges than LDH-HPO_4, which presented flake-like morphology probably due to the higher size of the organic anion.

3.3.1.e. Thermogravimetric analysis

The degradation of LDH took place in several stages, as it can be seen in the thermograms displayed in **Figure 3.6**. LDH-HPO_4 and LDH-DEHP registered a gradual mass loss around 100 and 200 °C, corresponding to surface and interlayer water respectively, while LDH-CO_3 did not lose significant mass until 200 °C, suggesting that most of its water content was located in the interlayer space.

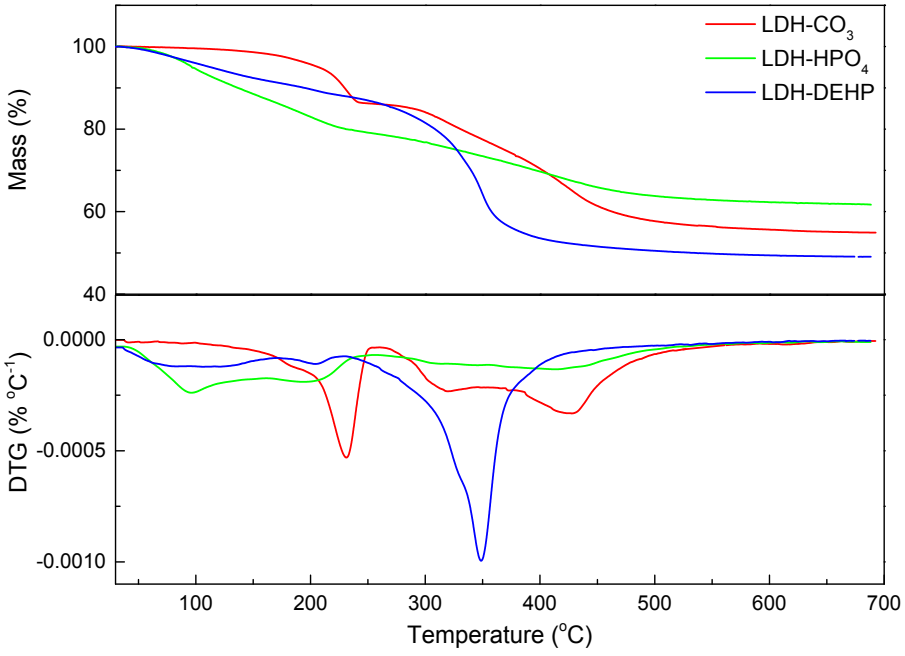

Figure 3.6. Mass loss and first derivative (DTG) curves of pristine and modified LDHs.

The mass loss from 250 to 500 °C corresponded to the release and/or the degradation of interlayer anions together with different steps of dehydroxylation of the metal hydroxide sheet layers, with the consequent brucite-like structure destruction and metal oxide formation (Taviot-Guého and Leroux, 2006).

The amount of residue collected at 700 °C was around 55, 62 and 49% of the initial mass of LDH-CO_3, LDH-HPO_4 and LDH-DEHP, respectively

3.3.2. Characterization of flexible polyurethane foam nanocomposites

3.3.2.a. Fourier transform infrared spectroscopy

Nanocomposite foams were characterized by FTIR in order to determine possible interactions between the fillers and the polyurethane matrix. **Figure 3.7** shows the spectra of the reference foam and those ones filled with 3 pphp of pristine and modified LDH. Urethane and urea characteristic bands appeared in the 3400-3200 cm^{-1} region, related to the N–H stretching vibration, and in the carbonyl (amide I) region, between 1750 and 1625 cm^{-1}. In the carbonyl region, besides the C=O stretching vibrations corresponding to the free urethane (1730 cm^{-1}) and urea (1715 cm^{-1}) and associated urea (1640 cm^{-1}), the characteristic C=O stretching vibration of the ester group from the polyol at 1742 cm^{-1} was also observed as a slight widening of the peak. The band appearing at 1532 cm^{-1} corresponded to the N–H bending and C–N stretching vibrations of the urethane and urea groups (amide II). The bands belonging to C–O–C asymmetric and symmetric stretching vibrations were observed at 1222 and 1090 cm^{-1}, respectively.

Besides the characteristic polyurethane absorption bands, it was observed in all foam samples the distinctive band of unreacted isocyanate groups at 2276 cm^{-1}, indicating that there still remained some isocyanate in the synthesized foams due to the used 20% excess for ensuring the reaction with the blowing agent. This remaining isocyanate is likely to react with ambient moisture and/or crosslink along the time (Lamba et al., 1997). Comparing the spectra of LDH containing foams with the spectrum of the reference foam, no relevant changes were observed suggesting no remarkable interactions between the filler and the polymeric matrix.

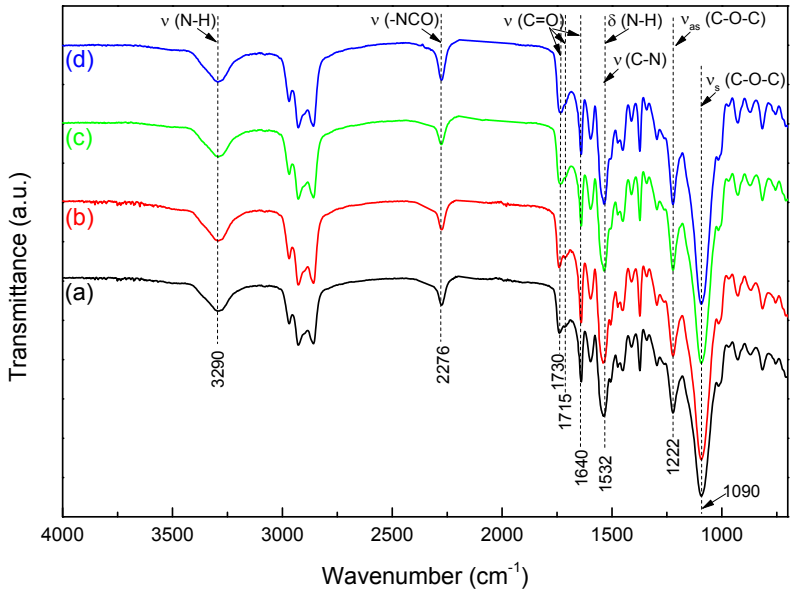

Figure 3.7. FTIR spectra of the reference foam, PUF-REF (a) and of those ones filled with 3 pphp of pristine and modified LDH, PUF-$LCO_3$3 (b), PUF-$LHPO_4$3 (c) and PUF-LDEHP3 (d).

3.3.2.b. Cell structure and morphology

The microstructure of the polyurethane foams was analyzed by X-ray diffraction to determine whether the layered double hydroxides were dispersed in the matrix unaltered as a microcomposite, or intercalated or exfoliated as a nanocomposite. **Figure 3.8** shows the diffraction patterns of the neat foam and nanocomposites filled with 1, 3 and 5 pphp of LDH-CO_3, LDH-HPO_4 and LDH-DEHP. The broad reflection around 20° corresponded to the crystalline fraction of the polyurethane. The presence of the (003) reflection in PUF-LCO_3 series at practically the same reflection angle of that observed in the LDH-CO_3 (11.77°) denoted that unmodified LDH was dispersed in the polymeric matrix maintaining its stacked structure practically unaltered, probably as a consequence of its high crystallinity. On the other hand, the increase in the basal distance from 23.12 in LDH-DEHP to 24.14 Å in PUF-LDEHP denoted that during polymerization the diffusion of polymeric chains among clay layers occurred, reaching an intercalated distribution of LDH-DEHP through the polyurethane matrix. Finally, the absence of the basal reflection in PUF-$LHPO_4$ foams suggested that polymer chains were introduced into the clay during the polymerization due to its low crystallinity as observed by XRD, moving away the layers of the LDH resulting in an exfoliated polymer

nanocomposite, therefore achieving a greater contact area between the clay layers and the polymeric matrix.

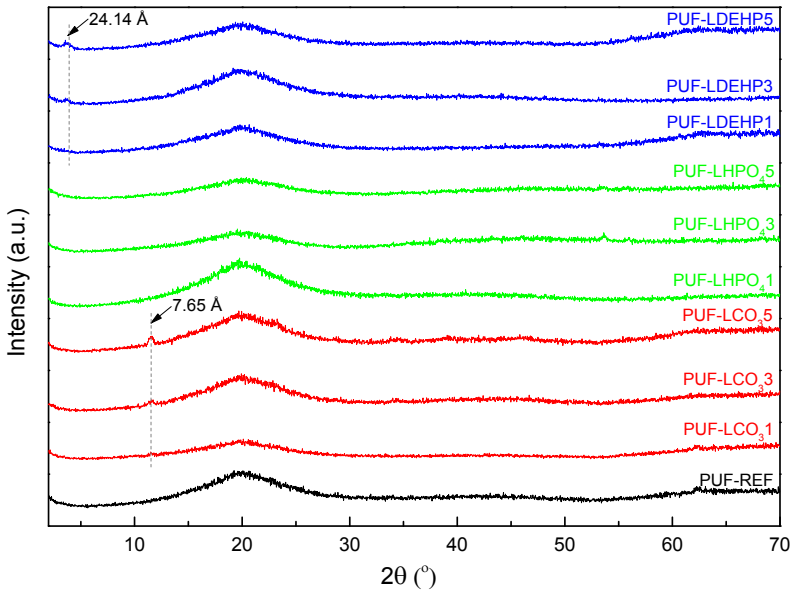

Figure 3.8. XRD patterns of the synthesized reference and nanocomposite foams filled with different amount of LDH-CO_3, LDH-HPO_4 and LDH-DEHP.

Thus, the modification of the pristine LDH enhanced the intercalation and exfoliation of the clay layers as a consequence of the loss of crystallinity during the rehydration process (He et al., 2006).

Figure 3.9 shows the SEM micrographs of the polyurethane nanocomposite foam surfaces, taken perpendicular to foam growth. Foam cells presented polyhedral shape consisting most of them in open cells. PUF-REF showed evidence of collapse of some cells that could be attributed to the low viscosity of the polyol. This resulted in a fast growing of the liquid mixture not crosslinked enough to avoid cell wall draining with the consequent bubble coalescence (Sharma et al., 2014). Nanocomposite foams showed an uneven cell size distribution, but cell structure did not appear collapsed or damaged probably due to an increase in the reactive mixture viscosity (avoiding in this way cell wall draining) along with the hindered bubble growth caused by the presence of LDH, thus favoring the formation of a heterogeneous structure (Javni et al., 2011).

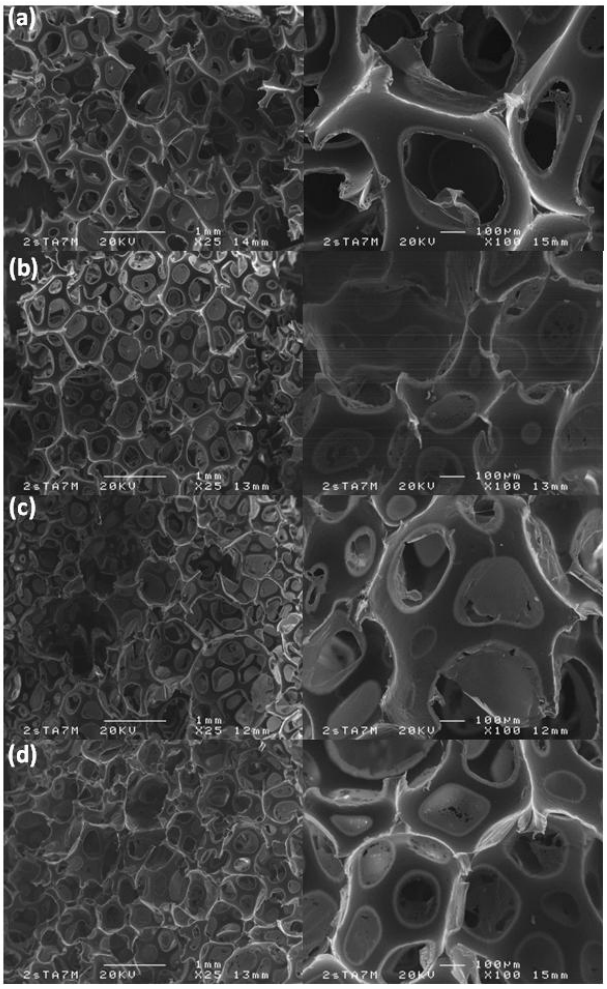

Figure 3.9. SEM micrographs with different magnifications (×25 on the left, ×100 on the right) of the polyurethane foam PUF-REF (a) and PUF nanocomposites PUF-$LCO_3$3 (b), PUF-$LHPO_4$3 (c) and PUF-LDEHP3 (d).

The microstructure and dispersion degree of the different LDH throughout the nanocomposite foam matrix was also analyzed by TEM in 3 pphp LDH containing samples. It was observed that the LDH were homogeneously dispersed within the polyurethane matrix (**Figure 3.10**), but clear differences were found in the morphology of the clays. Large stacks of clay were recognized in PUF-$LCO_3$3 (**Figure 3.10a**), whereas smaller and looser layer piles were observed in PUF-LDEHP3 (**Figure 3.10c**). Also, individual LDH layers distributed within PUF-$LHPO_4$3 (**Figure 3.10b**) were observed, confirming the exfoliated structure that was previously suggested by XRD.

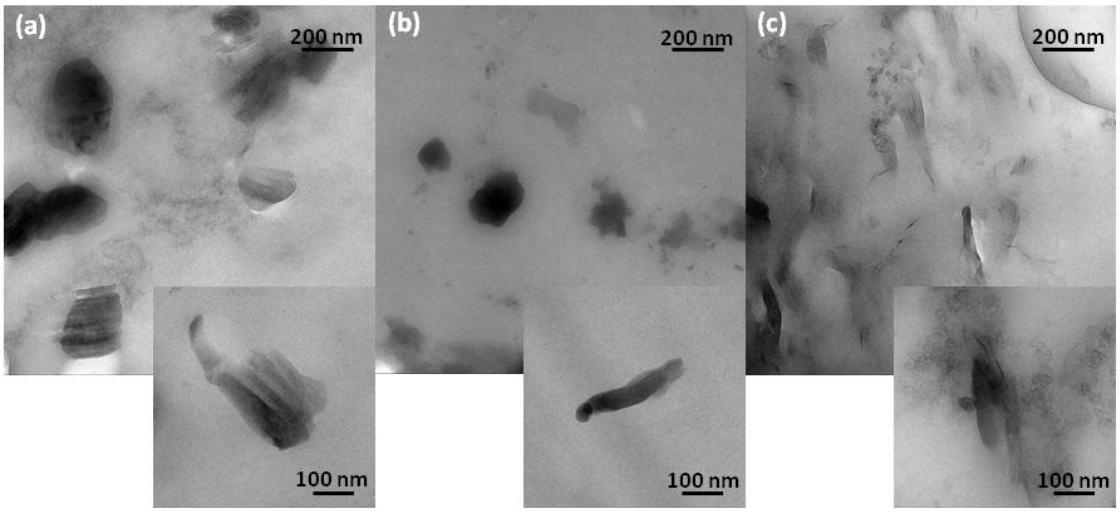

Figure 3.10. TEM micrographs of polyurethane foam nanocomposites, PUF-$LCO_3$3 (a), PUF-$LHPO_4$3 (b) and PUF-LDEHP3 (c).

Density is an important parameter of foam performance regarding comfort, support and durability of the flexible foams, consisting on the contribution of the weight and volume of the polymeric structure and also of the gases trapped in cells. The values of density and average cell size of the synthesized foams are listed in **Table 3.4**.

Table 3.4. Density and average cell diameter of the reference and LDH-containing polyurethane foams.

Sample	Density ($kg\ m^{-3}$)	Average cell diameter (μm)
PUF-REF	37.3 ± 0.8	362.3 ± 73.5
PUF-$LCO_3$1	43.5 ± 1.1	363.1 ± 94.3
PUF-$LCO_3$3	44.5 ± 0.5	319.3 ± 76.0
PUF-$LCO_3$5	46.5 ± 1.5	259.8 ± 70.7
PUF-$LHPO_4$1	51.9 ± 1.5	317.0 ± 90.9
PUF-$LHPO_4$3	44.1 ± 0.3	339.3 ± 96.7
PUF-$LHPO_4$5	52.8 ± 1.2	293.9 ± 92.3
PUF-LDEHP1	43.3 ± 0.4	286.1 ± 90.9
PUF-LDEHP3	44.3 ± 0.7	291.4 ± 92.0
PUF-LDEHP5	42.4 ± 1.5	306.9 ± 91.2

According to the literature, the presence of nanoparticles enhances the nucleation through an increase in the number of bubble sites thus achieving a reduced cell size (Javni et al., 2011; Madaleno et al., 2013). This was reflected in the increased density, and it was verified by the obtained cell size values, showing that when unmodified or modified LDH were incorporated into the polymeric matrix, lower

average cell diameter values were obtained. The nucleating effect of the clay depended on its dispersion degree and thus, on the number of dispersed nanoentities which acted as nucleating centers. The decrease of the cell diameter was also attributed to the hindered cell growth as a consequence of the increased viscosity of the reactive mixture caused by the addition of fillers. Therefore, denser foams were obtained with the addition of LDH.

Exfoliated samples, *i.e*. PUF-$LHPO_4$ foam series, presented the highest density reaching an increase of nearly 40% in case of PUF-$LHPO_4$1 with respect to reference foam. The presence of more individual clay layers promoted as mentioned before, the formation of more nucleation sites resulting in smaller cell diameter and higher density. PUF-LCO_3 and PUF-LDEHP foam series presented also an increase in density values but not as pronounced as PUF-$LHPO_4$ foams, reaching an increase of around 25% in both PUF-LCO_3 and PUF-LDEHP series.

The consideration of XRD results, which showed an exfoliated microstructure in the system with LDH-HPO_4, suggested that the smaller the filler size, the higher the density. The out of trend density value of the sample PUF-$LHPO_4$3 was attributed to the opposing effects of the nanoclay on nucleation and cell growth (Madaleno et al., 2013). At lower exfoliated clay content, more nucleation sites were formed due to the high amount of dispersed clay sheets until the percolation limit, where agglomerates could be formed reducing nucleation sites and viscosity, giving place to bigger cells as it was observed by SEM before.

3.3.2.c. Mechanical properties

Compression force deflection (CFD) values are given in **Figure 3.11** as a function of the filler content. In all cases, the firmness of the nanocomposite foams was higher than that of reference due to the reinforcing effect of the filler. The studied polymer nanocomposite series presented different behavior with increasing LDH content. In case of the PUF-LCO_3 system, the CFD value increased with filler content, being in concordance with the results obtained by Javni et al. (2011), reaching an increase of 43% in case of the sample containing 5 pphp of LDH-CO_3 comparing with the reference foam. The different behavior observed between the modified LDH could be related to

the size, crystallinity or degree of exfoliation/intercalation of the clay in the foam. The firmest foam of PUF-$LHPO_4$ series was the sample PUF-$LHPO_4$1, which showed an increase of 68% with respect to the unfilled foam. High reinforcement was achieved with low clay content as a consequence of the large contact area between the polymer and the exfoliated filler, with a decrease in the firmness at 3 pphp corresponding also to the observed out of trend density value of this sample. However, in case of LDH-DEHP containing samples, the higher CFD value was obtained at 3 pphp due to its intercalated structure, with an increase of nearly 100% with respect to the reference foam. These results suggested that the finer was dispersed the LDH in the matrix, the lower was the quantity required to act as reinforcement. Regarding the crystallite size between the incorporated structures, lower LDH content was required for the improvement of CFD as the crystallite size was reduced.

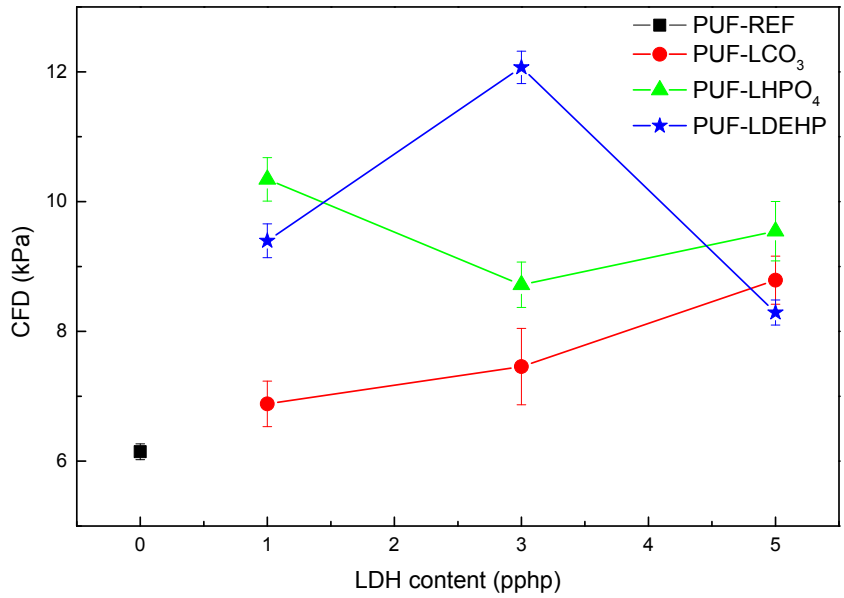

Figure 3.11. Compression force deflection values for polyurethane nanocomposite samples with different LDH content.

Elastic modulus and compressive stress at 10% of deformation were obtained from the stress-strain curves. These properties depend highly on density; hence in order to avoid the density effects, specific values are listed in **Table 3.5**. PUF-LCO_3 foam series showed an increase of specific compressive strength with increasing LDH-CO_3 content, following the same trend observed in CFD. In case of PUF-$LHPO_4$ and PUF-

LDEHP systems, the highest specific compressive strength values were obtained with 1 and 3 pphp of LDH, respectively, varying also as CFD did. In general, the compressive stress was higher for the LDH containing samples and was related to the reinforcing effect of the fillers. Regarding the specific elastic modulus, a slight decrease was observed with the LDH content in the PUF-LCO_3 series. The most pronounced decrease observed in PUF-$LHPO_4$ foams was attributed to the good dispersion of the clay throughout the polymeric matrix that might hinder the formation of hydrogen bonds between the urethane-urea hard domains of the polyurethane (Cao et al., 2005). However, the high specific elastic modulus observed in PUF-LDEHP series at 1 and 3 pphp clay content could be associated to the diffusion of the polyurethane chains between the organic intercalating anions, hindering the mobility of the polymeric chains thus resulting in stiffer foams.

Table 3.5. Specific compressive stress at 10% of deformation and specific elastic modulus of the reference and filled polyurethane foams.

Sample	Specific compressive stress ($kPa\ kg^{-1}\ m^3$)	Specific elastic modulus ($kPa\ kg^{-1}\ m^3$)
PUF-REF	0.45	1.16
PUF-$LCO_3$1	0.43	1.15
PUF-$LCO_3$3	0.48	1.13
PUF-$LCO_3$5	0.60	1.08
PUF-$LHPO_4$1	0.60	0.80
PUF-$LHPO_4$3	0.59	0.85
PUF-$LHPO_4$5	0.58	0.59
PUF-LDEHP1	0.60	1.19
PUF-LDEHP3	0.89	1.22
PUF-LDEHP5	0.63	0.55

The obtained resilience values for the different polyurethane foam systems are represented in **Figure 3.12** as rebound percentage. It was observed that the rebound values did not show a pronounced change. PUF-LCO_3 and PUF-LDEHP series showed similar resilience at low LDH contents (1 and 3 pphp) with respect to the reference foam, while exfoliated PUF-$LHPO_4$ foams (1 and 3 pphp) showed the lowest rebound values. Since resilience is a measure of the elasticity of the foam, the same trend observed in specific elastic modulus was followed in resilience values, obtaining the highest rebound in samples with the highest specific elastic modulus. Nevertheless,

foams containing 5 pphp of modified LDH showed an increase of rebound despite their lower elastic modulus.

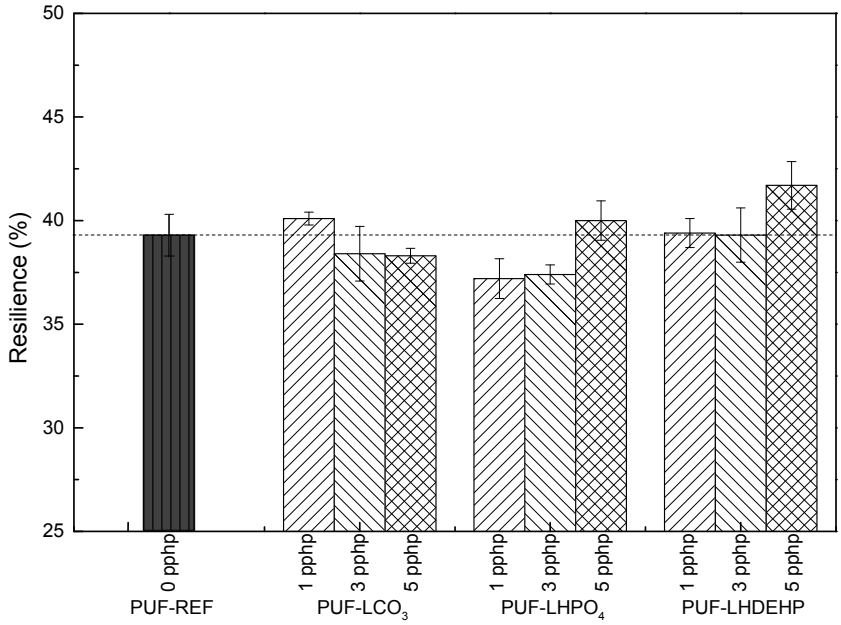

Figure 3.12. Resilience evolution for prepared polyurethane reference and nanocomposite foams with different filler content.

3.3.2.d. Thermal properties

The effect of the addition of the clays on the thermal behavior of the polyurethane foams was studied by thermogravimetric analysis (TGA) and pyrolysis combustion flow calorimetry (PCFC). Samples with intermediate filler content (3 pphp) were analyzed. **Figure 3.13** shows the TGA thermograms of the reference and the nanocomposite foams. The addition of LDH did not affect the degradation mechanism of PUF which occurred in two stages. The first mass loss (around 300 °C) corresponded to the decomposition of the hard domain, taking place the release of isocyanate, primary and secondary amines and alcohols.

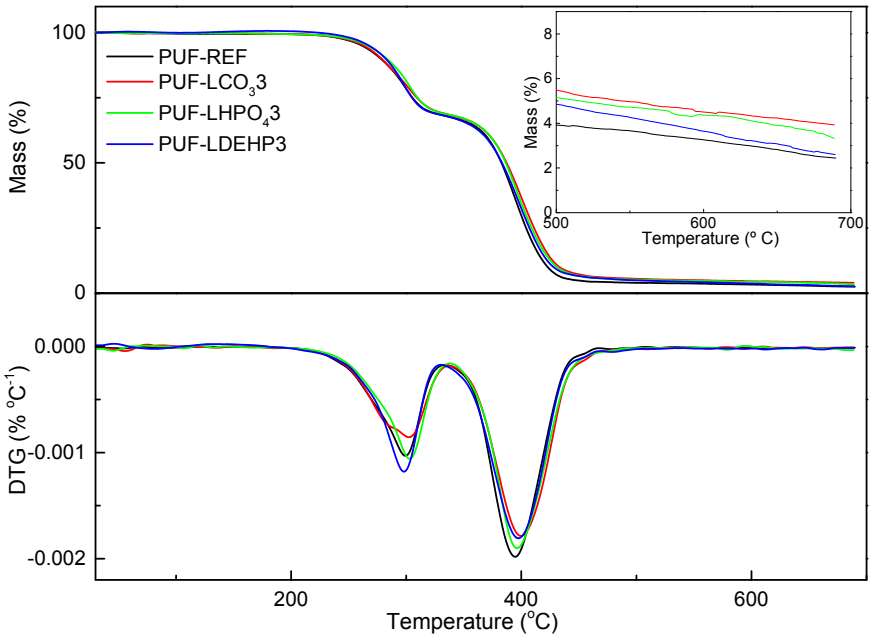

Figure 3.13. Mass loss and first derivative (DTG) curves of the reference foam and corresponding nanocomposites filled with 3 pphp of the different LDH. An amplification of the region between 500 and 700 °C is shown in the inset.

The onset (temperature at 5% mass loss, T_{onset}) and maximum degradation temperatures are shown in **Table 3.6**. Foam containing LDH-CO_3 presented a T_{onset} similar to reference, while in case of foams containing phosphorus modified LDH, PUF-$LHPO_4$3 and PUF-LDEHP3, the T_{onset} increased 2 and 4 °C respectively, which was attributed to a combined effect between phosphorus and the higher intercalation or exfoliation degree of modified LDH.

Table 3.6. Thermal degradation temperatures and residue content at 700 °C of the reference foam and the nanocomposites containing 3 pphp of LDH.

Sample	T_{onset} (°C)	T_{max1} (°C)	T_{max2} (°C)	Residue (wt. %)
PUF-REF	263	300	394	2.44
PUF-$LCO_3$3	262	302	400	3.96
PUF-$LHPO_4$3	265	303	397	3.59
PUF-LDEHP3	267	298	398	2.65

T_{onset}: Temperature at 5% mass loss.

T_{max1} and T_{max2}: Maximum degradation rate temperature, corresponding to first and second step.

Regarding the first maximum degradation rate temperature (T_{max1}) of phosphorus modified LDH containing foams, PUF-$LHPO_4$3 increased slightly in opposite to PUF-LDEHP3, whose T_{max1} decreased 2 °C. This decrease could be due to the

contribution of the hydrocarbon tail degradation as observed in **Figure 3.6**. Maximum degradation rate temperature of the second stage (T_{max2}) increased slightly in nanocomposites as a consequence of the barrier effect induced by the dispersed LDH, hindering the release of volatile compounds (Kotal et al., 2009). Concerning the obtained residue quantities, the LDH-CO_3 and LDH-HPO_4 containing nanocomposites presented higher residue amount than the reference foam at 700 °C, while the residue of the sample containing LDH-DEHP remained close to the reference, as a consequence of the lower hydroxide layer content owing to the dilution effect of the higher organic content of the $DEHP^-$ intercalating anion.

Pyrolysis combustion flow calorimetry provides a preliminary assess of the combustibility of samples through their pyrolysis under nitrogen atmosphere and the oxidation at high temperatures of the generated volatile compounds. **Figure 3.14** displays the heat release rate (HRR) curves of the reference foam and the nanocomposite foams containing 3 pphp of LDH.

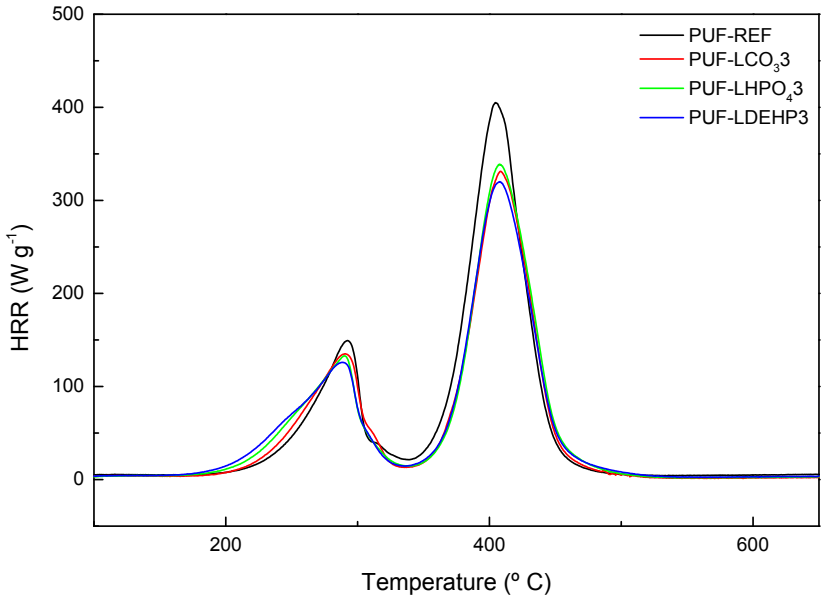

Figure 3.14. Heat release rate (HRR) curves of polyurethane reference foam and nanocomposites containing 3 pphp of the different LDH.

Correspondingly to the thermogravimetric analysis, the thermal decomposition of the samples took place in two differentiated stages. The first one was related to the

degradation of urethane-urea linkages of the hard domain, releasing low calorific capacity products (Ravey and Pearce, 1997).

Table 3.7 displays the most characteristic parameter obtained by PCFC. It was observed that although the temperature of the maximum heat release ($TPHRR_1$) was maintained nearly constant in this stage, the presence of LDH contributed to decrease of the peak heat release rate ($PHRR_1$). The second stage of decomposition corresponded to the degradation of polyol derived products which have higher calorific capacity than those derived from the isocyanate, releasing high quantity of gases in this stage.

Table 3.7. Pyrolysis combustion flow calorimetry results of the reference foam and the nanocomposites containing 3 pphp LDH.

Sample	$PHRR_1$ ($W\ g^{-1}$)	$TPHRR_1$ (°C)	$PHRR_2$ ($W\ g^{-1}$)	$TPHRR_2$ (°C)	THR ($kJ\ g^{-1}$)	HRC ($J\ g^{-1}\ K^{-1}$)	TTI (s)
PUF-REF	144.7 ± 6.5	290.6 ± 1.7	382.2 ± 6.8	405.4 ± 3.1	28.2 ± 0.6	420.3 ± 22.5	157.4
PUF-$LCO_3$3	136.4 ± 5.5	287.8 ± 2.9	333.5 ± 10.9	404.5 ± 3.7	26.9 ± 0.4	371.7 ± 11.2	138.6
PUF-$LHPO_4$3	138.4 ± 6.5	290.1 ± 0.5	327.2 ± 2.2	407.2 ± 1.5	26.5 ± 0.2	345.7 ± 2.1	169.8
PUF-LDEHP3	133.2 ± 11.0	288.8 ± 0.4	309.9 ± 2.3	404.6 ± 3.5	27.4 ± 0.8	334.5 ± 0.7	142.2

$PHRR_1$, $TPHRR_1$: Peak Heat Release Rate and Temperature of Peak Heat Release Rate in the first stage of decomposition.

$PHRR_2$, $TPHRR_2$: Peak Heat Release Rate and Temperature of Peak Heat Release Rate in the second stage of thermal decomposition.

THR: Total Heat Released (first and second stages).

HRC: Heat Release Capacity of the volatile compounds produced during pyrolysis.

TTI: Time to Ignition.

The decrease of $PHRR_2$ was more pronounced, achieving a reduction of 13, 14 and 19% in PUF-$LCO_3$3, PUF-$LHPO_4$3 and PUF-LDEHP3 respectively. The heat release capacity (HRC) is a parameter related to the fire hazard of the material and was calculated by the specific heat release and the heating rate. HRC value decreased with the addition of fillers, especially in those containing phosphorus. Therefore, the fillers might act diluting the flame and volatile compounds release by generating water and noncombustible gases, arising on a lower heat release. It was also observed that the fillers decreased the time to ignition of foams. This behavior suggested that phosphorus modified clays can be considered as good flame retardant candidates.

3.4. Conclusions

Starting from a synthetic hydrotalcite, LDH-CO_3, and following the calcination rehydration process, two phosphorus containing anions (HPO_4^{-2} and $DEHP^-$) were successfully intercalated into the Mg/Al hydroxide layers. The XRD analyses of the LDH showed that they presented different crystallinity degree and crystallite size, resulting the pristine LDH-CO_3 to be the most crystalline, followed by LDH-DEHP and LDH-HPO_4, being the latter the most amorphous one. The unmodified and modified LDH were added in different quantities (1, 3 and 5 pphp) to a flexible polyurethane foam matrix prepared with a castor oil based polyether polyol.

The XRD analyses of the nanocomposites showed that LDH-CO_3 did not lose its staked structure, while PUF-LDEHP series resulted in intercalated nanocomposites and PUF-LHPO_4 series reached an exfoliated dispersion as a consequence of the easy clay layer separation due to its less crystalline nature. TEM analysis revealed large stacks of clay in PUF-L$CO_3$3, smaller and looser layer piles in PUF-LDEHP3 and individual LDH layers within PUF-L$HPO_4$3. The addition of LDH and their dispersion degree throughout the polyurethane matrix influenced the properties of the foams. The density increased with the addition of fillers due to its nucleating effect and due to the increased viscosity of the reactive mixture. The dispersion degree of the LDH also affected the reinforcement of the foams, achieving the highest CFD values at 5, 3 and 1 pphp in PUF-LCO_3, PUF-LDEHP and PUF-LHPO_4, respectively, due to their crystallite size and intercalated or exfoliated distribution.

The evolution of resilience values corresponded to the behavior of the obtained elastic modulus for each foam series, increasing the bounce for modified LDH containing foams and decreasing for LDH-CO_3 containing nanocomposites. The thermal stability of the nanocomposites increased, especially in the second stage of degradation. Nanocomposite foams presented higher residue content due to the presence of metal oxides coming from the decomposition of the LDH.

Additionally, the LDH contributed to decrease the HRC of the foams and the PHRR on the second stage of decomposition. In general, PUF-LDEHP was the system

which decreased most the HRR acting as mentioned before in the second stage of decomposition.

These results showed that phosphorus modified LDH have the potential to be used as flame retardant additives.

3.5. References

Cao, X., Lee, L.J., Widya, T., Macosko, C., 2005. Polyurethane/clay nanocomposites foams: Processing, structure and properties. Polymer 46, 775–783.

Cavani, F., Trifirò, F., Vaccari, A., 1991. Hydrotalcite-type anionic clays: Preparation, properties and applications. Catal. Today 11, 173–301.

Chubar, N., Gerda, V., Megantari, O., Mičušík, M., Omastova, M., Heister, K., Man, P., Fraissard, J., 2013. Applications versus properties of Mg-Al layered double hydroxides provided by their syntheses methods: Alkoxide and alkoxide-free sol-gel syntheses and hydrothermal precipitation. Chem. Eng. J. 234, 284–299.

Costa, F.R., Leuteritz, A., Wagenknecht, U., Jehnichen, D., Häußler, L., Heinrich, G., 2008. Intercalation of Mg-Al layered double hydroxide by anionic surfactants: Preparation and characterization. Appl. Clay Sci. 38, 153–164.

Evans, D.G., Slade, C.T., 2006. Structural aspects of layered double hydroxides. Struct. Bond. 119, 1–87.

He, J., Wei, M., Li, B., Kang, Y., Evans, D.G., Duan, X., 2006. Preparation of layered double hydroxides. Struct. Bond. 119, 89–119.

Hernandez-Moreno, M.J., Ulibarri, M.A., Rendon, J.L., Serna, C.J., 1985. IR characteristics of hydrotalcite-like compounds. Phys. Chem. Miner. 12, 34–38.

Javni, I., Song, K., Lin, J., Petrovic, Z.S., 2011. Structure and properties of flexible polyurethane foams with nano- and micro-fillers. J. Cell. Plast. 47, 357–372.

Jiang, D.D., 2010. Polymer nanocomposites, in: Wilkie, C.A., Morgan, A.B. (Eds.), Fire

Retardancy of Polymeric Materials. CRC Press, Boca Ratón, pp. 261–292.

Kloprogge, J.T., Frost, R.L., 2001. Infrared and Raman spectroscopic studies of layered double hydroxides, in: Rives, V. (Ed.), Layered Double Hydroxides: Present and Future. Nova Science Publishers Inc, New York, pp. 139–192.

Kotal, M., Kuila, T., Srivastava, S.K., Bhowmick, A.K., 2009. Synthesis and characterization of polyurethane/Mg-Al layered double hydroxide nanocomposites. J. Appl. Polym. Sci. 114, 2–10.

Lamba, N.M.K., Woodhouse, K.A., Cooper, S.L., 1997. The chemistry of polyurethane copolymers, in: Polyurethanes in Biomedical Applications. CRC Press, Boca Ratón, pp. 5–23.

Li, F., Duan, X., 2006. Applications of layered double hydroxides. Struct. Bond. 119, 193–223.

Madaleno, L., Pyrz, R., Crosky, A., Jensen, L.R., Rauhe, J.C.M., Dolomanova, V., Madeira Viegas de Barros Timmons, A.M., Cruz Pinto, J.J., Norman, J., 2013. Processing and characterization of polyurethane nanocomposite foam reinforced with montmorillonite-carbon nanotube hybrids. Compos. Part A 44, 1–7.

Millange, F., Walton, R.I., Hare, D.O., 2000. Time-resolved in situ X-ray diffraction study of the liquid-phase reconstruction of Mg-Al-carbonate hydrotalcite-like compounds. J. Mater. Chem. 10, 1713–1720.

Miyata, S., 1980. Physico-chemical properties of synthetic hydrotalcites in relation to composition. Clays Clay Miner. 28, 50–56.

O'Neil, M.J., 2001. The Merck Index: An Encyclopedia of Chemicals, Drugs, and Biologicals. Merck Co, New Jersey.

Ravey, M., Pearce, E.M., 1997. Flexible polyurethane foam. I. Thermal decomposition of a polyether-based, water-blown commercial type of flexible polyurethane foam. J. Appl. Polym. Sci. 63, 47–74.

Sharma, C., Kumar, S., Unni, A.R., Aswal, V.K., Rath, S.K., Harikrishnan, G., 2014. Foam

stability and polymer phase morphology of flexible polyurethane foams synthesized from castor oil. J. Appl. Polym. Sci. 40668, 1–8.

Taviot-Guého, C., Leroux, F., 2006. In situ polymerization and intercalation of polymers in layered double hydroxides. Struct. Bond. 119, 121–159.

Wang, L., Su, S., Chen, D., Wilkie, C.A., 2009. Variation of anions in layered double hydroxides: Effects on dispersion and fire properties. Polym. Degrad. Stab. 94, 770–781.

Wypych, F., Satyanarayana, K.G., 2004. Clay Surfaces – Fundamentals and Applications, in: Wypych, F., Satyanarayana, K.G. (Eds.), Interface Science and Technology. Elsevier Ltd, UK, pp. 345–373.

Xu, Z.P., Lu, G.Q., 2005. Hydrothermal synthesis of layered double hydroxides (LDHs) from mixed MgO and Al_2O_3: LDH formation mechanism. Chem. Mater. 17, 1055–1062.

Zhao, Y., Li, F., Zhang, R., Evans, D.G., Duan, X., 2002. Preparation of layered double hydroxide nanomaterials with a uniform crystallite size using a new method involving separate nucleation and aging steps. Chem. Mater. 14, 4286–4291.

Zhou, Y., Sun, X., Zhong, K., Evans, D.G., Lin, Y., Duan, X., 2012. Control of surface defects and agglomeration mechanism of layered double hydroxide nanoparticles. Ind. Eng. Chem. Res. 51, 4215–4221.

“Maturity, one discovers, has everything to do with the acceptance of not knowing.”

M. Z. Danielewski. House of Leaves. United States: Pantheon, 2000.

Chapter 4

4

Flexible polyurethane foams with **phosphorus** containing oligomeric diol and **layered double hydroxides**

4. Flexible polyurethane foams with phosphorus containing oligomeric diol and layered double hydroxides

4.1. Introduction

In regard of the contribution of the phosphorus modified LDH to decrease the HRR of flexible polyurethane foams in **Chapter 3**, this chapter reports the effect of incorporating different amounts of a phosphorus containing oligomeric diol (E560) to flexible polyurethane foams prepared with LB50 and containing the layered double hydroxides used before (LDH-CO_3, LDH-HPO_4 and LDH-DEHP).

Modified clays and oligomeric diol mixture is expected to improve the flame retardant behavior of the foams owing to the presence of phosphorus in both modified LDHs and E560. The performed characterization in this chapter is parallel to the study carried out in **Chapter 3**, but with an intermediate LDH loading (3 pphp).

4.2. Experimental procedure

4.2.1. Materials

The PUF nanocomposites were prepared using toluene diisocianate, TDI (Desmodur T 80, Covestro) as A-side formulation and it was used without further purification. The B-side was constituted by Lupranol Balance® 50 (LB50), the castor oil based polyether polyol used in **Chapter 3,** which was blended with 5 and 10 parts per hundred of Exolit® OP 560 (E560), a reactive type flame retardant oligomeric phosphonate diol from Clariant. The general structural unit of a phosphonate diol is shown in **Figure 4.1**. Prior to their use, both polyol and oligomeric diol were dried in a rotary evaporator at 70 °C for 6 h.

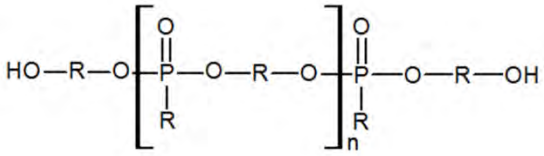

Figure 4.1. Structural unit of an oligomeric phosphonate diol.

The additives used for polyurethane foam synthesis and the preparation procedure of the different LDHs used (LDH-CO_3, LDH-HPO_4 and LDH-DEHP) were already detailed in **Chapter 2** (**Section 2.2**) and **Chapter 3** (**Section 3.2.2.**)**,** respectively.

4.2.2. Preparation of flexible polyurethane foam nanocomposites

The preparation of the polyurethane nanocomposite foams containing 3 pphp LDH (1.89 wt% of the total foam weight) was carried out by *in situ* polymerization process mixing the E560 diol with LB50 polyol prior to the addition of the foaming additives, as detailed in **Chapter 3** (**Section 3.2.3**).

A reference sample with LB50 as the unique polyol, denoted as PUF-REF, and foams with 5 and 10 pphp E560 (PUF-5E and PUF-10E respectively) were synthesized. The series of nanocomposites with 3 pphp of different type of LDH were denoted as follows. The foams synthesized with 100 pphp LB50 were named PUF-LCO_3, PUF-$LHPO_4$ and PUF-LDEHP; the foams containing 5 pphp E560 were denoted as PUF-5E/LCO_3, PUF-5E/$LHPO_4$ and PUF-5E/LDEHP and the foams with 10 pphp E560 PUF-10E/LCO_3, PUF-10E/$LHPO_4$ and PUF-10E/LDEHP. **Table 4.1** shows the LB50/E560 weight ratio and amount of TDI used for each sample, in order to balance the hydroxyl groups provided by the addition of E560. The same water, catalyst and surfactant content as in **Chapter 3** were used.

Table 4.1. Sample designation, used LB50/E560 ratio and TDI weight of each prepared polyurethane foam.

Sample	LB50/E560 weight ratio	TDI (g)
PUF-REF	100/0	32.3
PUF-5E	95/5	34.0
PUF-10E	90/10	35.7
PUF-LCO_3	100/0	32.3
PUF-5E/LCO_3	95/5	34.0
PUF-10E/LCO_3	90/10	35.7
PUF-$LHPO_4$	100/0	32.3
PUF-5E/$LHPO_4$	95/5	34.0
PUF-10E/$LHPO_4$	90/10	35.7
PUF-LDEHP	100/0	32.3
PUF-5E/LDEHP	95/5	34.0
PUF-10E/LDEHP	90/10	35.7

Prior to their morphological, mechanical and thermal characterization, the samples were stored at room temperature for one month until the complete cure of the foam, when the final properties were achieved.

4.3. Results and discussion

4.3.1. Fourier transformed infrared spectroscopy

Figure 4.2a shows the infrared spectra of LB50 and E560, as well as reference foam and foams containing 5 and 10 pphp E560. Apart from the broad band corresponding to O-H stretching appearing at 3490 and 3374 cm^{-1} in LB50 and E560 respectively, the characteristic N-H stretching vibration of urethane bond from the foams was observed at 3290 cm^{-1}. It was noteworthy that the intensity of the O-H stretching band from LB50 was very low due to the high molecular weight of the polyol. It was also observed a peak at 2276 cm^{-1} corresponding to unreacted isocyanate groups due to the excess of isocyanate used in the formulation, which 48 h after polymerization still remained visible. Isocyanate in excess reacts within time until the complete cure of the foam.

Figure 4.2b shows the spectra of LB50 and E560 and the foams in the interval between 2000 and 700 cm^{-1}. The stretching vibration band from the triglyceride ester carbonyl (C=O) appeared at 1742 cm^{-1} and the C-O-C symmetric stretching at 1094 cm^{-1} in LB50. The distinctive bands of E560 were attributed to the P=O stretching at 1221 cm^{-1} and P-O-C asymmetric (1021 and 955 cm^{-1}) and symmetric (808 cm^{-1}) stretching vibrations, respectively. The characteristic carbonyl stretching vibrations of urethane and urea bonds appear in the amide I (carbonyl) region, between 1750 and 1625 cm^{-1}. In this region, free urethane and urea absorption bands appeared at 1730 and 1715 cm^{-1}, respectively, in addition to associated urea (bidentate) stretching vibration at 1640

cm^{-1}. LB50 characteristic C=O vibration was also observed as a slight widening around 1740 cm^{-1}. The band corresponding to the N-H bending and C-N stretching vibrations of the urethane and urea groups (amide II) appeared at 1532 cm^{-1}. Additionally, the

band corresponding to asymmetric C-O-C stretching vibration was observed at 1221 cm^{-1}, which overlapped with the P=O stretching vibration, as can be observed from the increase in the intensity of this band with increasing amount of E560.

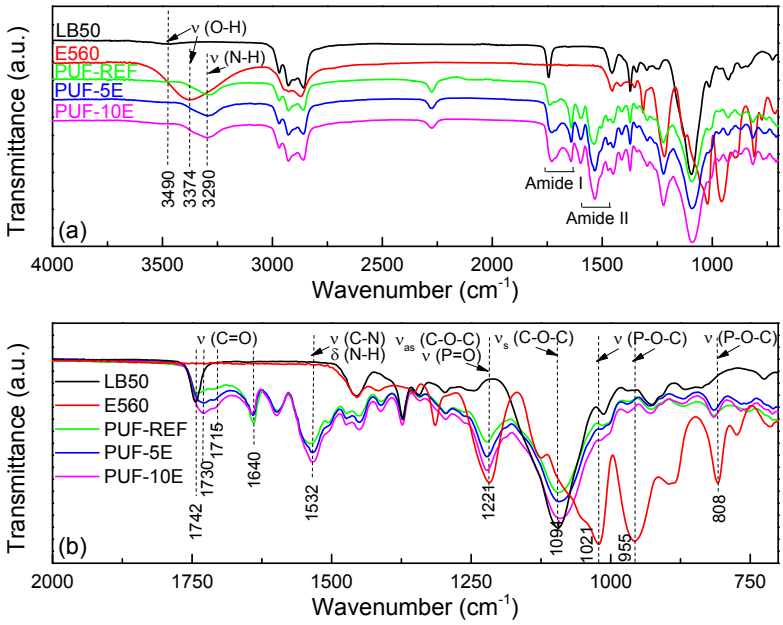

Figure 4.2. Infrared spectra of LB50 and E560, reference foam and foams containing 5 and 10 pphp E560 between 4000 and 700 cm^{-1} (a) and between 2000 and 700 cm^{-1} (b).

No significant changes were observed in the nanocomposite foams with respect to PUF-5E and PUF-10E samples, as shown in **Figure 4.3**. The absence of bands related to the metal-OH lattice vibrations in the nanocomposites could be attributed to the low LDH content, which corresponds to a 1.89 wt% LDH in the total weight of the foam. These peaks were observed elsewhere (Kotal et al., 2009) corresponding to nanocomposites containing 3 wt% LDH.

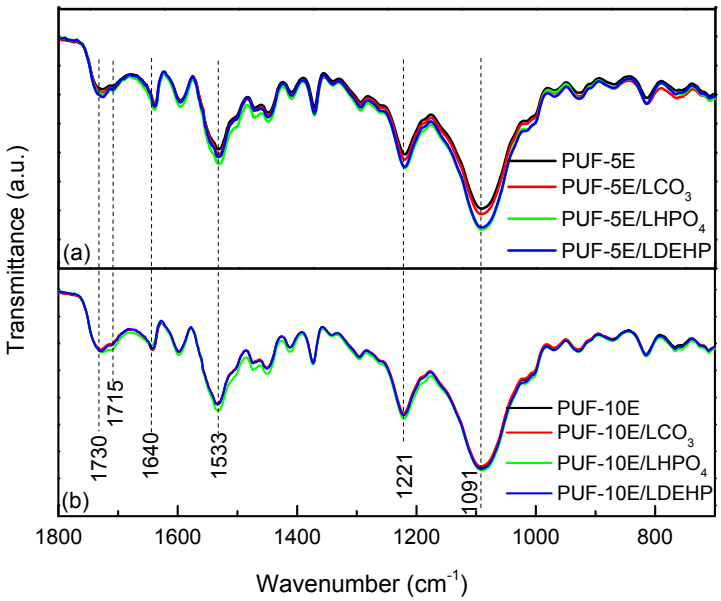

Figure 4.3. Infrared spectra of foams and nanocomposites with 5 (a) and 10 (b) pphp E560 from 1800 to 700 cm^{-1}.

4.3.2. Morphology and cell size

The diffraction patterns of the reference foams containing different amount of E560 and nanocomposites with 3 pphp LDH are displayed in **Figure 4.4**. The characteristic (003) reflection of clays, which determines the basal space between the layers of the clay, appeared at 11.77° (7.51 Å), 8.80° (10.04 Å) and 3.82° (23.12 Å) in LDH-CO_3, LDH-HPO_4 and LDH-DEHP respectively, as shown in **Chapter 3** (**section 3.3.1**). This reflection is related to the different size and arrangement of the intercalating anions. The intensity of the diffraction patterns and the crystallite size were also reported in **Chapter 3**. The pristine LDH was the most crystalline sample, while the phosphate intercalated LDH lost the original crystallinity during the rehydration process, resulting LDH-HPO_4 to be the less crystalline clay. Aside from the broad diffraction peak around 20° characteristic of the polyurethane, the appearance of a diffraction peak at 3.66° (24.14 Å) in case of LDH-DEHP containing nanocomposites was observed. The shift to lower angles of the (003) reflection indicated that polymeric chains had diffused between the clay layers leading to a higher basal spacing and thus, to an intercalated nanocomposite morphology. Those nanocomposites containing LDH-CO_3 presented a peak at 11.57° (7.65 Å), denoting that the clay was dispersed in

the polyurethane matrix maintaining practically unaltered its stacked structure probably as a consequence of its high crystallinity. In case of LDH-HPO_4 containing foams, no diffraction appeared around 8.80° suggesting that as a result of its low crystallinity, the layers of the clay were exfoliated during polymerization. The same behavior was observed in **Chapter 3** in foams containing 100 pphp LB50 and different LDH content.

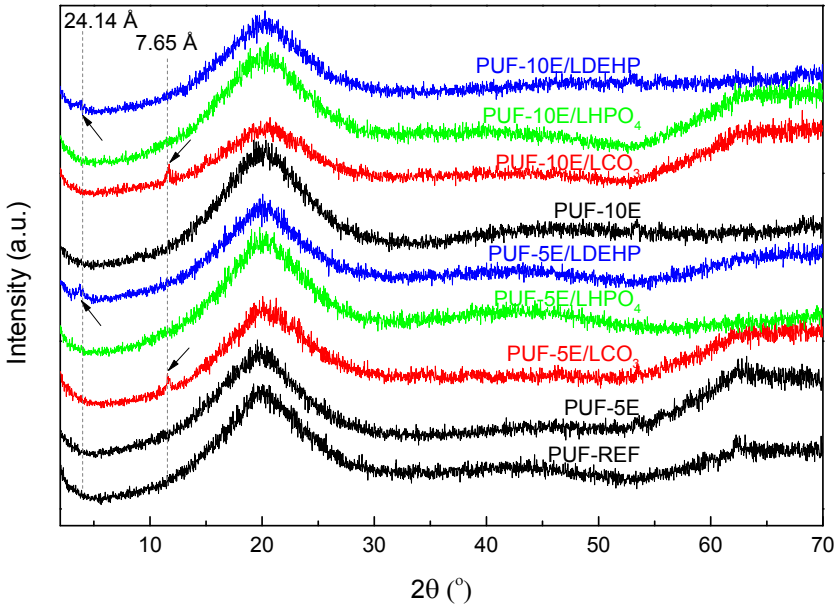

Figure 4.4. XRD patterns of the synthesized foams: references (PUF-REF, PUF-5E and PUF-10E) and nanocomposites filled with 3 pphp LDH.

Density and average cell size values of the synthesized foams are shown in **Table 4.2**. The density is an important parameter regarding foam comfort and support, which depends mainly on the used amount of blowing agent (Gao et al., 2014) and on the addition of additives such as fillers, which normally contribute to increase the density (Liang and Shi, 2011), (Widya and Macosko, 2005). It was observed in **Table 4.2** that the addition of E560 to the foam contributed to increase the density, resulting in a reduction of the average cell diameter. This effect could be attributed to the decrease of the chain length between crosslinking points when the low molecular weight E560 was incorporated (I_{OH} = 489 mg KOH g^{-1} and functionality of 2), thus increasing the crosslink density that resulted in a more compact disposition of the polymer chains. The addition of LDH promoted the bubble nucleation through an increase in the

number of bubble sites (Wee et al., 2004). The nucleating effect of the clay depends on its dispersion degree and hence on the number of dispersed nanoentities which act as nucleating centers. However, the addition of nanoclays also contributed to increase the viscosity of the reactive mixture, which is a critical parameter in polyurethane foaming process (Pan and Saddler, 2013).

Table 4.2. Density and average cell diameter of each unfilled and filled polyurethane foam samples.

Sample	Density ($kg\ m^{-3}$)	Average cell diameter (μm)
PUF-REF	37.3 ± 0.8	362.3 ± 73.5
PUF-5E	41.7 ± 0.7	286.9 ± 100.4
PUF-10E	47.9 ± 0.7	280.2 ± 83.4
PUF-LCO_3	44.5 ± 0.5	319.3 ± 76.0
PUF-5E/LCO_3	38.0 ± 0.5	333.6 ± 105.1
PUF-10E/LCO_3	38.7 ±0.5	355.6 ± 126.7
PUF-$LHPO_4$	44.1 ± 0.3	339.3 ± 96.7
PUF-5E/$LHPO_4$	46.2 ± 0.5	334.3 ± 81.0
PUF-10E/$LHPO_4$	44.2 ± 0.3	359.6 ± 99.1
PUF-LDEHP	44.3 ± 0.7	291.4 ± 92.0
PUF-5E/LDEHP	37.4 ± 0.5	344.0 ± 105.7
PUF-10E/LDEHP	35.0 ± 0.3	358.1 ± 111.7

Consequently, the blowing efficiency was conditioned by nucleation and viscosity, both of which affected the density of the foam. In case of LDH-HPO_4 containing foams, the values of density and cell size are quite similar independently of the E560 content. This effect could be attributable to the exfoliated dispersion of the LDH-HPO_4 clay layers, which increased the viscosity of the reactive mixture resulting in a hindered growth of the bubbles and leading to foams with thicker cell walls (Fan et al., 2012; Eaves, 2004). In foams with LDH-CO_3 and LDH-DEHP, the addition of LDH increased the density in foams fully synthesized with LB50 but decreased with the addition of E560, in contrast to those foams without fillers (PUF-REF, PUF-5E and PUF-10E). This sustained that these aforementioned LDH were less finely dispersed in the matrix than LDH-HPO_4, increasing the permeability to the blowing agent. In this way, their contribution to bubble nucleation together with the decrease in viscosity provided by E560 resulted in higher cell growth.

4.3.3. Mechanical properties

The firmness and support of the foams was measured by compression force deflection (CFD), one of the most indicative properties of flexible foams. The obtained CFD values for all the synthesized foams are shown in **Figure 4.5a**. It was observed that the CFD value of the unfilled foams increased nearly a 20% with the addition of E560.

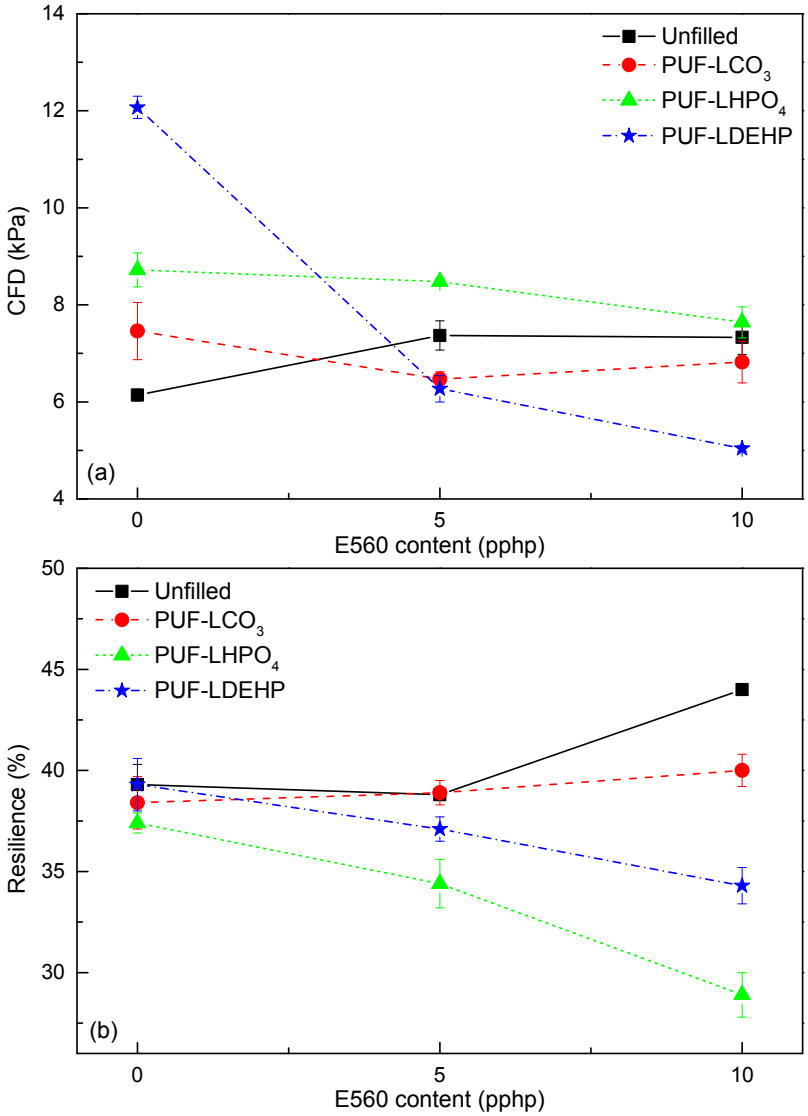

Figure 4.5. CFD (a) and resilience (b) evolution with E560 content of unfilled foams and nanocomposite foams with different LDH.

This occurred together with an increase of the density with higher E560 content, due to the higher material quantity available for load bearing when mass per

unit volume increases. The addition of LDH increased CFD for those foams synthesized with 100 pphp LB50 (PUF-LCO$_3$, PUF-LHPO$_4$ and PUF-LDEHP) with respect to PUF-REF, following the same behavior than density did. The addition of LDH-HPO$_4$ to foams containing E560 led to increase the CFD as a result of its fine dispersion through the matrix, but in contrast the presence of LDH-CO$_3$ and LDH-DEHP conferred lower CFD values than their respective unfilled foams.

The intercalated LDH-CO$_3$ and LDH-DEHP fillers did not contribute to increase the stiffness of the foam as they were more locally arranged in the cellular structure than the exfoliated LDH-HPO$_4$. CFD in sample PUF-10E/LDEHP decreased a 31% with respect to unfilled PUF-10E, probably due to the better compatibility between the organophosphorus intercalated LDH and the phosphonate oligomer, which provided a higher affinity with the polymeric chains leading to softer foam.

The recovery rate of the foams was measured as resilience (R) or bounce. In contrast to viscoelastic foams, high resilience foams (from R = 55%) are characterized for having a rapid recovery, bouncing back into its original shape immediately after compression. **Figure 4.5b** shows the evolution of the resilience with E560 content. It can be observed that the addition of 10 pphp E560 increased the bounce a 12% in case of unfilled foams. This could be attributed to the lower molecular weight of the phosphorus containing oligomeric diol, which contributed to increase the crosslinking density, and the additional aromatic molecules provided by the higher amount of used TDI for balancing the OH introduced by E560 (**Table 4.1**), leading to less viscoelastic foams (Ge et al., 2000). The addition of LDH to the PUF-REF foam did not vary notably the resilience value, but the differences in resilience were more evident with the increase of E560. LDH-CO$_3$ maintained the bounce nearly constant with E560, while LDH-HPO$_4$ and LDH-DEHP decreased the resilience value with respect to unfilled foams, being more pronounced in foams containing LDH-HPO$_4$. This behavior was attributed to the different dispersion degree of the LDH, since R decreased as the dispersion degree was higher. As it was mentioned before, the stacked structure of LDH-CO$_3$ was distributed along the polymeric matrix nearly unaltered due to its high crystallinity,

whereas the predominating amorphous character of LDH-HPO_4 allowed the exfoliation of the clay layers in the matrix.

In case of LDH-DEHP, its intermediate crystallinity between LDH-CO_3 and LDH-HPO_4 allowed partial intercalation of the matrix chains between the clay sheets as observed by XRD. In this way, it was found by Javni et al. (2011) that the addition of micro-sized fillers to polyurethane foam did not affect the rebound value, and also that the addition of a nanoclay with optimized polarity (which facilitates the intercalation or exfoliation) decreased strongly the resilience of the foam around a 30% for 3 wt% clay content. Hence, the presence of LDH and its dispersion through the polyurethane matrix counteracted the resilient contribution of E560 yielding to foams with more viscoelastic behavior.

4.3.4. Thermal properties

Thermal stability of the polyurethane foams was analyzed by TGA. **Figure 4.6** displays the thermograms of the synthesized foams. The degradation mechanism of the polyurethane did not change with the presence of E560 and LDH, which took place in two differentiated stages. The first one corresponded to the cleavage of the urethane-urea linkages and the second degradation step to the degradation of the polyol, as previously mentioned. **Figure 4.6a** and **Table 4.3** show that the phosphorus from E560 catalyzed the degradation of urethane-urea linkages shifting the T_{onset} and T_{max1} to lower values (13 and 14 °C, respectively, in PUF-10E), while helped to stabilize the second stage of degradation. This could be attributed to the formation of a char layer unstable at high temperatures, as can be observed by the lower residue content that remained in foams containing E560 in contrast with PUF-REF (Gaan et al., 2015).

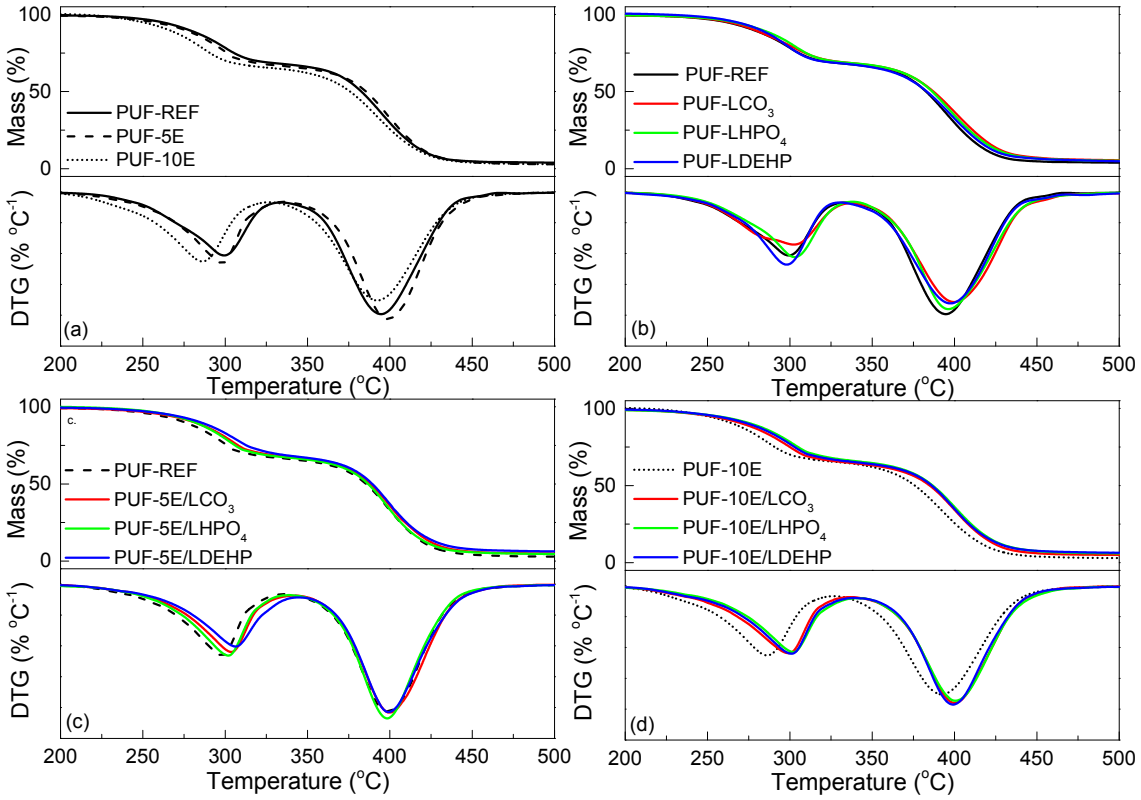

Figure 4.6. Mass loss (top) and first derivative (bottom) curves of the unfilled foams (a), nanocomposites without E560 (b) and with 5 pphp E560 (c) and 10 pphp E560 (d).

Figure 4.6b-d shows that in general, the addition of LDH helped to increase the thermal stability of foams delaying the T_{onset} and T_{max} of the first and second degradation stages, which could be attributed to the barrier effect caused by the layered structure of the LDH, leading to delay these temperatures by hindering the release of volatile compounds and the heat transmission into the polymeric matrix (Kotal et al., 2009; Guo et al., 2011). In the case of PUF-LDEHP, the T_{max1} value was shifted to lower temperatures attributed to the decomposition of the organic molecule intercalated between the clay layers. It was noteworthy that the LDH also contributed to the formation of a larger residue quantity, since the clays decompose from their metal hydroxide stacking structure to a mixture of metal oxides stable at high temperatures. Regarding the remaining residue, the phosphorus containing LDH led to the formation of a large amount of residue, especially LDH-DEHP which together with 5 and 10 pphp E560 were the combinations that most increase the thermal stability from all of the synthesized foams, yielding also to the formation of the higher residue

quantity at 700 °C, obtaining a 125, 178 and 234% more residue than unfilled PUF-REF, PUF-5E and PUF-10E respectively.

Table 4.3. Thermal degradation temperatures and residue content at 700 °C of the prepared foams.

Sample	T_{onset} (°C)	T_{max1} (°C)	T_{max2} (°C)	Residue (wt. %)
PUF-REF	263	300	394	2.44
PUF-LCO_3	262	302	400	3.96
PUF-$LHPO_4$	265	303	397	3.59
PUF-LDEHP	267	298	398	2.65
PUF-5E	257	298	399	1.98
PUF-5E/LCO_3	262	304	400	4.14
PUF-5E/$LHPO_4$	265	302	398	3.56
PUF-5E/LDEHP	266	306	399	5.50
PUF-10E	250	286	392	1.65
PUF-10E/LCO_3	252	299	400	4.08
PUF-10E/$LHPO_4$	256	302	400	5.09
PUF-10E/LDEHP	255	301	399	5.51

T_{onset}: Temperature at 5% mass loss.

T_{max1} and T_{max2}: Maximum degradation rate temperature, corresponding to first and second step.

Pyrolysis combustion flow calorimetry provides a preliminary fire behavior insight with the advantage of using milligram scale samples. **Figure 4.7a** shows the obtained heat release curves of the unfilled foams, which evidenced that the addition of E560 to the polyurethane foam had a catalyzing effect over the degradation of urethane-urea linkages, *i.e.* the first degradation stage, lowering the temperature of the peak release rate ($TPHRR_1$), as shown in **Table 4.4**.

Nevertheless, E560 contributed to decrease the THR and HRC of the whole process by means of reducing the $PHRR_1$ and $PHRR_2$, especially in PUF-10E decreasing both values around a 21% comparing with PUF-REF. The incorporation of LDH to the polyurethane foam matrix also contributed to reduce the THR and the HRC of the whole degradation process. It can be observed in **Figure 4.7b** that the addition of LDH to PUF-REF led to a decrease in the $PHRR_2$ of around a 13, 15 and 19% in case of LDH-CO_3, LDH-HPO_4 and LDH-DEHP respectively. This reduction could be due to the endothermic decomposition of the anionic clay and the contribution of the release of the interlayer water during this process, which confers a local cooling of the sample. Therefore, the addition of 10 pphp E560 to the unfilled foam decreased in higher extent the heat release of PUF-REF.

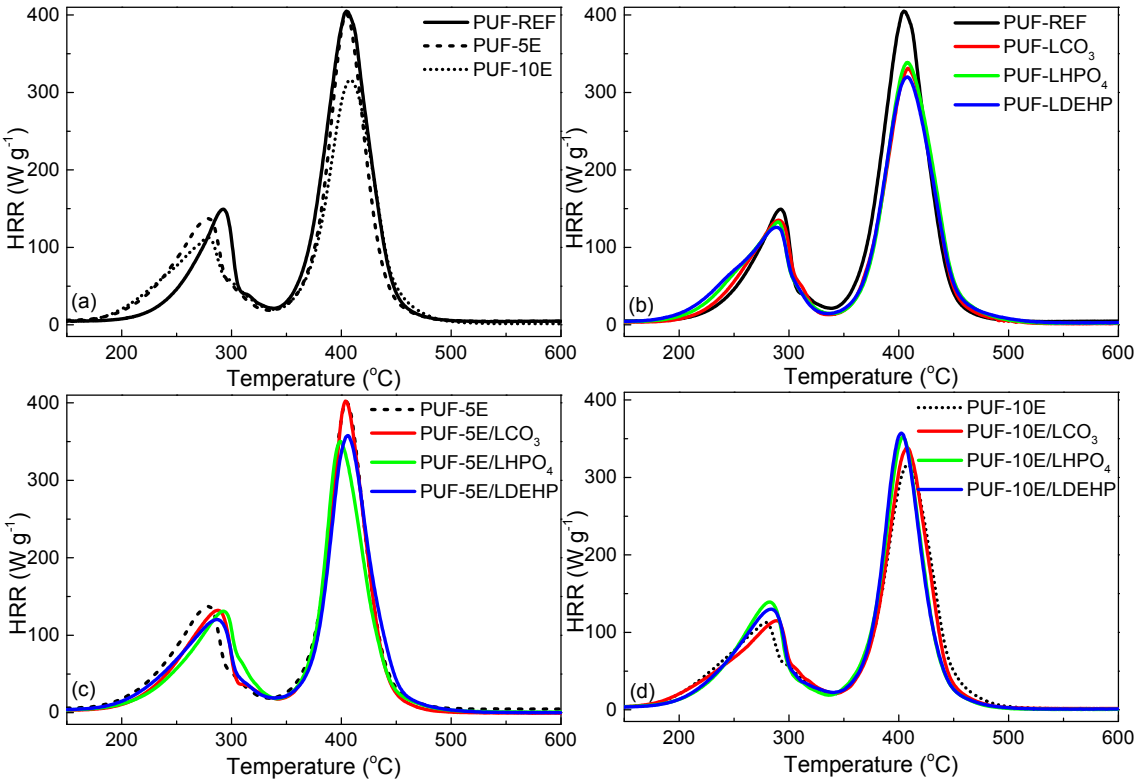

Figure 4.7. Heat release rate (HRR) curves of the unfilled foams with different amount of E560 (a) and nanocomposites without E560 (b), with 5 pphp E560 (c) and with 10 pphp E560 (d).

Table 4.4. Pyrolysis combustion flow calorimetry results obtained for unfilled foams and nanocomposite foams with different amount of E560 and with 3 pphp of the different LDH.

Sample	$PHRR_1$ (W g^{-1})	$TPHRR_1$ (°C)	$PHRR_2$ (W g^{-1})	$TPHRR_2$ (°C)	THR (kJ g^{-1})	HRC (J g^{-1} K^{-1})
PUF-REF	144.7 ± 6.5	290.6 ± 1.7	382.2 ± 6.8	405.4 ± 3.1	28.2 ± 0.6	420.3 ± 22.5
PUF-LCO_3	136.4 ± 5.5	287.8 ± 2.9	333.5 ± 10.9	404.5 ± 3.7	26.9 ± 0.4	371.7 ± 11.2
PUF-$LHPO_4$	138.4 ± 6.5	290.1 ± 0.5	327.2 ± 2.2	407.2 ± 1.5	26.5 ± 0.2	345.7 ± 2.1
PUF-LDEHP	133.2 ± 11.0	288.8 ± 0.4	309.9 ± 2.3	404.6 ± 3.5	27.4 ± 0.8	334.5 ± 0.7
PUF-5E	137.7 ± 5.1	279.7 ± 0.5	376.4 ± 3.1	404.7 ± 1.2	26.5 ± 0.4	414.2 ± 4.4
PUF-5E/LCO_3	132.7 ± 6.5	287.9 ± 0.4	388.7 ± 6.2	403.7 ± 0.3	26.1 ± 0.5	423.9 ± 3.9
PUF-5E/$LHPO_4$	136.0 ± 5.5	292.3 ± 0.5	336.1 ± 3.4	398.8 ± 0.4	26.2 ± 0.2	414.1 ± 6.6
PUF-5E/LDEHP	121.4 ± 6.0	287.1 ± 0.6	344.2 ± 5.2	406.0 ± 0.7	26.2 ± 0.5	378.2 ± 3.5
PUF-10E	114.0 ± 6.2	278.4 ± 0.7	300.9 ± 2.0	407.8 ± 0.8	26.1 ± 0.6	333.0 ± 6.2
PUF-10E/LCO_3	114.7 ± 7.3	287.5 ± 1.1	321.6 ± 4.7	407.9 ± 1.1	25.9 ± 0.2	356.0 ± 4.6
PUF-10E/$LHPO_4$	138.8 ± 6.2	282.7 ± 0.8	338.0 ± 2.1	403.5 ± 0.6	25.6 ± 0.5	368.0 ± 2.2
PUF-10E/LDEHP	131.0 ± 7.4	283.7 ± 0.3	339.8 ± 2.5	402.3 ± 0.5	25.9 ± 0.3	376.0 ± 4.4

$PHRR_1$, $TPHRR_1$: Peak Heat Release Rate and Temperature of Peak Heat Release Rate in the first stage of decomposition.

$PHRR_2$, $TPHRR_2$: Peak Heat Release Rate and Temperature of Peak Heat Release Rate in the second stage of thermal decomposition.

THR: Total Heat Released (first and second stages).

HRC: Heat Release Capacity of the volatile compounds produced during pyrolysis.

On the other hand, the addition of LDH seemed to be more effective than the addition of 5 pphp E560 on the improvement of the thermal properties of PUF-REF. As a consequence, a synergistic effect on the combustion properties could be expected by the combination of both E560 and LDH, which led to correct the catalyzing effect of E560 over the first stage delaying the $TPHRR_1$ (**Figure 4.7c-d**).

Their combination also contributed to reduce the THR and HRC of the foams, but in contrast contributed to increase the $PHRR_2$ in foams containing E560. This effect could be explained due to the contribution of the catalyzing effect of the phosphorus in E560 together with the barrier effect of the LDH, that might led to the generation of superheated conditions inside the polymeric matrix (Corcione and Frigione, 2012), causing a further release of heat and other generated volatile species. In regard to the most efficient LDH, phosphorus containing LDH were the clays that lowest PHRR values showed in 5 pphp E560 containing foams, and LDH-CO_3 was the clay that showed the lowest PHRR values in case of 10 pphp E560 containing foams.

Figure 4.8 shows the micrographs of the remaining residue of the nanocomposite foams with 3 pphp LDH synthesized with 100 pphp LB50 and with LB50/E560 (90/10 ratio) after PCFC testing. It can be observed that the presence of E560 changes the morphology of the char, leaving a higher amount of it and a continuous residue layer. As recorded by TGA, the presence of LDH increased the amount of char formed after pyrolysis, but forming discontinuous clusters of char in case of foams with 100 pphp LB50 as it can be observed in the figure. The combination of E560 with LDH also left a larger quantity of char, but the clay seemed to break the cohesion of the residue observed in PUF-10E. This could be related to the increase in the $PHRR_2$ registered by PCFC as a consequence of the release of heat after breaking the barrier formed by the clays along the matrix.

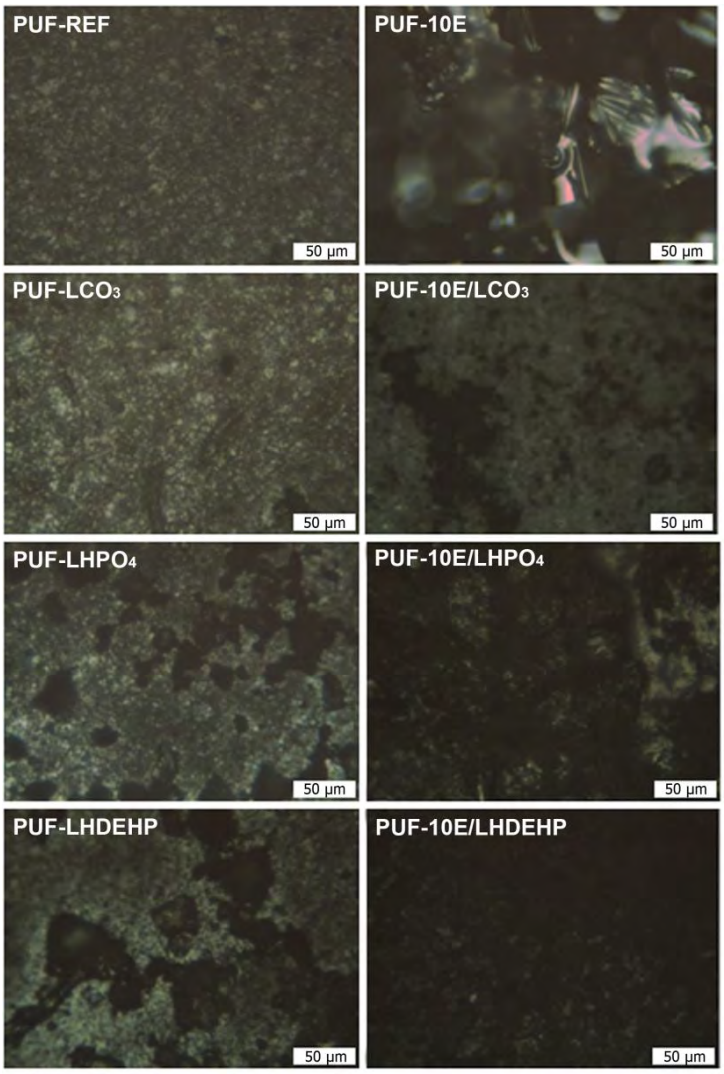

Figure 4.8. OM micrographs (x200 magnification) of the remaining residue at 750 °C after PCFC essay of nanocomposite foams with 3 pphp LDH fully synthesized with LB50 (left) and foams with 90/10 LB50/E560 (right).

4.4. Conclusions

Flexible polyurethane foams containing a commercial reactive phosphorus containing oligomeric diol (E560) and its combination with 3 pphp of a synthetic hydrotalcite (LDH-CO_3) and phosphorus intercalated LDH (LDH-HPO_4 and LDH-DEHP) were prepared aiming to study the effect of the addition of the reactive phosphorus containing compound and its combination with the different LDHs on the properties of the foams.

The density of the foams increased as E560 content was higher, whereas the effect of LDH in density depended on their dispersion degree. In this way, LDH-HPO_4 maintained the density nearly constant due to its exfoliated distribution meanwhile density values decreased in case of LDH-CO_3 and LDH-DEHP containing foams due to their lower dispersion degree. CFD values increased in unfilled foams with increasing E560 content as a consequence of the higher density of these samples. The addition of the different LDH led to a variable behavior, since the addition of LDH to PUF-REF contributed to increase the CFD but in combination with E560, LDH-HPO_4 was the only clay that increased the CFD as a consequence of its exfoliated dispersion, in contrast with LDH-CO_3 and LDH-DEHP which decreased CFD. Moreover, the presence of LDH did not affect strongly the resilience of the foams, but the differences were more evident with increasing E560 content, where the resilience decreased as the dispersion degree of the LDH was finer.

Regarding the thermal properties of the nanocomposite foams, E560 contributed to decrease the thermal stability in the first stage of degradation. However, the presence of LDH counteracted the catalyzing effect of E560 maintaining the initial degradation temperature and the first maximum degradation rate temperature constant while delaying the second stage degradation acting as a barrier against volatile compounds release. Additionally, the presence of LDH, especially those modified with phosphorus, led to the formation of a higher amount of residue. In PCFC studies, the catalyzing effect of E560 in the first stage was confirmed but in contrast, E560 contributed to decrease the PHRR and therefore the THR and HRC. Foams with 100 pphp LB50 and filled with LDH, particularly those modified with phosphorus, also contributed to decrease the PHRR of both degradation stages due to the barrier effect of the anionic clays, while the combination of E560 and LDH decreased the THR and HRC with respect to unfilled foams.

4.5. References

Corcione, C.E., Frigione, M., 2012. Characterization of nanocomposites by thermal analysis. Materials 5, 2960–2980.

Eaves, D., 2004. Flexible polyurethane foam, in: Eaves, D. (Ed.), Handbook of Polymer Foams. Smithers Rapra Publishing, UK, pp. 85–114.

Fan, H., Tekeei, A., Suppes, G.J., Hsieh, F., 2012. Properties of biobased rigid polyurethane foams reinforced with fillers: Microspheres and nanoclay. Int. J. Polym. Sci. 2012, 1–8.

Gaan, S., Liang, S., Mispreuve, H., Perler, H., Naescher, R., Neisius, M., 2015. Flame retardant flexible polyurethane foams from novel DOPO-phosphonamidate additives. Polym. Degrad. Stab. 113, 180–188.

Gao, L., Zheng, G., Zhou, Y., Hu, L., Feng, G., Zhang, M., 2014. Synergistic effect of expandable graphite, diethyl ethylphosphonate and organically-modified layered double hydroxide on flame retardancy and fire behavior of polyisocyanurate-polyurethane foam nanocomposite. Polym. Degrad. Stab. 101, 92–101.

Ge, J., Zhong, W.E.I., Guo, Z., Li, W., Sakai, K., 2000. Biodegradable polyurethane materials from bark and starch. I. Highly resilient foams. J. Appl. Polym. Sci. 77, 2575–2580.

Guo, S., Zhang, C., Peng, H., Wang, W., Liu, T., 2011. Structural characterization, thermal and mechanical properties of polyurethane/CoAl layered double hydroxide nanocomposites prepared via in situ polymerization. Compos. Sci. Technol. 71, 791–796.

Javni, I., Song, K., Lin, J., Petrovic, Z.S., 2011. Structure and properties of flexible polyurethane foams with nano- and micro-fillers. J. Cell. Plast. 47, 357–372.

Kotal, M., Kuila, T., Srivastava, S.K., Bhowmick, A.K., 2009. Synthesis and characterization of polyurethane/Mg-Al layered double hydroxide nanocomposites. J. Appl. Polym. Sci. 114, 2–10.

Liang, K., Shi, S.Q., 2011. Nanoclay filled soy-based polyurethane foam. J. Appl. Polym. Sci. 119, 1857–1863.

Pan, X., Saddler, J.N., 2013. Effect of replacing polyol by organosolv and kraft lignin on

the property and structure of rigid polyurethane foam. Biotechnol. Biofuels 6, 12–29.

Wee, D., Seong, D.G., Youn, J.R., 2004. Processing of microcellular nanocomposite foams by using a supercritical fluid. Fibers Polym. 5, 160–169.

Widya, T., Macosko, C.W., 2005. Nanoclay-modified rigid polyurethane foam. J. Macromol. Sci. Part B Phys. 44, 897–908.

“Without pain, without sacrifice we would have nothing. Like the first monkey shot into space.”

C. Palahniuk. Fight Club. United States: W. W. Norton & Company, 1996.

Chapter 5

5

Flexible polyurethane foams with isocyanate functionalized lignin

5. Flexible polyurethane foams with isocyanate functionalized lignin

5.1. Introduction

This chapter explores the functionalization of a commercial kraft lignin (k-lignin) by means of its reaction of an isocyanate group (NCO) from isophorone diisocyanate (IPDI) with the hydroxyl groups present in lignin (k-IPDI), in order to improve its reactivity for its further incorporation in a flexible polyurethane foam (PUF) formulation. The functionalization is monitorized by Fourier transformed infrared spectroscopy, OH group determinantion and by ^{13}C, ^{1}H and ^{31}P nuclear magnetic resonance.

The effect of the incorporation of k-lignin and k-IPDI in the final properties of flexible polyurethane foams is analyzed as well as their effect in the polymerization process. The density, cell size and lignin attachment to the foam is also studied by gravimetric measurements, optical microscopy and by an extraction process in dioxane, respectively. Additionally, glass transition temperature and the thermal stability measurements of the prepared PUFs are performed by differential scanning calorimetry and themogravimetric analysis and finally, the effect of the unmodified and functionalized lignin in the compressive properties of PUF is studied.

5.2. Experimental procedure

5.2.1. Materials

Southern pine kraft lignin, k-lignin (Domtar's BioChoice^{TM}) was kindly provided by UPM Biochemicals (Finland). K-lignin was acetylated for its further characterization by GPC and ^{13}C NMR, using acetic anhydride (98%, Panreac) and pyridine (99%, Panreac). Ethanol (>99.8%, Panreac), HPLC grade chloroform (>99.8%, Lab-Scan Analytical Sciences) and diethyl ether (99.7%, Panreac) were used in the process of washing the derivatized lignin (ac-lignin).

Additionally, lignin was phosphytilated for ^{31}P NMR analysis. Chromium (III) acetylacetonate (99.9%, Sigma-Aldrich) was used as relaxation agent and cyclohexanol

(Sigma-Aldrich) as reference compound. 2-Chloro-4,4,5,5-tetramethyl-1,3,2-dioxaphospholane (>95%, Sigma-Aldrich) was used as phosphytilation agent.

The functionalization of k-lignin with isocyanate groups was carried out using isophorone diisocyanate, IPDI (>99.5%, Desmodur® I, Covestro), with a NCO content of 37.8%. HPLC grade tetrahydrofuran, THF (>99.8%, Macron Fine Chemicals) was used as reaction medium and dibutyltin dilaurate, DBTDL (>95%, Sigma Aldrich) as selective catalyst for the reaction of hydroxyl groups from lignin with the secondary NCO groups of IPDI (Ono et al., 1985). HPLC grade toluene (>99.8%, Lab-Scan Analytical Sciences) was used to wash the functionalized lignin.

Flexible polyurethane foams were prepared according to the materials and procedure detailed in **Chapter 2** (**Section 2.2**) and **Chapter 3** (**Section 3.2.3**), respectively.

5.2.2. Lignin characterization procedures and techniques

5.2.2.a. Lignin content determination and characterization

The moisture content of the raw lignin was analyzed by TGA (TGA/SDTA 851, Mettler Toledo) in nitrogen atmosphere heating the sample from 25 to 200 °C at a heating rate of 10 °C min^{-1}. This value was confirmed gravimetrically drying the lignin in an oven at 50 °C for 24 h, so as to determine whether this temperature was enough to get a dried lignin at that time. Since the obtained values were similar, the average value of both was reported.

Acid insoluble lignin (AIL) was determined following TAPPI T 249 cm-85 (2009) and TAPPI T 222 om-02 (2011) methods. Briefly, 3.75 mL of ice-cooled 12 M sulfuric acid were added to 0.375 g of dried lignin (Gosselink et al., 2004a) and kept at 30 °C during 1 h. Demineralized water was then added and the mixture was kept boiling at 100 °C for 3 h. The suspension was cooled, filtered with a G4 glass filter and washed with hot water. The resulting solid was weighed after being dried at 105 °C and the filtrate was kept for measuring the acid soluble lignin (ASL) content. ASL was

determined by UV–vis spectroscopy (Dence, 1992) according to the procedure described in **Chapter 2** (**Section 2.3.2**).

The ash content of the kraft lignin was determined following the ASTM E1755-01 (2015) standard. Firstly, the lignin was oven-dried at 105 °C during 24 h. Two samples of approximately 1 g were treated in a muffle furnace at 525 °C during 5 h and the weight of the remaining residue was recorded as the ash content, given relative to the weight of dried lignin. This ash was thereafter used to calculate the acid insoluble ash (AI ash) content for correcting the AIL value following the TAPPI T 245 om-94 standard, adding firstly 20 mL of 65% (w/w) nitric acid to the ash, heating it up and keeping it boiling until having a residual volume of around 10 mL. Then, 4 mL of 96% (w/w) sulfuric acid were added and heated again until white fumes were evolved. The mixture was cooled down to room temperature and finally 50 mL of demineralised water were added and boiled for 5 min. After filtrating, washing and drying, the remaining solid was weighed for correcting the acid insoluble lignin content.

The presence of sugar impurities was evaluated by HPLC as detailed in **Chapter 2** (**Section 2.3.4**). Finally, the approximate hydroxyl number of both k-lignin and k-IPDI was determined following the ISO 14900 (2001) E standard for polyols with steric hindrance, carrying out the acetylation of the sample with a mixture of acetic anhydride and pyridine using imidazole as catalyst. After the acetylation, a back titration was performed with 0.5 N NaOH.

5.2.2.b. Lignin acetylation

The acetylation of lignin was performed following a method proposed by Lundquist (1992) in order to determine its molecular weight by GPC and also to quantify the hydroxyl content by quantitative ^{1}H and ^{13}C NMR. Briefly, 20 mg of **k-lignin** were dissolved in a 1/1 (v/v) acetic anhydride-pyridine mixture and were kept stirring 24 h at room temperature. The washing process was conducted as follows: absolute ethanol was added to the mixture, stirred during 30 min and then removed with a rotary evaporator, repeating this step for seven cycles using the ethanol to drag the pyridine and the acetic acid from the sample. Thereafter the **ac-lignin** was

dissolved in chloroform and added dropwise to diethyl ether, washed three times by centrifugation and dried under vacuum at 50 °C for 24 h.

5.2.2.c. NMR sample preparation

The hydroxyl number of k-lignin was confirmed by quantitative ^{1}H NMR, ^{13}C NMR and ^{31}P NMR, and the success of the functionalization of k-IPDI was qualitatively confirmed by solid state ^{13}C cross-polarization magic angle spinning (CP/MAS) NMR.

The ^{1}H NMR analysis was performed dissolving 22 mg of dried ac-lignin in 1 mL deuterated chloroform ($CDCl_3$, 99.96% atom D, Sigma-Aldrich) and 0.00659 g of 2,3,4,5,6-pentafluoroaldehyde (PFB, 98%, Sigma-Aldrich) were added as reference compound. The signals appearing between 1.6 and 2.2 ppm (aliphatic acetate, related to aliphatic OH) and between 2.2 and 2.6 ppm (aromatic acetate, related to aromatic OH) were integrated with respect to the signal associated to PFB between 10.2 and 10.4 ppm.

The samples for quantitative ^{13}C NMR analysis were prepared as follows. Dried k-lignin and ac-lignin samples were solved in deuterated dimethyl sulfoxide (DMSO-d_6, 99.9% atom D, Sigma Aldrich), weighing 10 mg of solid in 1 mL of solvent. The signals present in ac-lignin at 170.6, 169.9 and 169.1 ppm (corresponding to OH(I), OH(II) and OH(Φ), respectively) were integrated with respect to the aromatic region of lignin assuming the presence of six carbons between 100 and 160 ppm.

^{31}P NMR was performed by phosphytilation of lignin. The sample was prepared according to the procedure proposed by Granata and Argyropoulos (1995). Initially, a solvent mixture of dried pyridine and $CDCl_3$ in a 1.6/1 (v/v) ratio was prepared. A chromium (III) acetylacetonate relaxation agent solution (5 mg mL^{-1}) was prepared using the former solvent mixture. Cyclohexanol was used as a reference for the calculations of the ^{31}P nuclei present in the phosphytilated lignin since it reacts quantitatively with the phosphytilation agent. A solution (10.85 mg mL^{-1}) of cyclohexanol in the solvent mixture was also prepared. Then, the phosphytilated lignin was prepared. Briefly, 0.5 mL of the solvent mixture were added to a flask and 30 mg of dried lignin were added. Afterwards, 50 µL of the phosphytilation agent (2-chloro-

4,4,5,5-tetramethyl-1,3,2-dioxaphospholane) were added and subsequently, 100 µL of both relaxation agent and reference solutions were added. Finally, solvent mixture was added until 1 mL. For calculation purposes it was essential to calculate accurately the amount of lignin and cyclohexanol added. Thus, the integrals of the ^{31}P NMR spectrum were calculated as a function of the intense peak appearing at 145.5 ppm, corresponding to the phosphytilated OH group from cyclohexanol (Argyropoulos, 1994). The values related to aliphatic and phenolic OH contents were compared with those obtained by ^{1}H and ^{13}C NMR spectroscopy.

5.2.3. Preparation of isocyanate functionalized lignin

Kraft lignin was grounded in a mortar and dried at 50 °C for 24 h prior to its functionalization with IPDI. Once dried, k-lignin (20 g) was dissolved in 100 mL of THF using a magnetic stirrer. Afterwards IPDI was weighed into a round bottom flask in a 3/1 NCO/OH molar ratio and heated up to 60 °C under nitrogen atmosphere. Then, DBTDL (0.1% of the total weight) was added to the IPDI and stirred (at 600 rpm) during few minutes, followed by the addition of the lignin solution to the flask using a dropping funnel while maintaining the vigorous stirring in the flask. The reaction was kept at 60 °C for 24 h. Thereafter, the formed solid was separated by centrifugation, washed with toluene and centrifuged repeatedly (at least three times) at 4500 rpm during 5 min, replacing the used toluene for fresh one after each centrifugation in order to remove the remaining unreacted IPDI. Finally, the slurry was dried in a vacuum oven at 75 °C for 24 h and then the vacuum was kept at room temperature for the following 48 h. The obtained k-IPDI was grounded and sieved in order to obtain a homogeneous particle size.

5.2.4. Preparation of flexible polyurethane foams

Two series of flexible polyurethane foams containing the same amount of lignin regardless the isocyanate content of the k-IPDI (which was taken into account to maintain the NCO/OH ratio) were produced, in addition to a reference foam without

lignin (PUF-REF). The lignin content of the foams was set at 3, 5 and 10% (by weight) for both k-lignin (PUF-3%kl, PUF-5%kl and PUF-10%kl) and k-IPDI containing foams (PUF-3%kIPDI, PUF-5%kIPDI, PUF-10%kIPDI). PUF with k-lignin were prepared dissolving previously dried lignin in 50 mL THF. Then, the k-lignin solution was added slowly to the polyol and stirred vigorously during 1 h at room temperature. The THF was then removed using a rotary evaporator until constant mass was achieved. The k-lignin precipitated during THF removal, forming a stable and fine dispersion of the solids in the polyol. Once the k-lignin/LB50 mixture was prepared, the polyurethane foams were manufactured according to the same procedure reported in **Chapter 3** (**Section 3.2.3**) by one shot open mold polymerization, plus a postcuring process at 150 °C for 24 h. After this thermal treatment, the disappearance of free NCO groups was confirmed by FTIR in different regions of the foams. In case of k-IPDI containing samples, the functionalized lignin was introduced directly into the polyol and homogenized by rotor-stator mixing at 12000 rpm during few minutes. All the foams were formulated with the same amount of blowing agent and surfactant than in **Chapters 3** and **4**, but with an excess of 10% of isocyanate (corresponding to an isocyanate index of 110) without taking into account the OH content of the lignin in the formulation owing to its low reactivity.

Nevertheless, the catalyst formulation had to be increased in case of k-lignin containing samples, since the presence of lignin affected the reactivity in the polymerization process hampering the formation of acceptable foams. Thus, amine and organometallic catalyst were adjusted (increasing their amount to 0.5 and 0.6 pphp, respectively, with respect to PUF-REF and k-IPDI containing foams) in order to yield the gelling time quickly enough to avoid the collapse of the foam (Szycher, 2013). Thermal, morphological and mechanical characterization of the foams was performed to postcured samples.

5.2.5. Lignin extraction from the foam

Polyurethane foams containing lignin were subjected to extraction with a mixture of 1,4-dioxane/water (90/10, v/v) to determine to what extent was the lignin

chemically attached to the polymeric matrix. Briefly, around 0.7 g of foam were cut into cubes of approximately 5 x 5 x 5 mm^3 and were placed inside a cellulose cartridge, performing thereafter the extraction with the dioxane/water mixture using a Soxhlet extraction kit during 24 h. The mass of the foams was weighed before and after the extraction process. The procedure was performed once per sample, as a preliminary study of the chemical attachment of the lignins to the matrix. The mass loss related to polyurethane, which was registered in PUF-REF, was corrected in lignin containing foams in order to consider solely the lignin mass loss.

5.3. Results and discussion

5.3.1. Lignin characterization

5.3.1.a. Lignin content determination

The determination of total lignin content was carried out in order to confirm the purity of the k- lignin. The lignin was characterized without further purification than drying in an oven (24 h at 50 °C) owing to its high moisture content (28.43%). **Table 5.1** shows the composition of the k-lignin on a dry basis, reflecting that it was a high purity lignin, reaching nearly a 90% of total lignin content even though having detected a small amount of sodium and sulfur due to its kraft origin, as shown in **Table 5.2**.

Table 5.1. Composition of k-lignin.

	k-lignin
Total lignin content (wt.%)	89.38
AIL	88.27
ASL	1.11
Ash (wt.%)	1.28
AI ash (wt.%)	ND
Sugars (wt.%)	0.79
Arabinose	ND
Glucose	ND
Xylose	0.79
Mannose	ND
$\overline{M}_n$ (g mol^{-1})	3696
$\overline{M}_w$ (g mol^{-1})	7780
PD	2.10

ND: Not detected

Not only was low the sugar impurity content (0.79%), perceiving only the presence of xylose, but also the inorganic impurities (ash content, 1.28%), as it is common in kraft lignins due to the precipitation method from the black liquor.

These values are in agreement with those reported in the literature for other industrial kraft lignins (Gosselink et al., 2004b; Passoni et al., 2016). Regarding the average molecular weight determination of the k-lignin by GPC, it was derivatized to ac-lignin in order to get increased solubility in the mobile phase (THF) (Gellerstedt, 1992). The average molecular weight resulted to be relatively low (7780 g mol^{-1}), whereas the PD of the sample indicated a narrower weight distribution than that usually found in commercial industrial lignin (Sarkanen et al., 1984).

Regarding the functionalization of the k-lignin sample, it was mandatory to quantify the amount of hydroxyl groups in its structure by means of OH number determination by ISO 14900 (2001) E standard. **Table 5.2** shows that the hydroxyl content of the k-lignin was in accordance to those values from other commercial kraft lignins (Cateto et al., 2008). A distinct decrease in the hydroxyl content was registered in k-IPDI as a consequence of the reaction between some of the hydroxyl groups of the lignin with the IPDI, evidencing the different reactivity of the hydroxyls of the lignin depending of their chemical environment. Therefore, the difference between the OH number of k-lignin and k-IPDI showed up that 3.81 mmol OH g^{-1} reacted with isocyanate. The conversion of this OH consumption into nitrogen percentage (5.33%) was in accordance with the nitrogen content obtained by elemental analysis in k-IPDI (5.29%), included in **Table 5.2**.

Table 5.2. Chemical composition and hydroxyl number of k-lignin and k-IPDI.

	k-lignin	k-IPDI
Elemental analysis (wt.%)		
C	64.1	63.37
H	5.80	6.81
N	0.25	5.29
O	29.13	21.22
S	1.78	1.84
Na	0.68	0.01
Total OH content (mmol g^{-1}) according to *ISO14900:2001(E)*	7.33	3.52

5.3.1.b. Structural characterization

FTIR allows distinguishing the most relevant units composing the lignin structure. **Figure 5.1** and **Table 5.3** show the most representative functional group vibrations in the infrared spectrum. The bands appearing at 1269, 1146, 853 and 814 cm^{-1} in k-lignin are the characteristic vibrations of the guaiacyl units (G), common in softwood lignin.

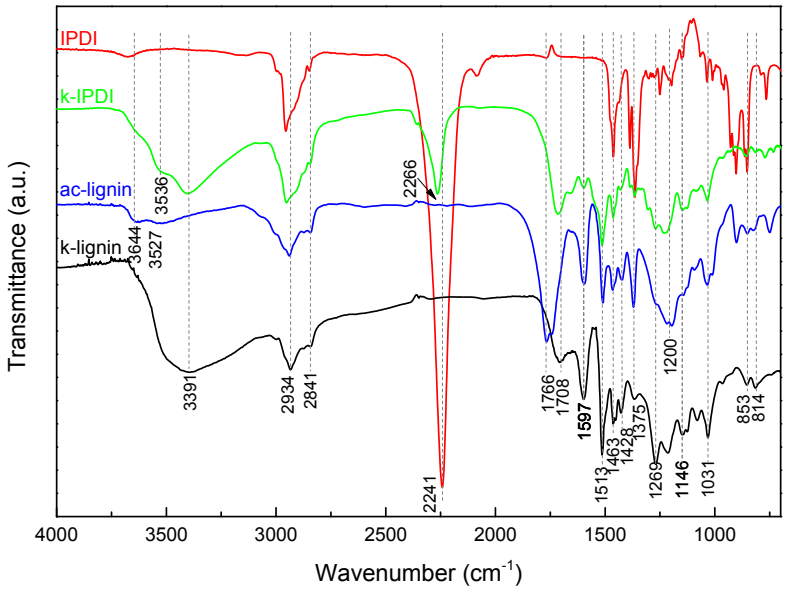

Figure 5.1. Infrared spectra of k-lignin, ac-lignin, k-IPDI and IPDI.

The broad peak corresponding to O-H stretching vibration at 3391 cm^{-1} in k-lignin decreased drastically in ac-lignin corroborating the consumption of hydroxyl groups during its chemical treatment. The broad O-H peak appearing as an average of the hydrogen bonded and free hydroxyl groups in the unmodified lignin, was replaced by two low intensity peaks at around 3644 and 3527 cm^{-1}, reflecting non-hydrogen bonded aliphatic and phenolic OH groups (Stuart, 2004). Moreover, the appearance of an intense peak at 1766 cm^{-1} with a shoulder at 1740 cm^{-1} corresponding to aliphatic and aromatic C=O stretching vibration respectively, and a broad signal around 1200 cm^{-1} related to C-O-C and C-C stretching vibrations in esters, confirmed the successful acetylation of k-lignin.

Table 5.3. k-lignin, ac-lignin and k-IPDI functional groups and their respective wavenumber.

Functional group	k-lignin Wavenumber (cm^{-1})	ac-lignin Wavenumber (cm^{-1})	k-IPDI Wavenumber (cm^{-1})
Free aliphatic and aromatic O-H str	-	3644, 3527	3644, 3536*
O-H str	3391	-	3391
N-H str	-	-	3391
C-H str in methylene (-CH_2-)	2934	2934	2951
C-H str in methyl (CH_3-)	2841	2841	2848
NCO str	-	-	2266
C=O str (aliphatic)	-	1766	-
C=O str (aromatic)	-	1740	-
C=O str of fatty esters, unconjugated ketones, carbonyls and ester groups	1708	-	1712
Urethane C=O str	-	-	1712
C-H aromatic ring skeletal vibration and C=O str	1597	1597	1597
C-H aromatic ring skeletal vibration	1513	1513	1513
C-H asymmetrical deformation in -CH_2- and CH_3-	1463	1463	1463
Aromatic ring skeletal vibrations, C-H in-plane deformation	1428	1428	1428
Phenyl -OH, aliphatic str in -CH_3	1375	1375	1375
G ring breathing and C=O str	1269	1269	1269
C-O-C and C-C str	1211	1200	1224
Aromatic C-H in plane deformation (typical from G units)	1146	1146	1146
Aromatic C-H in plane deformation, -OH deformation in primary alcohols and unconjugated C=O str	1031	1031	1031
C-H out of plane in 2, 5 and 6- positions of G units	853, 814	853, 820	853, 814

*Shoulder

The functional group content per lignin empirical C_9 unit formula was estimated by means of NMR spectroscopy (**Figure 5.2**). This formula is an approximation calculated to give an idea of the functional groups available in the C_9 structural unit of lignin. Quantitative ^{13}C NMR spectroscopy, with a wider spectral width and better resolution than ^{1}H NMR, allowed reporting the functional groups per aromatic ring in k-lignin, distinguishing primary, secondary and phenolic hydroxyl groups in acetylated lignin samples (Faix et al., 1994). The value of the signal integration can be considered as mol% and its conversion to mmol g^{-1} required the estimation of the empirical C_9 unit formula of k-lignin in order to compare the NMR results with the OH number determined by titration following the ISO 14900 (2001) E standard.

Therefore, the estimation of the empirical C_9 unit formula, collected in **Table 5.4**, was calculated according to the values obtained by elemental analysis and the methoxyl group (OCH_3) content calculated by the integration of the signal at 56.6 ppm of the ^{13}C spectrum of k-lignin.

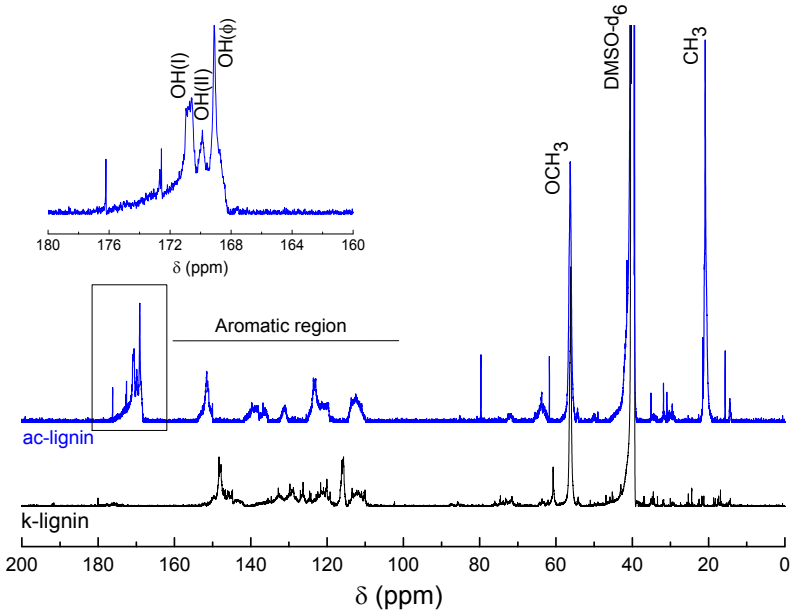

Figure 5.2. ^{13}C NMR spectra of unmodified (k-lignin) and acetylated lignin (ac-lignin).

Table 5.4. C_9 empirical formula estimation by elemental analysis results and ^{13}C NMR.

	k-lignin	k-IPDI
C_9 unit formula*	$C_9H_{8.28}S_{0.10}O_{2.58}(OCH_3)_{0.74}$	$C_9H_{10.84}S_{0.11}O_{1.14}(OCH_3)_{0.77}(NHCO)_{0.38}(NCO)_{0.38}$
C_9 unit Mw (g mol^{-1})	184	193

*C_9 unit formula of k-IPDI was calculated assuming that the same amount of OCH_3 in k-lignin, calculated by ^{13}CNMR, was present in k-IPDI sample, and that only half of the nitrogen present reacted with the hydroxyl groups from lignin.

The value of the integrations of methoxyl, carbonyl and carboxyl groups calculated in k-lignin (number of carbon atoms per C_9 unit) together with the values corresponding to the OH(I), OH(II) and OH(Φ) content calculated in the carbonyl region of ac-lignin, are shown in **Table 5.5.**

^1H NMR spectrum of ac-lignin (**Figure 5.3**) was recorded aiming to confirm the aliphatic and phenolic hydroxyl content of k-lignin determined by ^{13}C NMR (**Figure 5.3**). ^{31}P NMR was also performed (**Figure 5.4**) since it allows discerning the aliphatic and the different types of phenolic hydroxyl groups in lignin, such as condensed phenolic,

guaiacyl (G), syringyl (S) and *p*-hydroxyphenyl (H) units. The integrals of the peaks of the ^{31}P NMR spectrum were calculated as mentioned before, as a function of the intense peak appearing at 145.5 ppm. The values related to total aliphatic and phenolic OH contents were in accordance with those obtained by ^{1}H and ^{13}C NMR spectroscopy, and additionally it was evidenced that guaiacyl hydroxyl groups were predominant in k-lignin due to its softwood origin.

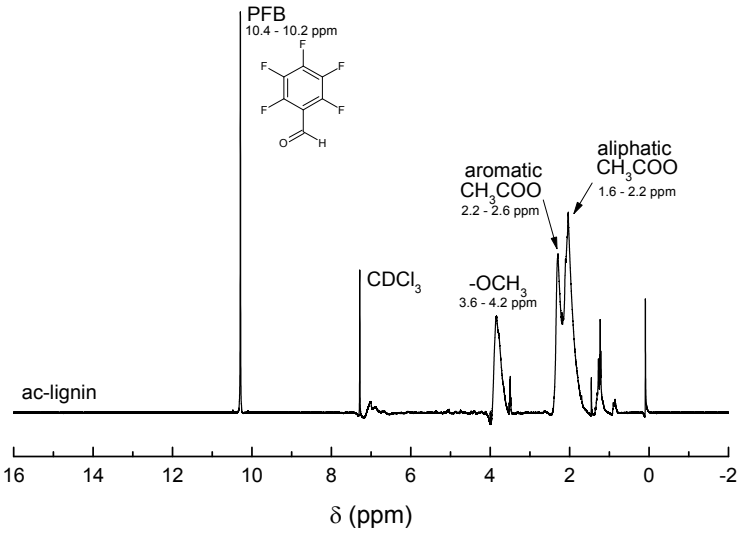

Figure 5.3. ^{1}H NMR spectrum of acetylated lignin (ac-lignin).

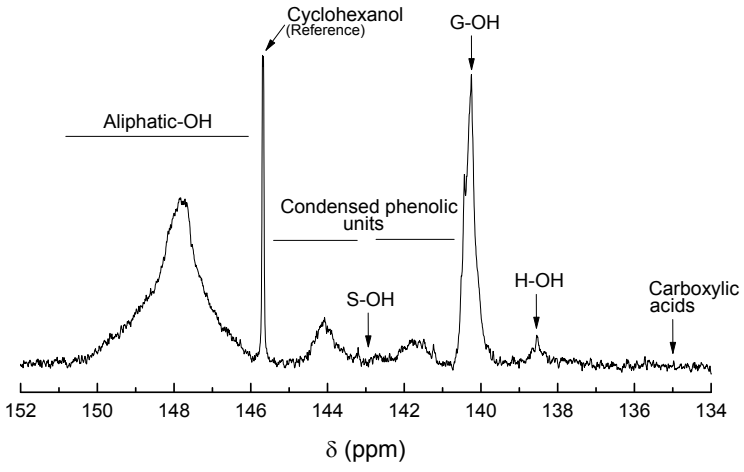

Figure 5.4. ^{31}P NMR spectrum of phosphytilated lignin.

Table 5.5. k-lignin functional group content determination by quantitative ^{13}C NMR, ^{1}H NMR and ^{31}P NMR.

	Functional group		δ (ppm)	C atoms per C_9 unit	Amount in lignin (mmol g^{-1})
^{13}C NMR	COOH and CHO		160-200	0.01	0.054
	Total OH		168-178	1.28	6.957
	OH(ϕ)		168-169.9	0.46	2.500
	OH(aliphatic)		169.9-172	0.82	4.456
	OH(I)		*170.3-172*	*0.59*	*3.207*
	OH(II)		*169.9-170.3*	*0.23*	*1.250*
	OCH_3		55.4-58	0.74	4.022
			Integral value		
^{1}H NMR	OCH_3		3.6-4.2	8.50	4.098
	Total OH		1.6-2.6	-	6.869
	OH(ϕ)		2.2-2.6	4.61	2.225
	OH(aliphatic)		1.6-2.2	9.62	4.644
^{31}P NMR	COOH		134.0-136.0	ND	ND
	Total OH		-	-	6.526
	OH(ϕ)	OH(H)	138.0-139.0	0.35	0.125
		OH(G)	138.0-141.0	4.17	1.490
		OH(S)	142.5-143.5	ND	ND
		OH(condensed)	141.0-142.5	2.11	0.754
		Total OH(ϕ)	138.0-145.0	6.63	2.37
	OH(aliphatic)		146.0-150.5	11.63	4.156

ND: Not detected

The molecular weight value obtained per C_9 unit (**Table 5.4**) was in accordance with the values reported for other softwood kraft lignins, which are usually around 180 g mol^{-1} (Crestini, 2012). The total hydroxyl content calculated by ^{13}C NMR (6.96 mmol g^{-1}) approached the value obtained by titration (7.33 mmol g^{-1}). These values were similar to those reported by Cateto et al. (2008) for another commercial kraft lignin, although in their case the phenolic OH content was higher (3.95 mmol g^{-1}). The aliphatic OH content in k-lignin was nearly twice times the amount of phenolic OH (often referred as the reactive group of lignin) (Paulsson and Simonson, 2002), being primary OH more abundant than secondary ones.

The absence of signals corresponding to syringyl (S) units between 103 and 105 ppm (C-2, C-6 from S), and between 152 and 153 ppm (C-3 and C-5 from 4-O-alkylated S group) confirmed the predominant presence of guaiacyl (G) units, as it was expected owing to the softwood origin of k-lignin. These characteristic signals from carbons related to G units appeared in the aromatic region of the ^{13}C NMR spectrum (**Figure 5.2**), between 100 and 160 ppm. The lignin functionalization with IPDI was confirmed qualitatively by ^{13}C CP/MAS NMR spectroscopy (**Figure 5.5** and **Table 5.6**).

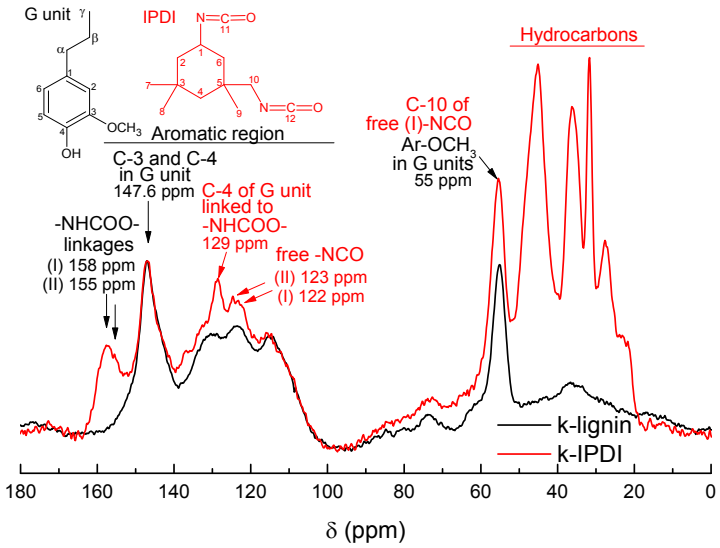

Figure 5.5. ^{13}C CP/MAS NMR spectra of k-lignin and k-IPDI.

Table 5.6. ^{13}C CP/MAS NMR spectra signal assignments.

Sample	δ (ppm)	Assignment
k-IPDI	157.6	Secondary urethane linkage
	155.2	Primary urethane linkage
	146.9	Superposition C-3 and C-4 of G unit
	129.1	C-4 of G unit connected to -NHCOO-
	123.1	Free secondary -NCO
	122.4	Free primary -NCO
	56.6	Superposition aromatic -OCH_3 in G + primary carbon (C-10) of unreacted -NCO from IPDI
	45.1	Carbon attached to secondary isocyanate (C-1) from IPDI C-1 from unreacted secondary -NCO C-10 from reacted primary -NCO C-2 and C-4 (-CH_2) from IPDI C-1 and C-6 from reacted secondary -NCO
	36.2	-CH_2- (C-6) from IPDI
	31.7	CH_3- (C-7 and C-8) from IPDI
	27.6	CH_3- (C-9) from reacted primary NCO
	23.1	CH_3- (C-9) from unreacted primary NCO
k-lignin	147.0	Superposition of signals: C-4 in G etherified unit C-3 in G non-etherified unit
	55.1	Aromatic methoxyl (-OCH_3) from G units

The appearance of new signals between 20 and 70 ppm corresponded to hydrocarbons of the isocyanate structure, whereas the reaction between the isocyanate and the hydroxyl groups from lignin was evidenced by the appearance of new signals corresponding to urethane (-NHCOO-) linkages at 155.2 and 157.6 ppm (secondary and primary urethane linkages, respectively). The new signal appearing at 129.1 ppm was attributed to C-4 from G unit connected to -NHCOO-.

The availability of free isocyanate groups for further reaction with the matrix was confirmed by the appearance of new signals at 122.4 and 123.1 ppm, corresponding to free primary and secondary NCO groups, respectively (Bialas et al., 1990), superimposed with the signals corresponding to aromatic carbons in lignin.

5.3.1.c. Morphology and particle size

As it can be observed in **Figure 5.6**, k-IPDI is perfectly discernible from k-lignin, as the former presents a yellowish color and looser texture. SEM images (**Figure 5.6**) revealed that k-IPDI presented lower particle size than the unmodified k-lignin, probably due to changes in surface energy as a consequence of the modification with isocyanate, as it was suggested by Chauhan et al. (2014).

Figure 5.6. Images and SEM micrographs of dried k-lignin (left) and k-IPDI (right). SEM micrographs with x10000 magnification.

Nevertheless, the particle size of k-lignin was not relevant since it was added to the polyurethane formulation as a solution in THF, removing afterwards the solvent and keeping the k-lignin solved in the polyol. But in case of k-IPDI the particle size, ranging from 400 to 700 nm was significant as it was found to be insoluble in organic solvents and had to be added to the polyurethane formulation by direct mixing with the polyol.

5.3.1.d. Thermal properties

The effect of isocyanate functionalization on the glass transition temperature (T_g) of lignin was analyzed by DSC. **Figure 5.7** shows the DSC thermograms of IPDI, k-lignin and k-IPDI. The T_g of k-lignin was found to be 151.2 °C, which was consistent with the reported values from other commercial kraft lignins (Gellerstedt, 2015; Lora, 2008).

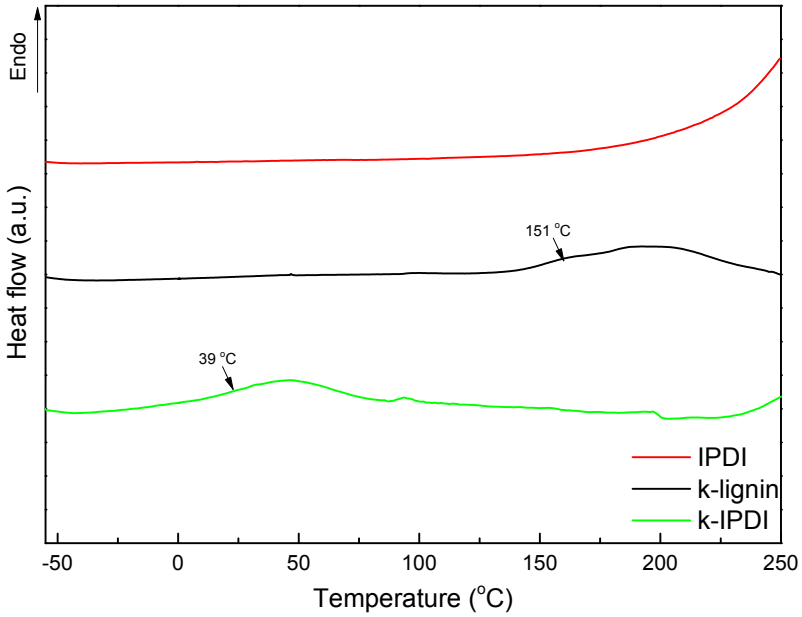

Figure 5.7. DSC thermograms of IPDI, k-lignin and k-IPDI.

Nevertheless, it was observed that the T_g in k-IPDI was shifted 112 °C below the T_g of the unmodified lignin, resulting in a T_g of 39.2 °C. This was attributed to the introduction of the urethane linkages that increased the mobility of the lignin structure as a consequence of the lower hydroxyl content, which resulted in the reduction of hydrogen bonding. Other works suggested that derivatization of lignin decreased the

Tg value due to a plasticization effect of the derivatization process (Lisperguer et al., 2009).

Table 5.7. Glass transition, degradation temperatures, mass loss and residue at 800 °C of k-lignin and k-IPDI.

	T_g (°C)	T_{max} (°C)	Mass loss (wt%)	Residue (wt%)
k-lignin	151.2	386	60.15	39.87
k-IPDI	39.2	333	74.83	25.04

$T_{max:}$ temperature at maximum degradation rate.

Figure 5.8 shows the thermal degradation of lignin under inert atmosphere, which was broader than that of the IPDI that presented a sharp mass loss at 221 °C. This was attributed to the different groups and heterogeneous molecular weight moieties forming the complex lignin structure. **Figure 5.8** and **Table 5.7** show that the degradation of k-lignin occurred between 300 and 400 °C as a consequence of the cleavage of C-C and β-β linkages of lignin's main structure (Ferry et al., 2015). The rearrangement of the lignin backbone occurred from 450 °C, giving place to high yields of char (39.87% in k-lignin). The maximum degradation temperature was shifted 53 °C towards lower temperatures in k-IPDI as a consequence of the combined degradation of the urethane linkages formed between the isocyanate and the lignin. Despite the previous drying of k-lignin and the organic modification of k-IPDI, some amount of moisture was lost between 65 and 105 °C (2 and 3%, respectively).

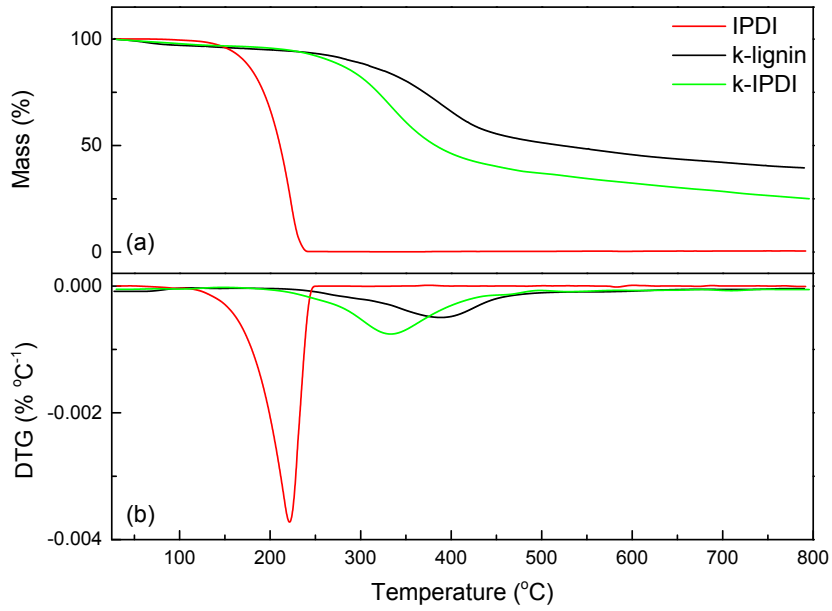

Figure 5.8. Mass loss (up) and first derivative (down) curves of IPDI, k-lignin and k-IPDI.

The lack of residue in the degradation of IPDI contributed to decrease the residue of k-IPDI by 37% with respect to k-lignin. Hence, the functionalization of lignin produced a decrease on its thermal stability.

5.3.2. Characterization of flexible polyurethane foams

5.3.2.a. Effect of lignin in polymerization

The effect of the presence of k-lignin and k-IPDI in the reactivity of the polyurethane foam formation was studied by FTIR (**Figure 5.9**), calculating the area of the remaining isocyanate stretching vibration at 2276 cm^{-1} 24 h after the polymerization, and normalizing it with respect to the signal of a group that did not take part into the polymerization process, *e.g*. the C=C aromatic stretching vibration at 1598 cm^{-1}. The area of this band was deconvoluted and calculated in PUF-REF and was taken as a reference, since the lignin contributed also with C=C groups. **Table 5.8** shows NCO/C=C ratio and the timings of the different steps of the foaming process, as well as the maximum height of the final foams.

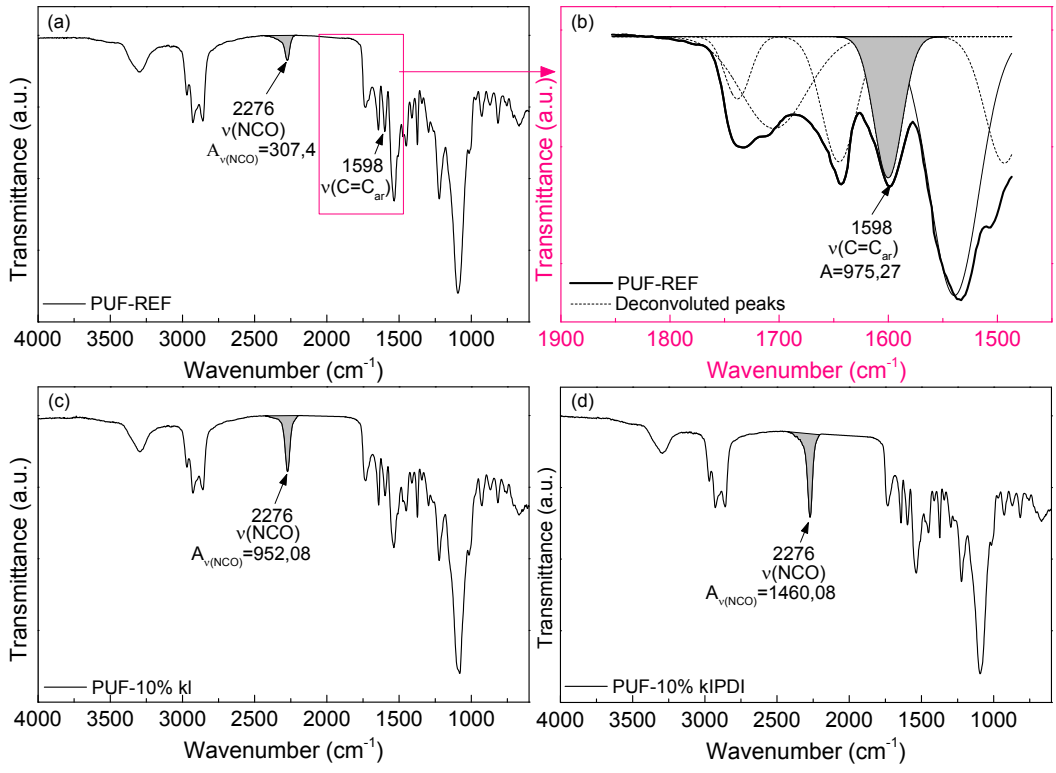

Figure 5.9. Infrared spectra of PUF-REF (a), deconvolution of the aromatic C=C band in PUF-REF (b), PUF-10%kl (c) and PUF-10%kIPDI (d).

Table 5.8 evidenced that the timings of the different foaming stages increased when both unmodified and IPDI-modified lignin were added to the foam, suggesting that its complex structure hindered the reaction between the hydroxyl groups of the polyol and the isocyanate, as it was also appreciated in the increased NCO/C=C ratio.

Comparing the timings between k-lignin and k-IPDI containing foams, it was mandatory to take into consideration that the used catalyst quantity had to be increased in case of k-lignin containing foams to avoid the collapse of the structure, as a consequence of the decreased polymerization rate caused by the presence of lignin. The effect of this higher catalyst content was clearly observed in the lower cream, rise and gel time values as well as lower NCO/C=C ratios at low k-lignin content, since this accelerating effect was lost at 10% k-lignin content.

Table 5.8. Reaction times of the different stages in the foaming process and NCO/C=C ratio.

Sample	Cream time (s)	Rise time (s)	Gel time (s)	Tack-free time (h)	Max. height (mm)	Area ν(NCO/C=C)
PUF-REF	7	83	160	2.00	98	0.315
PUF-3%kl	11	88	167	3.00	88	0.709
PUF-5%kl	15	124	260	4.50	84	0.869
PUF-10%kl	23	225	859	6.00	73	0.976
PUF-3%kIPDI	20	125	300	3.83	95	0.969
PUF-5%kIPDI	24	163	310	4.25	87	0.973
PUF-10%kIPDI	26	168	632	5.83	75	1.497

The use of this catalyst formulation in k-IPDI containing foams caused their shrinkage due to the exceeding catalyst content, so it was expected that if it could be possible to prepare foams with the same catalyst formulation, the timings of the k-lignin containing ones would be much higher than those containing k-IPDI.

5.3.2.b. Density, cell size and lignin attachment to the foam

Density is a key parameter in the final properties of the materials, since the mechanical properties depend directly apart from the nature of the material, on the amount of the material available and its distribution along the cellular structure. **Table 5.9** shows that despite all foams were prepared using the same blowing agent amount, meaning that the same amount of CO_2 was generated during the foaming process, the

addition of either k-lignin or k-IPDI contributed to increase the density of the foams. As it was mentioned before, the addition of lignin increased the gelling time that could lead to the loss of CO_2 during the polymerization, resulting in structures with smaller cells and thicker walls, yielding higher density values as it was reported by Mahmood et al. (2015). The lower size of the cells and the higher width of the struts were attributed to the increase in the viscosity of the polyol-lignin mixture, being the values in accordance with the density values, as they contained more material in the same volume. It was noteworthy that in general the density and the average cell size and strut width values evolved in the same extent regardless of the type of lignin, having slightly higher average cell size values in case of k-IPDI containing foams, probably due to its higher reactivity.

Table 5.9. Density, average cell size, strut width, open cell content, viscosity of the polyol-lignin mixture and mass loss after extraction of the k-lignin and k-IPDI containing foams.

Sample	Density (kg m^{-3})	Average cell size (μm)	Average strut width (μm)	Open cell content (%)	Viscosity of the polyol-lignin mixture (mPa s)	Mass loss after extraction (wt.%)
PUF-REF	32.4 ± 0.8	215.7 ± 58.3	39.7 ± 7.5	21.7 ± 0.6	837	-
PUF-3%kl	32.3 ± 0.2	202.5 ± 65.6	59.5 ± 12.0	30.3 ± 1.5	1265	0.48
PUF-5%kl	36.2 ± 0.3	197.1 ± 51.0	63.7 ± 11.7	32.7 ± 2.1	1458	3.31
PUF-10%kl	42.2 ± 0.3	176.5 ± 59.3	89.4 ± 25.0	36.0 ± 4.3	1837	3.85
PUF-3%kIPDI	34.5 ± 0.9	220.1 ± 59.3	55.9 ± 8.7	49.2 ± 2.5	1283	0.53
PUF-5%kIPDI	36.9 ± 0.6	233.6 ± 62.1	66.7 ± 14.4	54.7 ± 4.2	1743	1.02
PUF-10%kIPDI	41.8 ± 0.7	204.2 ± 53.2	88.0 ± 18.3	55.7 ± 1.5	3497	1.12

Figure 5.10 shows SEM images of foam sections perpendicular to the growth (**Figure 5.10a**) and also in growth direction (**Figure 5.10b**). It was observed that the cellular structure of the reference foam was formed by both small and large voids with thin struts. Also, the cells were slightly larger in the growth direction, denoting that the foam rise took place rapidly giving place to elongated cells. This oriented effect was hindered in foams containing lignin, where more homogeneous pores and wider struts were observed, which could be attributed to the higher viscosity of the part B reactant mixture. It shall be noted that the k-IPDI containing foams presented more voids in their walls suggesting the presence of more open cells. This higher open cell content was confirmed by measuring the air passing through the structure of the foam, as

shown in **Table 5.9**. Both k-lignin and k-IPDI containing foams presented higher open cell content than PUF-REF, since lignin particles acted as a breaking point of the cell walls. Notwithstanding, k-IPDI containing foams show more open cells than unmodified lignin containing ones. This could be owing to the fact that k-lignin was introduced in the formulation in solution with THF, resulting in a more homogeneous distribution of the lignin in the matrix, while k-IPDI was introduced by dispersing the solid into the polyol. The presence of these coarser distributed solid particles could enhance in a higher extent the breakage of the walls.

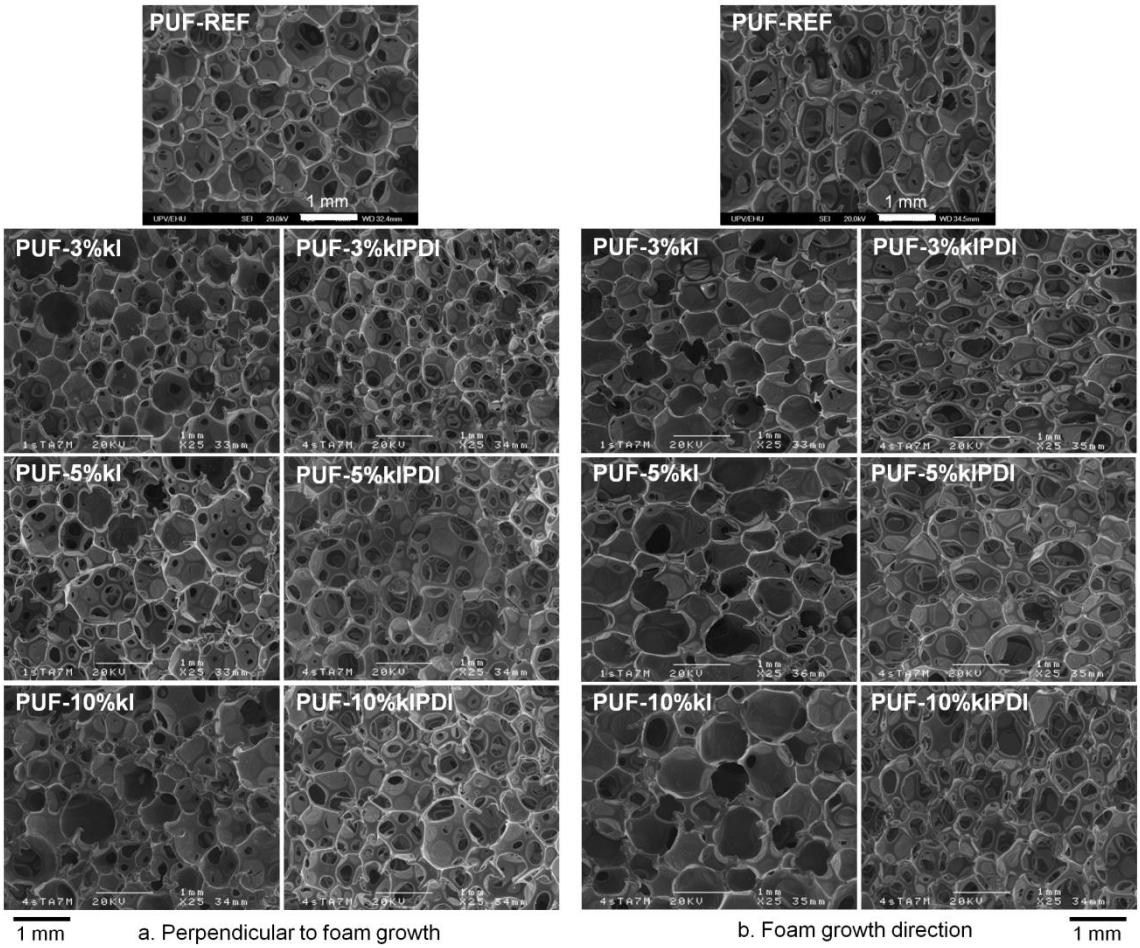

Figure 5.10. SEM micrographs of the sections perpendicular (a) and parallel (b) to foam growth, of PUF-REF and foams containing k-lignin and k-IPDI.

The interaction between lignin and polyurethane matrix was determined extracting foams with a dioxane/water (9/1, v/v) mixture, which is a good medium for dissolving lignin. The PUF-REF mass loss after the extraction was registered in order to take into account only the lignin mass loss in the k-lignin and k-IPDI containing foams

as shown in **Table 5.9**. It was observed that in both k-lignin and k-IPDI, the extracted lignin content was lower than the added. This suggested that part of the k-lignin was also chemically linked to the polyurethane matrix, but in lesser extent than k-IPDI, as a consequence of the isocyanate groups anchored to k-IPDI. These results suggested that the presence of isocyanate groups in lignin increased its reactivity. Moreover, the chemical linkage of the lignin would prevent it from migration during its application.

5.3.2.c. Thermal properties

The determination of the glass transition temperature was performed by DSC. **Table 5.10** and **Figure 5.11** thermograms show the T_g of the different polyurethane foams, which were in accordance with T_g values reported before for flexible PUF (Herrington and Hock, 1998).

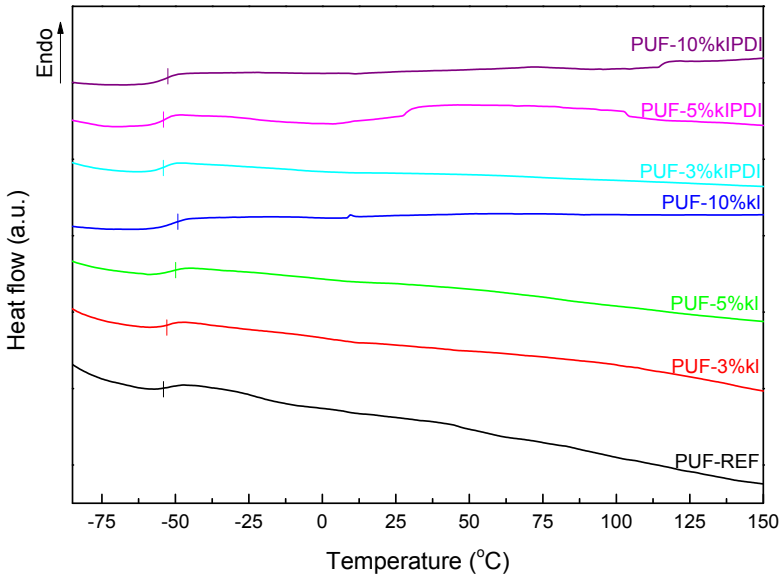

Figure 5.11. DSC thermograms of PUF-REF and foams containing k-lignin and k-IPDI.

The presence of k-lignin yielded to slightly higher T_g values, in the same way as it was reported elsewhere (Wang et al., 2013; Yoshida et al., 1990). This effect was attributed to the fine dispersion of k-lignin in the polyurethane matrix as a consequence of its introduction in THF solution into the formulation. This finer dispersion, together with the higher T_g of k-lignin, could have caused the increase of the T_g of k-lignin containing foams as a result of the increased interaction between

lignin and the matrix. In contrast, the rougher dispersion of k-IPDI through the matrix and its lower T_g value, which was reflected in a slight decrease in the T_g of the k-IPDI containing foams.

Table 5.10. Glass transition, degradation temperatures and residue at 800 °C of the prepared polyurethane foams.

Sample	T_g (°C)	T_{onset} (°C)	T_{max1} (°C)	T_{max2} (°C)	Residue (wt.%)
PUF-REF	-53.0	266.7	296.6	396.6	0.00
PUF-3%kl	-52.6	269.1	298.6	392.5	1.97
PUF-5%kl	-51.6	269.9	299.5	395.3	3.73
PUF-10%kl	-50.8	262.2	294.8	396.1	5.52
PUF-3%kIPDI	-54.1	267.4	293.8	399.4	1.89
PUF-5%kIPDI	-54.2	268.6	296.9	400.8	3.23
PUF-10%kIPDI	-53.6	267.9	293.9	402.6	4.85

T_{onset}: Temperature at 5% mass loss.

T_{max1} and T_{max2}: Maximum degradation rate temperature of first and second stages, respectively.

The thermal stability of the flexible polyurethane samples was analyzed by TGA (**Figure 5.12)** and the most characteristic values are included in **Table 5.10**. The addition of lignin did not change the thermal degradation mechanism, which took place in two stages regardless of the presence of both types of lignin. The first degradation step corresponded to the degradation of the isocyanate-urea related domains whereas the second step was attributed to the decomposition of the soft domains, which are related to the polyol.

T_{onset} shifted slightly towards higher temperatures in case of PUF containing k-lignin at the lowest content, probably due to the stabilizing effect of the lignin distributed along the polyurethane matrix, whereas it remained practically unaltered in case of k-IPDI containing foams. In regard of the first stage maximum degradation temperature (T_{max1}), it decreased in k-IPDI containing foams, as it was expected from the previous TGA analysis of k-IPDI, since it presented lower thermal stability than k-lignin, which contributed to delay between 2 and 3 °C the first degradation of PUF. Moreover, it should be noted that the mass loss related to this step decreased in both kinds of lignin containing foams, being function of the lignin content.

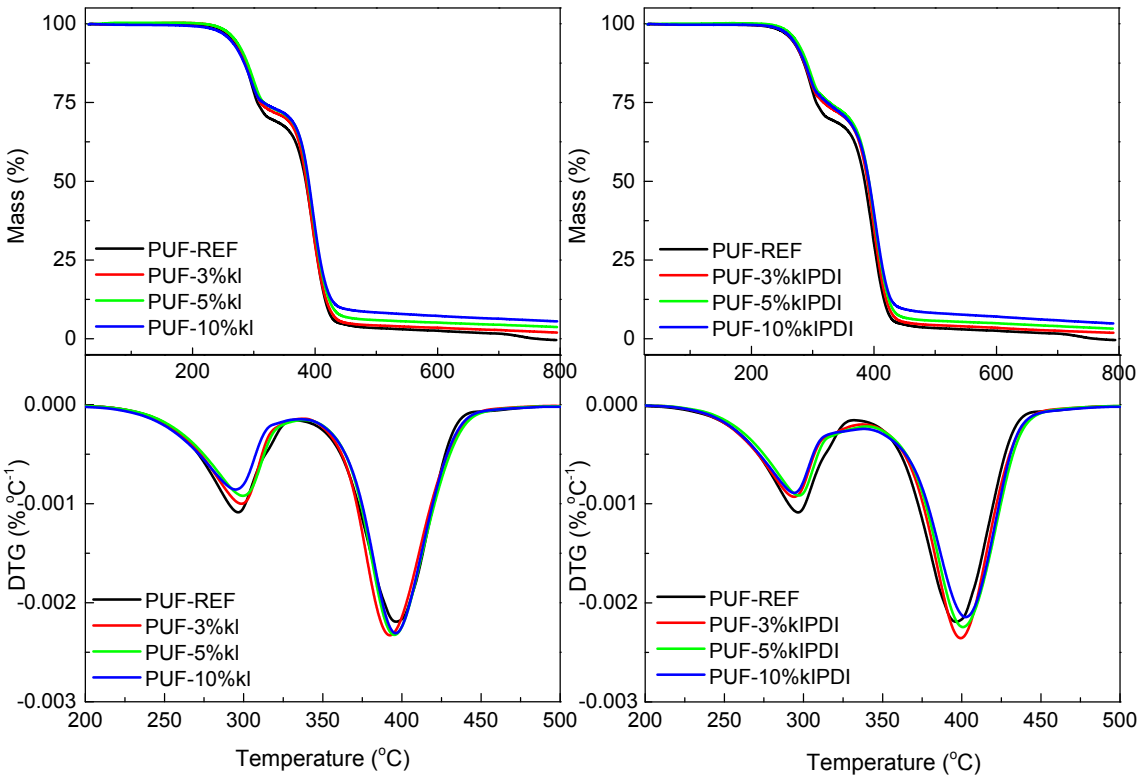

Figure 5.12 Mass (top) and first derivative (bottom) curves of the reference and k-lignin and k-IPDI containing foams.

Despite the presence of k-IPDI did not contribute to improve the thermal stability of the first stage of degradation, the chemical attachment of the lignin with the polymeric matrix contributed to increase up to 6 °C the maximum mass loss rate in the second stage. In relation to the residue, more quantity was formed with increasing lignin content as it was expected; in greater extent in case of k-lignin (5.52% in case of PUF-10%kl) than k-IPDI(up to a 4.85% in case of PUF-10%kIPDI) owing to the low thermal stability of the urethane-urea linkages formed between the isocyanate modified lignin.

5.3.2.d. Mechanical properties

The capacity of the foam to absorb elastic energy and to recover its original shape after being deformed was measured as resilience. The obtained resilience values are shown on **Table 5.11** and demonstrated that the addition of k-lignin yielded to less resilient, *i.e.* more viscoelastic foams, and which needed more time to recover their original shape. Apart from other parameters, resilience could be related to the density

of the foam; therefore those with lower density would take less time to recover (Mills et al., 2009). This was fulfilled in case of k-lignin containing foams, which resilience decreased at higher density (and higher lignin content). In case of k-IPDI filled foams, the resilience decreased a 15% with respect to PUF-REF when adding a 3% k-IPDI and remained practically constant with increasing k-IPDI content, in spite of their higher density. This effect was also observed in **Chapter 4** in foams containing LDH and E560, suggesting that reactive modifiers such as E560 or k-IPDI could affect the crosslink density, thus showing lower resilience values.

On the other hand, firmness of the foam was studied by CFD test, which together with the density is one of the most important characteristics of the flexible foams. **Table 5.11** shows that the addition of lignin to the cellular polyurethane caused an increase in the CFD of the foams. Unmodified lignin containing foams resulted to be more rigid than those containing k-IPDI due to the rougher particle dispersion.

Table 5.11. Mechanical properties of the prepared flexible polyurethane foams. Specific compressive stress is given at 10% strain and energy absorption per volume unit at 50% strain.

Sample	Resilience (%)	CFD (kPa)	Specific compressive stress (kPa kg^{-1} m^3)	Specific elastic modulus (kPa kg^{-1} m^3)	Energy absorption / volume (J m^{-3} 10^{-2})
PUF-REF	45.8 ± 1.1	4.46 ± 0.33	0.10	3.05	192.97
PUF-3%kl	40.0 ± 0.8	6.06 ± 0.33	0.11	2.36	200.71
PUF-5%kl	34.8 ± 0.9	6.81 ± 0.10	0.14	2.86	250.27
PUF-10%kl	33.3 ± 0.3	9.51 ± 0.15	0.13	3.17	312.23
PUF-3%kIPDI	39.1 ± 0.3	4.59 ± 0.41	0.11	2.29	172.09
PUF-5%kIPDI	38.9 ± 0.8	5.21 ± 0.13	0.06	1.82	120.74
PUF-10%kIPDI	38.7 ± 0.3	5.53 ± 0.29	0.03	1.58	103.33

The compressive stress-strain curves (**Figure 5.13a**) of the lignin containing foams evidenced that those containing k-lignin presented higher elastic modulus than PUF-REF, having the highest modulus at a k-lignin load of 10%. The opposite effect was observed in k-IPDI containing foams, presenting modulus below that of the PUF-REF, being especially low in case of 10% k-IPDI containing sample. Nevertheless, in order to avoid the effect of the density in the compressive characteristics of the foams, the specific compressive stress at 10% strain and the specific compressive modulus were calculated (**Table 5.11**).

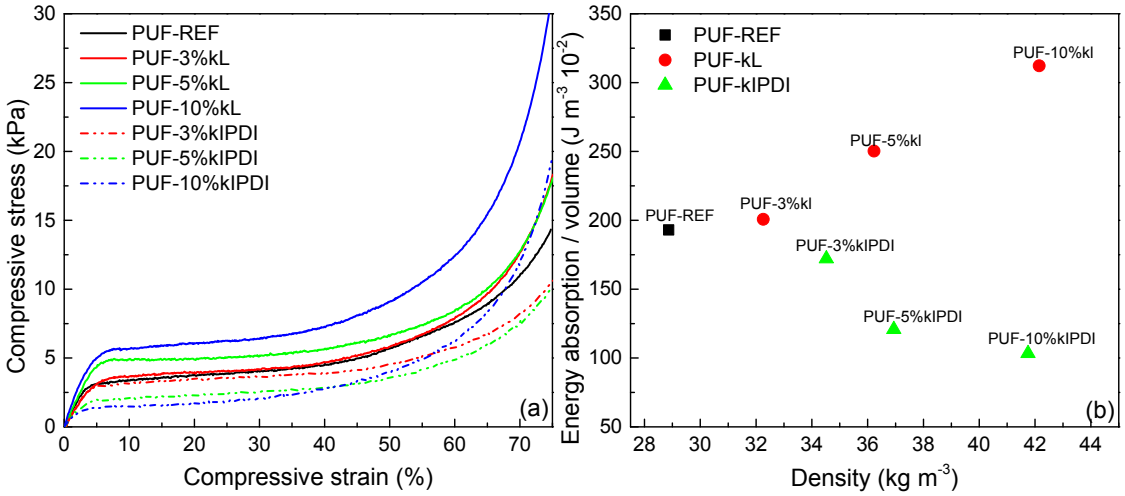

Figure 5.13. Compressive stress-strain curves (a) and energy absorption capability according to density (b) of reference and foams containing k-lignin and k-IPDI.

The trend followed by the CFD values was confirmed with higher specific compressive stress values than PUF-REF in case of k-lignin containing foams. The specific modulus did not change much when using k-lignin with respect to PUF-REF, but did present a growing trend at higher k-lignin content, whereas more flexible foams were obtained using k-IPDI, presenting lower specific compressive stress at 10% strain and lower specific modulus than PUF-REF, which could be related to the lower crosslink density of k-IPDI containing foams. Additionally, the energy absorption per unit volume of foam (toughness) was calculated as the area below the stress-strain curves until 50% deformation. This parameter is critical in applications involving safety, such as seat cushioning in automotive industry, where the foam acts as a passive protective element for the dissipation of the energy absorbed during the impact. **Figure 5.13b** shows the different trend followed by foams containing k-lignin and k-IPDI.

The higher stiffness of k-lignin containing foams provided with higher energy absorption capacity with increasing lignin content, while k-IPDI containing samples presented a lower area under the curve due to their higher flexibility, thus having a lower ability to absorb energy. This was because k-lignin acted as a filler, whereas k-IPDI acted as a reactive filler that interfered with foam crosslinking.

5.4. Conclusions

A commercial softwood kraft lignin (k-lignin) was successfully functionalized with an aliphatic diisocyanate (IPDI) in order to increase its chemical attachment to a flexible polyurethane foam matrix. Approximately half of the hydroxyl groups present in lignin reacted with IPDI, as it was suggested by the OH consumption determined in k-IPDI by the ISO 14900:2001(E) standard, which was in agreement with the nitrogen content detected by elemental analysis. Its functionalization was also confirmed by FTIR and ^{13}C CP/MAS NMR spectroscopy, through the appearance of new signals related to urethane groups and free isocyanate groups. Thermogravimetric analyses also showed that the degradation of k-IPDI occurred in one stage, having a maximum degradation temperature intermediate to that of k-lignin and neat IPDI.

Moreover, flexible polyurethane foams containing 3, 5 and 10% of lignin were successfully manufactured. It was observed that the presence of lignin hindered the foam formation increasing the times for each stage of the foaming process with higher lignin contents. This was more pronounced in case of k-lignin containing foams which needed more catalyst amount in order to avoid the foam collapse due to the slower polymerization caused by the presence of lignin. Density increased in both k-lignin and k-IPDI containing foams, regardless the type of lignin, owing to the higher viscosity of the reactive mixture.

More rigid foams were obtained with the addition of k-lignin to the polyurethane matrix, as it was observed by the higher CFD values obtained, suggesting that k-lignin acted as reinforcement in the polyurethane matrix. This reinforcing effect was also reflected in lower resilience values, meaning that k-lignin containing foams needed more time to recover their original shape. The lower resilience and CFD of 3% k-IPDI containing foams was a consequence of the less fine dispersion and to the lower crosslink density compared to foams containing k-lignin.

In terms of the strain-stress curves, it was observed that the modulus and the ability to absorb energy increased when k-lignin was used, whereas those containing k-IPDI were softer (with lower elastic modulus) but with lower energy absorption

capacity. These properties will condition the application field of these foams. High energy absorption capacity would be needed in protective or safety-related applications, while comfort intended ones would be more focused on the flexibility of the foam.

5.5. References

Argyropoulos, D.S., 1994. Quantitative phosphorus-31 NMR analysis of lignins, a new tool for the lignin chemist. J. Wood Chem. Technol. 14, 37–41.

ASTM E1755-01, 2015. Standard test method for ash in biomass.

Bialas, N., Höcker, H., Marschner, M., Ritter, W., 1990. ^{13}C NMR studies on the relative reactivity of isocyanate groups of isophorone diisocyanate isomers. Die Makromol. Chemie 1852, 1843–1852.

Cateto, C.A., Barreiro, M.F., Rodrigues, A.E., Brochier-Salon, M.C., Thielemans, W., Belgacem, M.N., 2008. Lignins as macromonomers for polyurethane synthesis: A comparative study on hydroxyl group determination. J. Appl. Polym. Sci. 109, 3008–3017.

Chauhan, M., Gupta, M., Singh, B., Singh, A.K., Gupta, V.K., 2014. Effect of functionalized lignin on the properties of lignin-isocyanate prepolymer blends and composites. Eur. Polym. J. 52, 32–43.

Crestini, C., 2012. Conversion of lignin: Chemical technologies and biotechnologies, in: Aresta, M., Dibenedetto, A., Dumeignil, F. (Eds.), Biorefinery - From Biomass to Chemicals and Fuels. Walter de Gruyter GmbH, Berlin/Boston, pp. 167–206.

Dence, C.W., 1992. The determination of lignin, in: Lin, S.Y., Dence, C.W. (Eds.), Methods in Lignin Chemistry. Springer-Verlag, Berlin, pp. 33–61.

Faix, O., Argyropoulos, D.S., Robert, D., Neirinck, V., 1994. Determination of hydroxyl groups in lignins. Evaluation of ^{1}H-, ^{13}C-, ^{31}P-NMR, FTIR and wet chemical methods. Holzforschung 48, 387–394.

Ferry, L., Dorez, G., Taguet, A., Otazaghine, B., Lopez-Cuesta, J.M., 2015. Chemical modification of lignin by phosphorus molecules to improve the fire behavior of polybutylene succinate. Polym. Degrad. Stab. 113, 135–143.

Gellerstedt, G., 2015. Softwood kraft lignin: Raw material for the future. Ind. Crops Prod. 77, 845–854.

Gellerstedt, G., 1992. Gel permeation chromatography, in: Lin, S.Y., Dence, C.W. (Eds.), Methods in Lignin Chemistry. Springer-Verlag, Berlin, pp. 487–497.

Gosselink, R.J.A., Abächerli, A., Semke, H., Malherbe, R., Käuper, P., Nadif, A., Van Dam, J.E.G., 2004a. Analytical protocols for characterisation of sulphur-free lignin. Ind. Crops Prod. 19, 271–281.

Gosselink, R.J.A., Snijder, M.H.B., Kranenbarg, A., Keijsers, E.R.P., De Jong, E., Stigsson, L.L., 2004b. Characterisation and application of NovaFiber lignin. Ind. Crops Prod. 20, 191–203.

Granata, A., Argyropoulos, D.S., 1995. 2-Chloro-4,4,5,5-tetramethyl-1,3,2-dioxaphospholane, a reagent for the accurate determination of the uncondensed and condensed phenolic moieties in lignins. J. Agric. Food Chem. 43, 1538–1544.

Herrington, R., Hock, K., 1998. Flexible Polyurethane Foams. Dow Chemical Co., Midland, MI.

ISO 14900, 2001. Plastics - Polyols for use in the production of polyurethane - Determination of hydroxyl number.

Lisperguer, J., Perez, P., Urizar, S., 2009. Structure and thermal properties of lignins: Characterization by infrared spectroscopy and differential scanning calorimetry. J. Chil. Chem. Soc. 54, 460–463.

Lora, J., 2008. Industrial commercial lignins: Sources, properties and applications., in: Belgacem, M.N., Gandini, A. (Eds.), Monomers, Polymers and Composites from Renewable Resources. Elsevier Ltd, Amsterdam, pp. 225–241.

Lundquist, K., 1992. Proton (^{1}H) NMR Spectroscopy, in: Lin, S.Y., Dence, C.W. (Eds.),

Methods in Lignin Chemistry. Springer-Verlag, Berlin, pp. 242–249.

Mahmood, N., Yuan, Z., Schmidt, J., Xu, C.C., 2015. Preparation of bio-based rigid polyurethane foam using hydrolytically depolymerized Kraft lignin via direct replacement or oxypropylation. Eur. Polym. J. 68, 1–9.

Mills, N.J., Stämpfli, R., Marone, F., Brühwiler, P.A., 2009. Finite element micromechanics model of impact compression of closed-cell polymer foams. Int. J. Solids Struct. 46, 677–697.

Ono, H.K., Jones, F.N., Pappas, S.P., 1985. Relative reactivity of isocyanate groups of isophorone diisocyanate. Unexpected high reactivity of the secondary isocyanate group. J. Polym. Sci. Polym. Lett. Ed. 23, 509–515.

Passoni, V., Scarica, C., Levi, M., Turri, S., Griffini, G., 2016. Fractionation of industrial softwood kraft lignin: Solvent selection as a tool for tailored material properties. ACS Sustain. Chem. Eng. 4, 2232–2242.

Paulsson, M., Simonson, R., 2002. Acetylation of lignin and photostabilization of lignin-rich mechanical wood pulp and paper, in: Hu, T.Q. (Ed.), Chemical Modification, Properties and Usage of Lignin. Springer Science+Business Media, LLC, New York, pp. 227–245.

Sarkanen, S., Teller, D.C., Stevens, C.R., McCarthy, J.L., 1984. Associative interactions between kraft lignin components. Macromolecules 17, 2588–2597.

Stuart, B.H., 2004. Organic molecules, in: Infrared Spectroscopy: Fundamentals and Applications. Wiley & Sons, Ltd, Chichester, UK, pp. 71–93.

Szycher, M., 2013. Flexible and Semiflexible foams, in: Szycher's Handbook of Polyurethanes. CRC Press, Boca Ratón, pp. 181–255.

TAPPI T 222 om-02, 2011. Acid-insoluble lignin in wood and pulp. Technical Association of the Pulp & Paper Industry.

TAPPI T 249 cm-85, 2009. Carbohydrate composition of extractive-free wood and wood pulp by gas-liquid chromatography. Technical Association of the Pulp &

Paper Industry.

Wang, Z., Yang, X., Zhou, Y., Liu, C., 2013. Mechanical and thermal properties of polyurethane films from peroxy-acid wheat straw lignin. BioResources 8, 3833–3843.

Yoshida, H., Mörck, R., Kringstad, K.P., Hatakeyama, H., 1990. Kraft lignin in polyurethanes. II. Effects of the molecular weight of kraft lignin on the properties of polyurethanes from a kraft lignin polyether triol polymeric MDI system. J. Appl. Polym. Sci. 40, 1819–1832.

„Wer will dass die Welt so bleibt wie sie ist, der will nicht das sie bleibt.“

(Erich Fried)

E. Budzinski. Mauerbild. Berlin, 1990.

Chapter 6

6

Fire behavior: Combination of **layered double hydroxides**, phosphorus containing oligomeric **diol** and **lignin**

6. Fire behavior: Combination of layered double hydroxides, phosphorus containing oligomeric diol and lignin

6.1 Introduction

Given the results obtained in the preceding chapters and with the objective of performing a more thorough study of fire behavior, different flexible polyurethane foams are prepared in this **chapter** containing the previously used eco-friendly fillers such as layered double hydroxides (LDH) and kraft lignin, in combination with the phosphorus containing oligomeric diol (E560). The combination of these two additive compounds and the reactive E560 is expected to improve the flame retardancy owing to the sum of the effects provided by each one.

Lignin was selected to give added value to an industrial byproduct that can act as a potential **charring agent** owing to its aromatic structure. This particular unsaturated structure can yield high amounts of char in presence of an **acid source**. In this way, E560 was selected as acid source to promote the charring efficiency of lignin, due to the presence of phosphorus in its structure that upon degradation produce phosphorus containing acids which can enhance the dehydration and the degradation of lignin. This char has an important role as a heat and oxygen barrier of the burning polymer, delaying or even avoiding the penetration of flames in the material. Nevertheless, this char shield cannot be fully efficient if cracks are present on its surface. For this reason, LDH were selected not only due to the barrier effect provided by its lamellar structure that can also hinder the penetration of oxygen and heat through the burning polymeric substrate, but also because LDH can act as a **char reinforcing filler** avoiding the formation of cracks in a more advanced stage of burning.

In this **chapter**, due to its higher availability carbonate interlayered LDH (LDH-CO_3) is selected whereas kraft lignin is chosen due to the superior mechanical properties observed in **Chapter 5**. Two series of foams are prepared containing separately lignin and LDH, and combining both of them: one of the series without E560 (0E foam series) and the other with 5 parts per hundred of E560 polyol (5E series) in order to avoid a pronunciated increase of viscosity.

In addition to Fourier transform infrared spectroscopy, thermogravimetric analysis and mechanical tests, different techniques for the evaluation of flame

response of the manufactured foam samples are employed, such as cone calorimetry, limiting oxygen index and UL94 horizontal burning test for foamed materials. Despite these techniques do not determine the real response of the materials under real fire conditions; they can be used as a preliminary assess of the effect on the flame retardancy of these potential eco-friendly flame retardants.

6.2 Experimental procedure

6.2.1. Materials

In this chapter, FPUF were prepared with a fossil derived trifunctional polyether polyol (Alcupol® F4811). The isocyanate (TDI) and foaming additives, as well as the Exolit® OP 560 (E560) oligomeric diol which was used as reactive flame retardant, and the eco-friendly fillers carbonate interlayered LDH (Sigma-Aldrich) and kraft lignin (BioChoice™, UPM) are all described in **Chapter 2** (**Section 2.2**).

6.2.2. Flexible polyurethane foam preparation

In the preceding chapters it has been observed that density plays an important role in the final properties of flexible polyurethane foams. For this reason, in this chapter foams with densities of 40 ± 2 kg m^{-3} were prepared. This condition necessitated varying the formulations (shown in **Table 6.1**) in relation to the additive or additive mixture used, in order to maintain constant density values, but the isocyanate index was held constant (110) in all cases. In general, the use of lignin and LDH contributed to increasing the viscosity of the reactive mixture, hindering the growth of the bubbles and yielding more compact foam. To counteract this effect, higher blowing agent content was needed in some formulations in order to maintain the density. The use of higher amounts of water had also an impact on the hard segment (HS) content of the foams, as shown in **Table 6.1**, which was calculated as the grams of water and isocyanate divided by the total weight of the foam (Sonnenschein et al., 2007). A series of foams with only polyether polyol (0E), with 5 wt% of lignin (0E-

5%L), with 3 parts per hundred of polyol (pphp) of LDH (0E-3LDH), and combining 5%wt lignin and 3 pphp LDH (0E-5%L/3LDH) was prepared. The same pattern was repeated to prepare foams containing a mixture of 95 pphp of polyether polyol and 5 pphp of E560 (5E, 5E-5%L, 5E-3LDH and 5E-5%L/3LDH, respectively). The sample identification according to the additives used is also shown in **Table 6.1**.

The foams were prepared following the procedure explained in **Chapter 3** (**Section 3.2.3**). Foams containing E560 were prepared by mixing both polyol and oligomeric diol for 30 s at 2000 rpm prior to addition of the additives and the eco-friendly fillers. When the foams contained E560, lignin and/or LDH, the E560 was always mixed with the polyol first, and then the fillers were added according to the aforementioned procedure, incorporating and dispersing first the LDH and then the lignin, which were previously dried as explained in **Chapter 3** (**Section 3.2.3**) and **Chapter 5** (**Section 5.2.2**). Then, the amine catalyst, surfactant and blowing agent were added to the mixture and stirred with a radial turbine at 2000 rpm for 60 s. Afterwards the organometallic catalyst was added and mixed another 30 s, resulting in a ready-to-use part B of the formulation. Finally the TDI (part A) was incorporated and stirred for a few seconds with a turbohelix-shaped stirrer at 2500 rpm in order to obtain a faster homogenization. Finally, the mixture was poured quickly into an open mold allowing free rise of the foam. The hydroxyl number of lignin was not taken into consideration in foam formulation.

Table 6.1. Additives, isocyanate and hard segment (HS) content of the prepared flexible polyurethane foams.

Sample	Additive content						HS (%)
	Exolit OP 560® (pphp)	Lignin (%*)	LDH (pphp)	Water (pphp)	Isocyanate content I.I.= 110 (%*)	Organotin/amine catalyst ratio	
0E	-	-	-	2.30	33.21	0.96	25.9
0E-5%L	-	5	-	2.40	34.18	1.67	26.5
0E-3LDH	-	-	3	2.35	33.65	1.27	26.2
0E-5%L/3LDH	-	5	3	2.40	34.18	1.67	26.5
5E	5	-	-	2.40	38.02	0.25	28.5
5E-5%L	5	5	-	2.40	38.07	0.20	28.5
5E-3LDH	5	-	3	2.40	38.02	0.21	28.5
5E-5%L/3LDH	5	5	3	3.00	44.53	1.00	31.8

*Given as a percentage of the total foam weight.

6.3 Results and discussion

6.3.1. Foam morphology and structural characterization

Firstly, the viscosity of the reactive mixture was measured since it is a critical parameter affecting the foaming process. Increased viscosity hinders bubble growth, yielding foams with lower cell size. **Figure 6.1** shows the viscosity of the part B precursors of the foams (corresponding to the polyol or polyol-diol mixture plus the additives and fillers used in each formulation), evidencing that the viscosity increased in the presence of fillers. The effect of this higher-viscosity formulation was counteracted by the addition of more blowing agent.

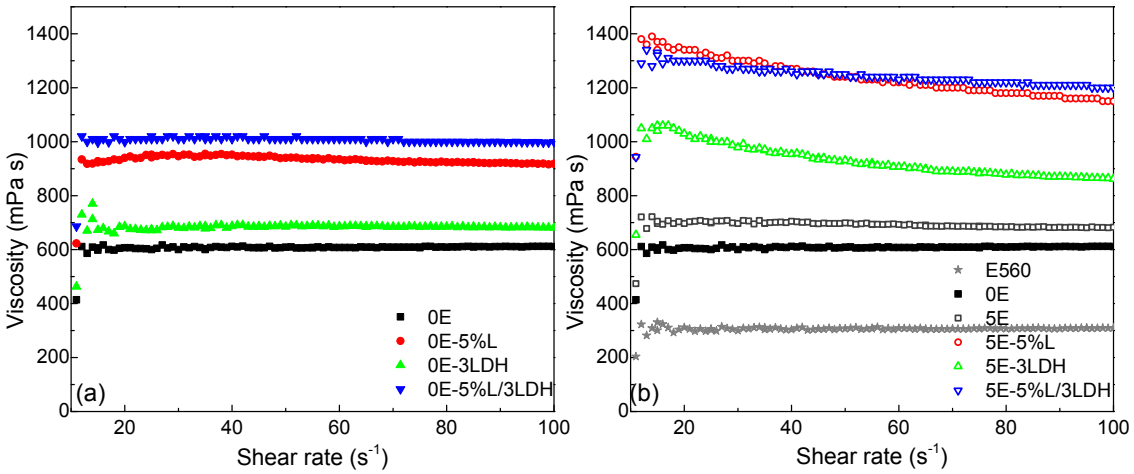

Figure 6.1 Viscosity of the part B precursors (polyol or polyol-diol mixture, 0E and 5E respectively, plus additives and fillers used in each series of foams: 0E series (a) and 5E series (b)

Figure 6.2 shows the infrared spectra of the prepared foams, all of which confirmed the complete reaction of isocyanate groups with the polyol or polyol-diol mixture and the blowing agent due to the absence of the characteristic –NCO band at 2276 cm^{-1}. Foams belonging to the 0E series (using only polyether polyol) exhibited some differences owing to the formulation of the foams. The slightly higher hard segment content in the foams containing LDH and/or lignin was reflected in the increased intensity of the bands associated with urea bonds found in the 0E foams. This increased intensity was observed in the characteristic bands of hydrogen bonded N-H (3296 cm^{-1}), the associated urea carbonyl stretching vibration band (1640 cm^{-1}), and also in the N-H bending vibration band (1533 cm^{-1}), which overlapped with C-N

stretching. The intensity of the C-O-C asymmetric (1222 cm^{-1}) and symmetric (1088 cm^{-1}) stretching remained practically unaltered. In case of 5E foams, the band appearing at 3296 cm^{-1} related to N-H stretching vibration, presented higher intensity than 0E series owing to their higher HS content.

The 0E sample showed lower intensity in the bidentate urea band (1640 cm^{-1}) due to its lower blowing agent content. Moreover, the higher intensity of this band in filled foams (0E-5%L, 0E-3LDH and 0E-5%L/3LDH) also reflected that urea microdomain separation was favored. With regard to the foams containing 5 pphp E560, the intensity of the bidentate urea band at 1640 cm^{-1} in 5E increased over that of 0E due to the higher water in the formulation, and thus the higher urea content in the 5E formulation. Nevertheless, the intensity of this band decreased in filled 5E foams due to the higher viscosity of the reactive mixture in the presence of either LDH or lignin, which hindered separation of the urea microphase (Das et al., 2009). On the other hand, the low LDH and lignin content in foams made it difficult to discern their characteristic bands due to their low relative intensity.

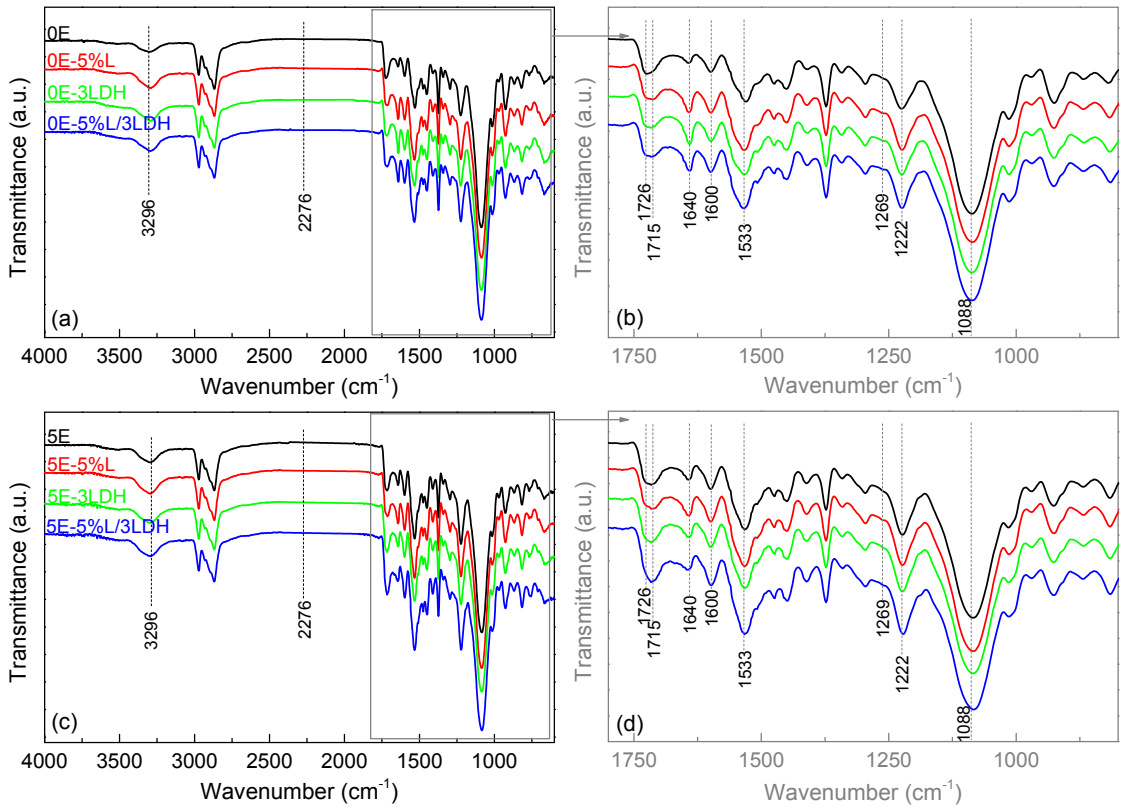

Figure 6.2. Infrared spectra of the 0E (top) and 5E (bottom) series of foams.

In terms of foam morphology, since the foams were formulated in order to achieve similar density values, the effect of this parameter was omitted within the characterization studies of the foams and focused on the outcome of the fillers used, or in combination with E560. **Table 6.2** shows that the density values were maintained around 40 ± 2 kg m^{-3}. These values were adjusted by varying the amount of blowing agent used.

Table 6.2. Density, open cell content and average cell size of the foams.

Sample	Density (kg m^{-3})	Open cell content (%)	Average cell size (µm)
0E	41.5 ± 0.2	30.5 ± 1.4	240.4 ± 75.2
0E-5%L	38.8 ± 0.6	23.8 ± 1.5	242.6 ± 81.2
0E-3LDH	41.3 ± 0.5	27.0 ± 1.6	240.9 ± 66.8
0E-5%L/3LDH	39.5 ± 0.9	25.7 ± 1.9	241.9 ± 69.8
5E	41.1 ± 0.8	22.4 ±1.5	239.7 ± 64.8
5E-5%L	41.2 ± 0.7	29.5 ± 2.3	237.7 ± 72.8
5E-3LDH	40.2 ± 0.9	35.4 ± 2.8	238.3 ± 77.0
5E-5%L/3LDH	39.4 ± 1.2	34.7 ± 3.3	234.4 ± 68.6

Figure 6.3 also shows that the cell heterogeneity of the foams was maintained regardless of whether they were filled or unfilled, and whether or not they contained E560.

When comparing 0E to 5E foam series, similar average cell size values perpendicular to foam growth were obtained, as expected since the formulation was adjusted to have the same density. The only sample that presented a slightly lower average cell size was 5E-5%L/3LDH, probably as a consequence of the combined effect of the higher viscosity of the reactive mixture and also due to its higher catalyst and HS content.

The porosity (or open cell content) of polyurethane foams is influenced by several factors (Szycher, 2013), including the viscosity of the reactive mixture (Turner et al., 1989), the isocyanate index, the type of surfactant used, the amount of organometallic catalyst used (which hinders wall breaking by favoring polymerization) (Mahmoud et al., 2017) and the presence of fillers in the matrix (Danowska et al., 2013). In the case of 0E foams, the porosity decreased from 30.5% in 0E to 23.8% in 0E-5%L, and to 27.0% for 0E-3LDH, owing to the higher viscosity that hindered wall

breakage. Nevertheless, while the addition of LDH decreased the open cell content (25.7%) in 0E-5%L/3LDH as compared with 0E due to increased viscosity, the filler amount in the matrix was saturated enough to contribute to facilitating wall breakage, in contrast to the open cell content of 0E-5%L (23.8%). In the case of foams containing E560, the open cell content in the 5E sample was lower than in the 0E samples, also as a consequence of the increased viscosity. Nevertheless, this effect was counteracted by the presence of fillers that facilitated wall breakage (Harikrishnan et al., 2006) and due to the lower organotin catalyst content (Mahmoud et al., 2017).

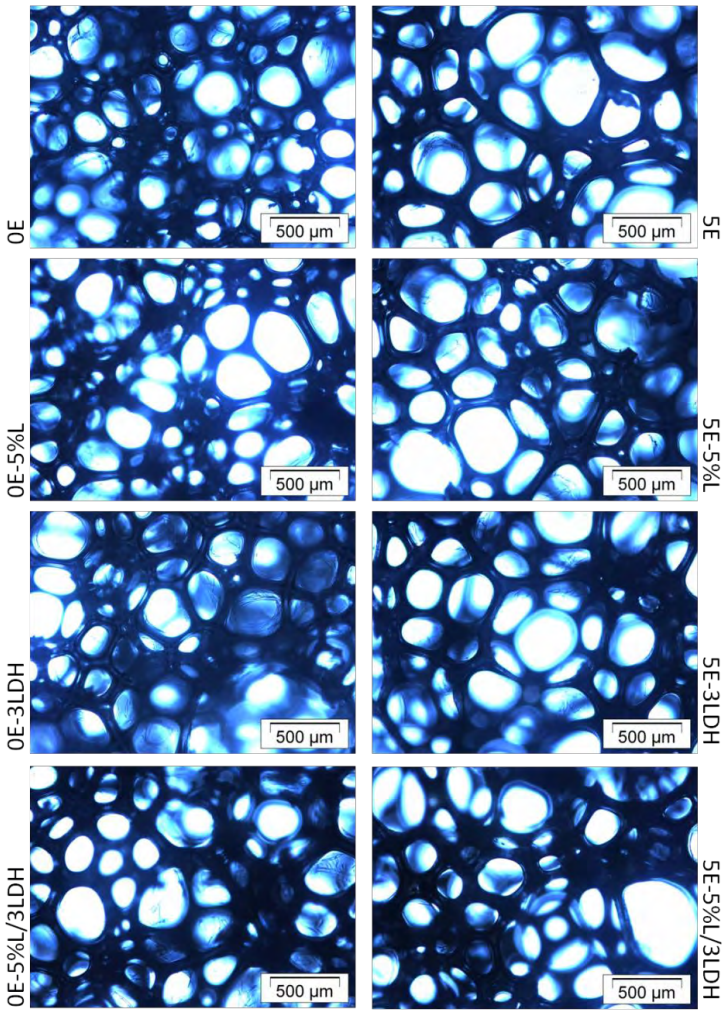

Figure 6.3. OM micrographs (x50) of the foams prepared with 100 pphp polyether polyol (left) and with 95 pphp polyether polyol and 5 pphp E560 (right).

6.3.2. Thermal properties

The thermal stability of the foam samples was analyzed by TGA, and the mass loss curves are shown in **Figure 6.4**. As it was previously observed, the decomposition of PUF occurred in two stages: the first corresponding to the degradation of the hard segment (urethane and urea linkages) at T_{max1}, and the second to the degradation of the soft segment (polyol backbone) at T_{max2}. In 0E foams, the presence of lignin and LDH decreased the T_{onset} slightly due to their intrinsic lower decomposition temperatures (**Table 6.3**). Regarding the maximum degradation rate temperatures T_{max1} and T_{max2}, LDH decreased the T_{max1} slightly, but did not affect the T_{max2}. When lignin and LDH were combined in the formulation, the LDH presented a stabilizing effect of T_{max1} and T_{max2}, preventing the earlier degradation of PUF and lignin in both decomposition stages. This was attributed to the barrier effect of the lamellar geometry of LDH together with the charring effect of lignin, which contributed to delay the release of volatile products (Liu et al., 2015).

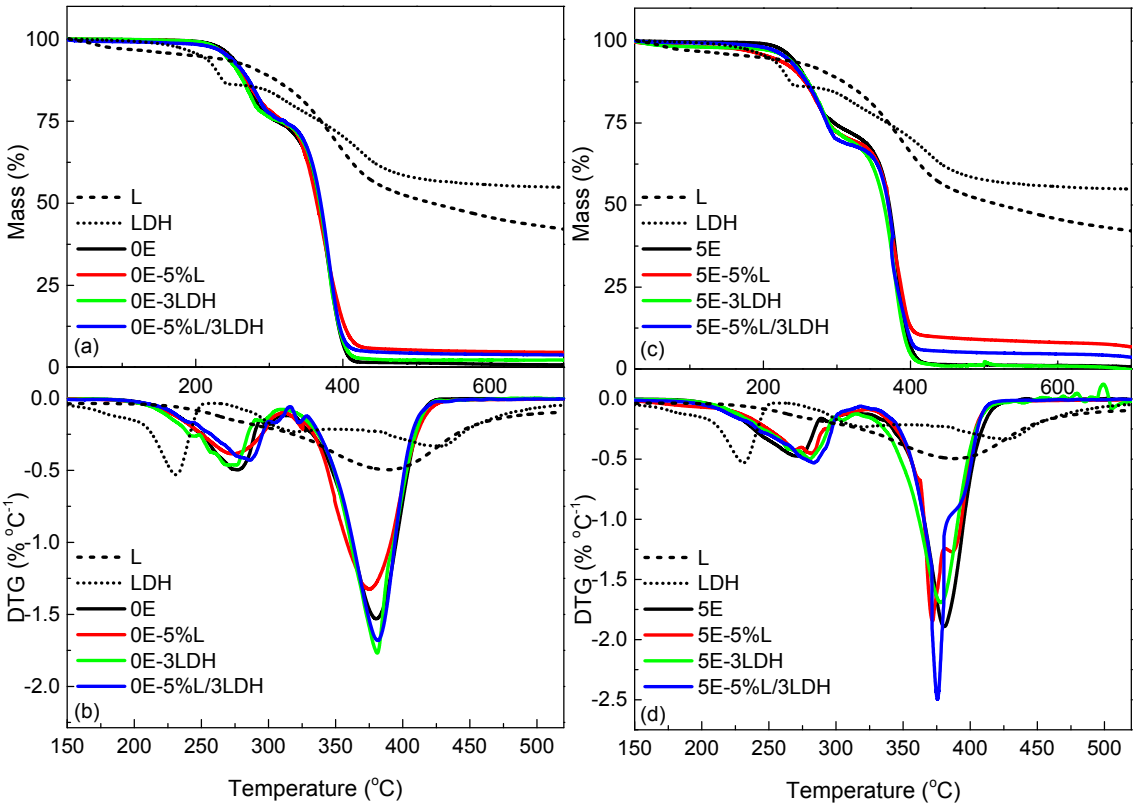

Figure 6.4. Mass loss and derivative mass loss (DTG) curves of the foams prepared only with polyether polyol (a, b) and combining polyether polyol with E560 (c, d).

Table 6.3. Thermal degradation temperatures obtained from TGA and glass transition temperatures of the different foams obtained by DMA.

Sample	T_{onset} (°C)	T_{max1} (°C)	T_{max2} (°C)	T_g (°C)
Lignin	196	386	-	-
LDH	207	231	318/429	-
0E	247	277	380	-39
0E-5%L	243	274	375	-40
0E-3LDH	240	273	380	-39
0E-5%L/3LDH	243	285	381	-38
5E	238	271	381	-33
5E-5%L	210	281	372/386	-35
5E-3LDH	231	280	378	-37
5E-5%L/3LDH	230	283	376/390	-32

T_{onset}: Temperature at 5% mass loss

$T_{max1,2}$: Temperature of maximum degradation rate in the first (1) and second (2) stage

T_g: Glass transition temperature measured by DMA as the maximum of tan δ

On the other hand, the use of E560 had a catalyzing effect on the T_{onset}, especially in the presence of lignin, as a consequence of the acid nature of the phosphorus contained in the polyol, which contributed to accelerating the dehydration of lignin (Fierro et al., 2005), decreasing the T_{onset} by up to 28 °C in 5E-5%L as compared with 5E. The combination of lignin and LDH contributed to delaying this dehydration by 20 °C in 5E-5%L/3LDH as compared with 5E-5%L. While the presence of E560 increased the decomposition of the urethane/urea linkages slightly in the first stage, it certainly affected the second stage, showing two different mass losses when combined with lignin (5E-5%L and 5E-5%L/3LDH). These two different mass losses were attributed to the catalyzing effect of the phosphorus during the decomposition of the polyol backbone, during the second stage of which the degradation of the polyol (taking place at 372 °C and 376 °C in 5E-5%L and 5E-5%L/3LDH, respectively) could be differentiated from the degradation of the lignin (at 386 and 390 °C in 5E-5%L and 5E-5%L/3LDH, respectively). It was observed that the introduction of fillers yielded a slight increase in residue as a consequence of its low loading content. Nevertheless it was worth noting that samples containing lignin, due to the aromatic structure of this substance, exhibited the highest char yield, especially when combined with E560. The phosphorus contained in the polyol acted as an acid source, enhancing the char formation of lignin.

Figure 6.5 shows the storage modulus, E´, and tan δ curves as a function of temperature, obtained by DMA. The glass transition temperature was calculated as the maximum value of the loss factor (tan δ) (**Table 6.3**). The tan δ profiles remain similar regardless of the fillers used, and a single transition is observed in all foams, corresponding to the T_g of the polyol. The most relevant change observed was the broader transition and higher T_g value of the foams containing E560 with respect to 0E foams, as a consequence of the lower molecular weight of the phosphorous oligomeric diol and the increased crosslinking density (Zhang, 2008) due to the higher amount of isocyanate required to compensate for the OH introduced by E560. As regards the storage modulus (E') of the 0E and 5E series, the latter presented a higher E' value, owing to its increased crosslink density. Moreover, the addition of lignin to both series of foam resulted in foams with a lower E' than their respective 0E and 5E counterparts, and this effect is attributed to the increased viscosity that hindered the crosslink formation during the foaming process.

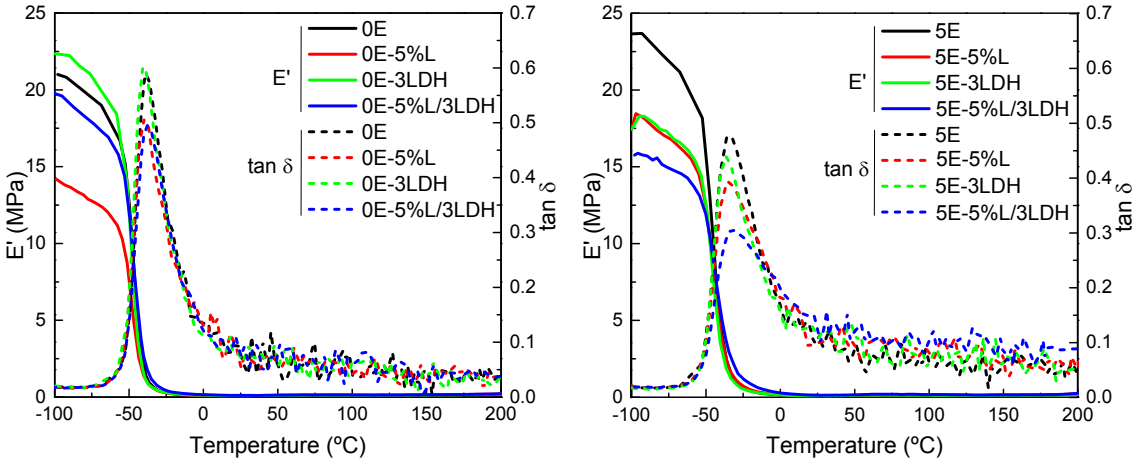

Figure 6.5. Storage modulus (E') and tan δ as a function of temperature of 0E (left) and 5E (right) series of polyurethane foams.

6.3.3. Mechanical properties

Resilience is a parameter related to the quality and durability of flexible open-cell foams, which gives a notion of the support of the cellular material. Flexible foams can be divided into highly resilient or viscoelastic foams. Those classified in the former group have resilience values higher than 55% and are characterized by a high support factor, firmness, and fast recovery after compression, along with higher durability.

Those included in the second group, which are also known as memory foams, have resilience values below 20%, and are characterized by their softness, better pressure distribution and slower recovery than high resilient foams, which are desirable for motion isolation in bedding. Conventional slabstock foams have resilience values around 40%, which was the case of the present foams shown in **Table 6.4**. The addition of E560 to the formulation contributes to increase resilience of 5E foam, in accordance with **Chapter 4** (**section 4.3.3**), which is related to the higher crosslink density of the foam due to the higher hydroxyl index of the E560, which requires more TDI and thus creates more crosslinking points and a tighter structure.

Table 6.4. Mechanical properties of the prepared flexible polyurethane foams. Specific compressive stress is given at 10% strain and compression set and energy absorption per volume unit are both given at 50% strain.

Sample	Resilience (%)	CFD (kPa)	Compression set (%)	Elastic Modulus (kPa)	Compressive stress (kPa)	Energy absorption/ volume ($J\ m^{-3}$)
0E	30.0 ± 2.7	3.97 ± 0.61	5.02 ± 1.46	56.1 ± 0.5	3.39	192.40
0E-5%L	38.7 ± 3.6	4.61 ± 0.30	4.38 ± 2.40	118.8 ± 5.0	5.49	285.35
0E-3LDH	39.2 ± 3.9	4.47 ± 0.19	3.51 ± 0.31	78.4 ± 1.1	4.02	212.12
0E-5%L/3LDH	38.2 ± 3.2	4.37 ± 0.11	4.25 ± 0.31	79.7 ± 5.6	3.38	192.86
5E	34.0 ± 2.3	3.71 ± 0.47	5.04 ± 1.16	64.1 ± 1.6	2.81	160.57
5E-5%L	27.7 ± 1.6	4.12 ± 0.29	5.13 ± 0.69	76.6 ± 3.7	3.57	196.65
5E-3LDH	32.0 ± 2.9	3.52 ± 0.18	4.96 ± 1.34	44.9 ± 2.8	2.28	130.17
5E-5%L/3LDH	34.4 ± 2.0	4.69 ± 0.46	6.43 ± 1.12	81.4 ± 5.1	4.54	248.93

In spite of this behavior, **Table 6.4** shows that the addition of fillers had opposite effects in the two systems. In the case of 0E foams, the addition of lignin and LDH, alone or in combination, led to higher resilience values (up to 9% higher than 0E), thus resulting in foams with faster recovery after deformation, due to the urea segregation. The same effect was observed in **Chapter 4** (**section 4.3.3**) when LDH were present in the formulation. Nevertheless, the behavior observed with lignin in **Chapter 5** (**section 5.3.2**) which decreased resilience values, was only observed when lignin was combined with E560. This different behavior in lignin in presence or not of E560 could be attributed to the different polyol (ALC) used in this **chapter**. In the case of foams containing E560, as it was observed in **Chapter 4** (**section 4.3.3**), the presence of fillers led to unchanged or even decreased resilience values, due to the viscosity of

the reactive mixture that hindered urea microphase separation as well as due to the increased crosslinking density.

Another parameter related to the quality of flexible foams is compression force deflection (CFD), which is related to the firmness (or load-bearing capacity) of the foam. It gives a measure of the pressure needed to maintain compression of the foam to 50% of its original thickness. **Table 6.4** reveals that the CFD values of the 0E system were generally higher than those of 5E samples, in contrast of what was observed in **Chapter 4** (**section 4.3.3**) where CFD increased slightly with E560 content. These results indicate the reinforcing effect of the urea microdomain segregation in 0E, acting to reinforce the foam structure owing to the differences in the foam formulation to maintain the density constant. Moreover, CFD increased when using lignin, due to its aromatic and rigid structure as it was observed in **Chapter 5** (**section 5.3.2**), which effect was added to the reinforcing effect of the microdomains, thus increasing the compression strength of the foam. In the case of 5E foams, the presence of lignin also contributed to increase CFD values, with a more pronounced increase when in combination with LDH, but values generally remained below those of the 0E system, due to the lower microdomain separation of the foam.

The compression set quantifies the permanent deformation after a material is compressed under constant deformation and temperature. This property is critical in the final application of flexible polyurethane foams, and is related to the relative flow of the hard segment to the soft domains of the polyurethane under thermal and compressive stress, forming to new interactions in the new deformed conformation (Sonnenschein et al., 2007).

It was observed that in general the compression set of 0E foams was slightly lower as a consequence of their better segregation of hard segments, as established by Armistead et al. (1988). Nevertheless, the addition of lignin and/or LDH to 0E acts to hinder the relative flow between domains, with the effect of decreasing the permanent deformation compared to the unfilled 0E sample. On the other hand, the lower microphase separation of filled 5E foams resulted in slightly higher permanent deformation.

The values for elastic modulus, compressive stress at 10% and energy absorption up to 50% of deformation were obtained from the **compressive stress-strain** curves of the foams (**Figure 6.6**). Comparing 0E and 5E foams, the higher crosslink density resulted in higher elastic moduli in 5E foams, while phase separation in 0E favored higher compression strength values. In both series the addition of lignin led to higher E and compressive strength values due to its complex and rigid structure.

The elastic modulus and compressive stress values of the foams determined their energy absorption per volume unit, which is related to the density of the material and is a critical parameter in applications involving safety. In this case, since the density was constant for all the foams, urea microdomain separation was evident in the curves. In general, 0E series foams showed higher microphase separation, especially 0E-5%L, generally presenting higher energy absorption than 5E series foams, which were softer and, with the exception of 5E-5%L/3LDH foam, presented higher energy dissipation due to the reinforcing effect of lignin in combination with LDH. As it was observed in **Chapter 5** (**section 5.3.2**) the presence of lignin contributed to increase the energy absorption per unit volume of the foams.

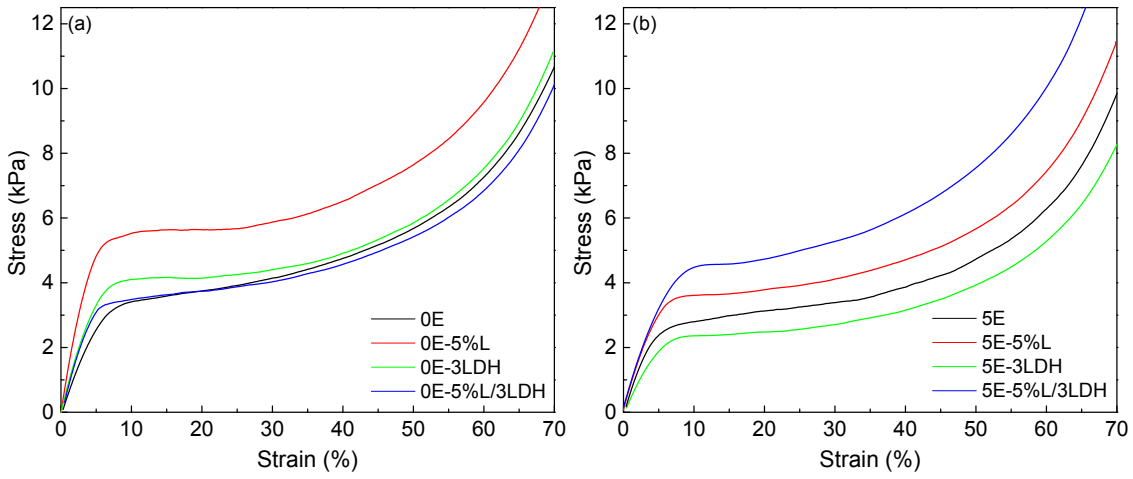

Figure 6.6. Compressive stress-strain curves of the foams prepared with polyether polyol (a) and with 5 pphp E560 (b).

6.3.4. Flammability

LOI defines the minimum oxygen concentration necessary to support the combustion of a specimen under a specified candle-like fire scenario, and thus it is a

method for classifying the flammability of a polymer. Increasing the LOI value of a material is indicative of reduced flammability. Polymeric materials with LOI values higher than 26–30 % are usually considered flame retardant (Schartel, 2010).

While the LOI value (**Table 6.5**) increased somewhat when using the phosphorous oligomeric diol in the foam (from 18.2 to 20.0), it decreased in the presence of lignin. The same behavior was observed by Xing et al. (2013), who attributed this effect to lignin's intrinsic flammability (Cheng et al., 2012). Considering the small amount of lignin used and that the intrinsic flammability of PU is even higher than that of lignin, this explanation was dismissed. The deterioration of LOI upon the addition of lignin or LDH, respectively, is proposed to be due to the increased viscosity of the pyrolyzing melt, which results in more fuel being allocated to the actual pyrolyzing zone. This effect has been described before for nanocomposites (Schartel et al., 2006; 2015). Adding the flame retardant E560 to the samples with lignin and LDH appears to compensate for the effects, yielding unchanged LOI values (around 18.2) for the 0E series. The amount of additives used was far too small to improve LOI.

Table 6.5. Limiting oxygen index values, melt polymer layer thickness after 20 s of combustion and burning rate (BR) obtained from UL 94 test.

Sample	LOI	Melt layer thickness (mm)	BR (mm min^{-1})
0E	18.2	3.02 ± 0.34	59.7 ± 3.4
0E-5%L	17.0	1.10 ± 0.29	50.9 ± 4.7
0E-3LDH	17.1	2.60 ± 0.35	65.8 ± 3.4
0E-5%L/3LDH	17.2	0.96 ± 0.31	51.8 ± 2.4
5E	20.0	2.98 ± 0.56	45.4 ± 1.2
5E-5%L	18.5	2.49 ± 0.45	42.4 ± 1.7
5E-3LDH	18.2	1.54 ± 0.32	45.3 ± 2.8
5E-5%L/3LDH	18.4	0.95 ± 0.20	43.9 ± 1.4

The viscosity of the molten pyrolyzing polymer in the pyrolysis zone can be critical in flame propagation. Lower viscosities enhance the dripping of combustible polymers, creating pool fires but also removing fuel from the flame. The thickness (**Figure 6.7**) and the viscosity (**Figure 6.8**) of the molten polymer layers were measured by quenching the burning sample in the cone calorimeter 20 s after ignition.

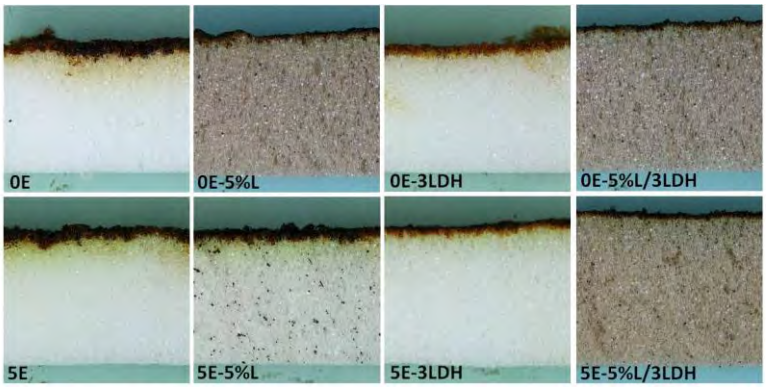

Figure 6.7. Images of the transversal cut of the molten polymer layer of the quenched foam samples after 20 s of ignition.

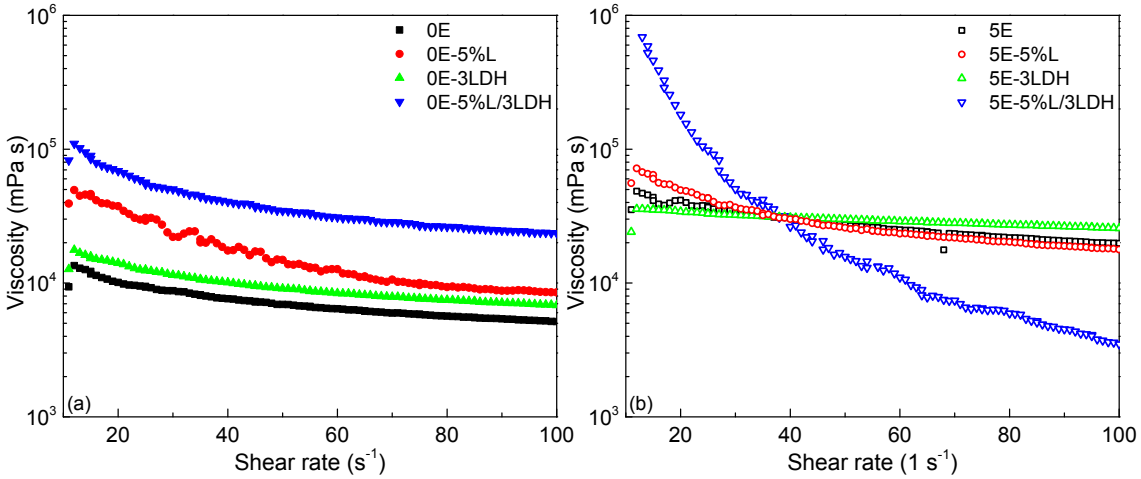

Figure 6.8. Viscosity of the molten polymer layer remaining after 20 s of combustion. 0E (a) and 5E (b) samples.

Cross sections of quenched foams showed that the liquid accumulated on the surface of the foam, as was reported by Krämer et al. (2010). **Figure 6.8** displays the viscosity of the liquid pyrolysis products. Since pyrolysis products on the surface of burning items are not exposed to shear stress in fire scenarios, zero viscosity is a crucial factor when it comes to dripping. **Figure 6.8** shows that the use of lignin and LDH, and especially their combination, yielded significantly higher viscosity at zero shear rates. It was observed that the increase in melt viscosity resulted in a decreased thickness of the melt layer in foams containing lignin and LDH.

These results show that the mixture of the three compounds at such low contents did not enhance the flame retardancy of PUF, but provided increased

viscosity, which reduces melt flow and can prevent the polymer from dripping, and thus hinder the ignition of adjacent objects in a fire scenario.

UL 94 is another preliminary test to assess the flammability of materials that is widely used in industry since it provides different rates depending on which test standard is performed to measure the behavior of the material. The UL 94 tests evaluate the behavior of materials under short-term fire exposure, determining their capacity for self-sustained flame propagation. For cellular materials such as polyurethane foams, the horizontal burning test is applied (UL 94-HB) according to ISO 9772. Despite the fact that all of the foam samples tested in our study failed to achieve classification according to the UL 94 standard, the results were recorded in order to determine and compare the burning rates of the different samples. Analogous to LOI, adding small amounts of lignin and LDH, respectively, had hardly any relevant effect. **Table 6.5** shows that the presence of E560 generally reduced the burning rate. When it was used alone, the burning rate was reduced by 24% as compared to 0E (14.3 mm min^{-1}), and by 26% when it was used in combination with lignin and LDH. It was noteworthy that in accordance to the increased melt viscosity, lignin and its combination with LDH reduced the flame propagation speed, which would result in increased time to escape to the victims trapped in a hypothetical fire scenario.

Cone calorimetry (CC) is a bench scale test designed to study the heat release of materials by simulating forced flaming fire conditions, which is generally performed in a horizontal orientation. The time to ignition (TTI) of polyurethane foams, due to their low density, is characterized by low thermal inertia, leading to a quick temperature rise on the surface once the specimen is exposed to an external heat flux (in this case 50 kW m^{-2}, which is considered the heating intensity in a fully developed fire (Drysdale, 1986; Krämer et al., 2010; Tsai, 2009). Therefore, these materials present practically immediate time to ignition (in this case all the samples presented TTI values ranging between 1 and 2.5 s) and rapid fire growth, as described by Schartel and Hull (2007).

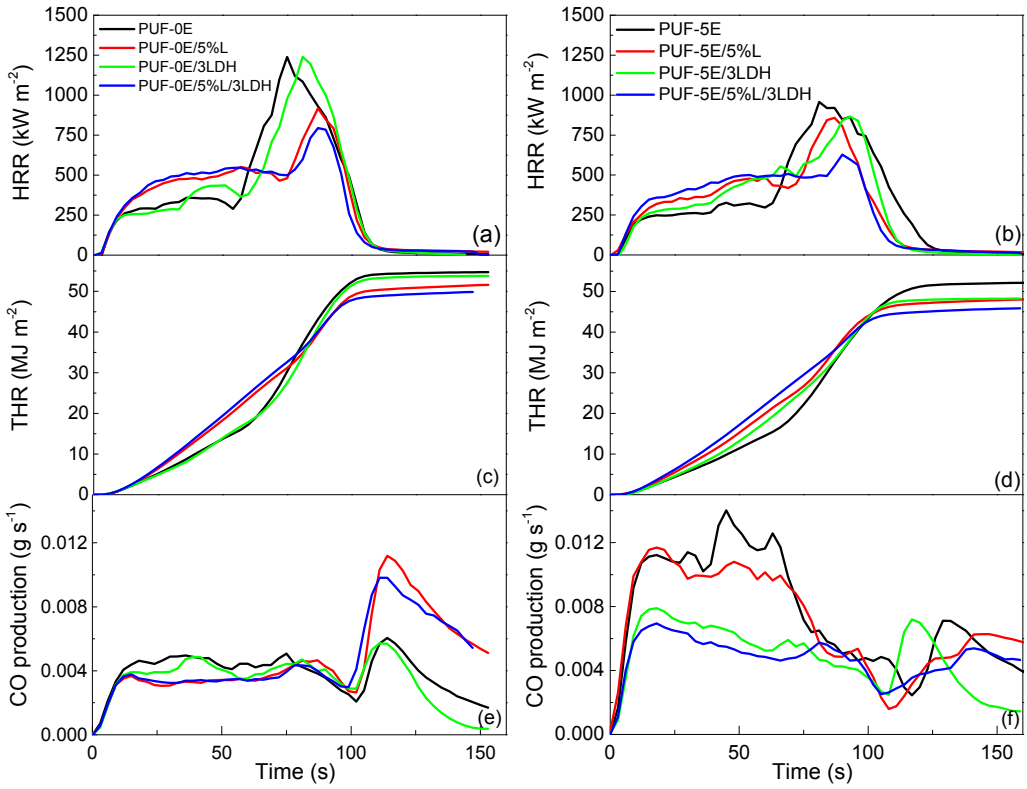

Figure 6.9. HRR, THR and CO production curves of unfilled and filled foams containing 0 (left) and 5 (right) pphp E560.

Figure 6.9 shows the HRR curves of the horizontal CC measurements of the series of foams with 100 pphp of polyether polyol (**Figure 6.9a**) and foams containing 5 pphp E560 (**Figure 6.9b**). The curves showed two distinct stages. According to Vanspeybroeck et al. (1993), the heat released in flexible polyurethane foams is proportional to the amount of mass burned, commencing with a fast melting of the samples to the bottom of the holder. This rapid advance of the pyrolysis front was reflected in the first decomposition stage, where the decomposition of the isocyanate took place, releasing a yellow smoke that decomposes into cyanhydric acid. Subsequently and as a consequence of the burning of the polyol (soft segment), the formation of a pool fire took place (Alongi and Carosio, 2017). The time to pool fire (t_{pool}) was defined to quantify the time at which the second stage of decomposition started, which was observed in the burning process to coincide with the decrease in the heat release rate before the maximum HRR (pHRR) of the second stage.

The pHRR is an important parameter since it is believed to indicate the moment when the fire is most likely to spread to adjacent objects (Schartel and Hull, 2007). The

pHRR for all tested samples occurred in the second stage as a consequence of the pool fire, as previously reported by Krämer et al. (2010). The flammable liquid resulted from the decomposition of the urethane and urea linkages, leading to the rupture of the crosslinked structure. Compared to the 0E samples, pHRR was reduced by 47% and t_{pool} was delayed 30 s when lignin, LDH and E560 (5E-5%L/3LDH) were combined. LDH contributed to a protective layer because of its inert filler character and its high aspect ratio (Zammarano et al., 2005). Therefore, the time to pHRR (tpHRR) in the case of 0E-3LDH was slightly delayed as compared with 0E. This protective effect was more evident in foams containing E560, where higher amounts of residue were formed (**Table 6.6**). In general, 0E foams containing lignin exhibited a higher heat release during the first stage of combustion, but a lower pHRR and delayed tpHRR. A similar behavior was observed for 5E foams. Differences between the materials were not as significant as within the group of 0E foams, which indicates that burning behavior was dominated by the phosphorus containing oligomeric diol.

Figure 6.10 shows the images of the residues collected in the pan after cone calorimeter measurements. Differences were observed between the residue obtained from the 0E and 5E foam series due to the presence of E560, which slightly promoted char formation. However, after flameout all samples presented very low amounts of residue compared to charring materials such as rigid PUF (Lorenzetti et al., 2012). Since the pool fire stage is characterized by intense bubbling of the liquid pyrolysis products, and the char yield is very low, the formation of a protective char layer with a closed surface is hindered during combustion. Being very thin and cracked, the char layers formed by the tested foams under forced flaming conditions do not act as an efficient heat shield.

Table 6.6 shows that in addition to decreasing the HRR, the presence of the fillers and E560 also delayed the t_{pool}, thus delaying the second stage of decomposition in which the highest amount of heat was released. The total heat release (THR) gives insight into the fire load of the material. It was observed that the THR did not change significantly, because the samples burned completely. Nevertheless, THR decreased slightly (**Figures 6.9c**, **d** and **Table 6.6**) because of polyurethane weight replacement with fillers and increased residue. For the 0E and 5E foams, not only the THR, but also

the effective heat of combustion of the volatiles (EHC) were lower in the first stage than the THR and EHC in the second pool fire stage. When the samples contained lignin and/or LDH this behavior changed, increasing the heat released in the first stage, indicating that these change the pyrolysis front and contribute to a more gradual heat release. The incorporation of the phosphorous oligomeric diol contributed to a decrease in THR and EHC in both stages for the 5E foam series. In fact, THR decreased by up to 13.5% as compared with 0E when lignin, LDH and E560 were combined.

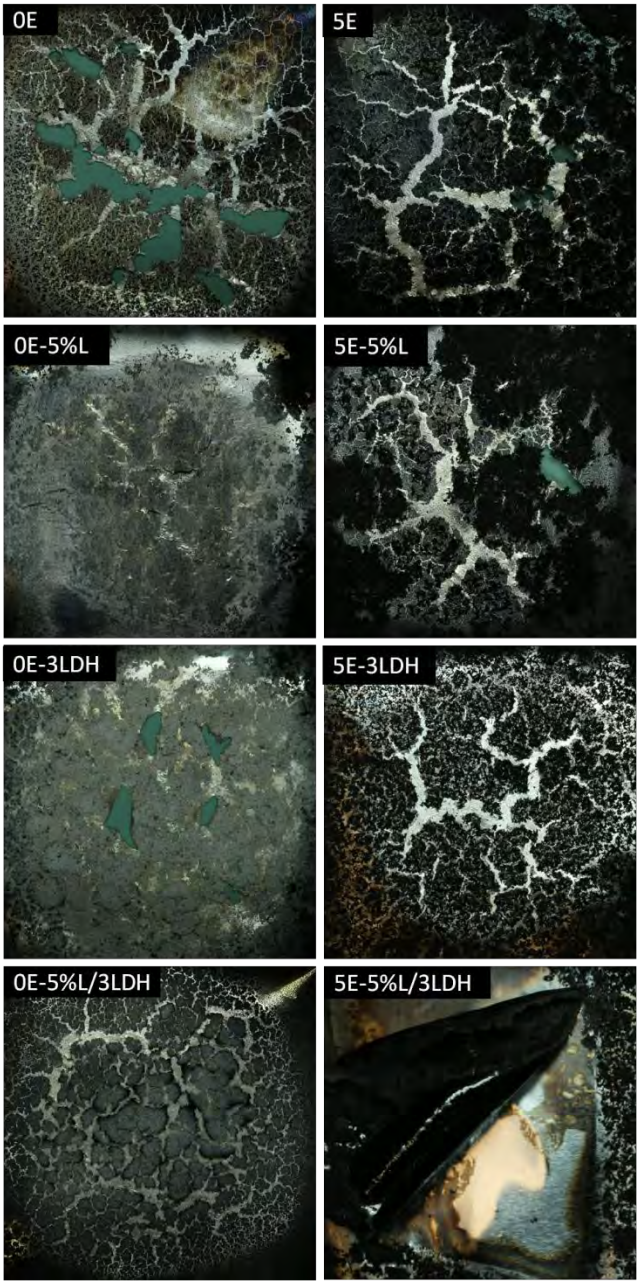

Figure 6.10. Images of fire residues obtained in the cone calorimeter for 0E and 5E foam series after flameout and afterglow.

Table 6.6. Cone calorimetry test data of the prepared flexible polyurethane foams.

Sample	pHRR ($kW\ m^{-2}$)	tpHRR (s)	pHRR/ tpHRR ($kW\ m^{-2}s^{-1}$)	1st stage		t_{pool} (s)	2nd stage		THR ($MJ\ m^{-2}$)	EHC ($MJ\ kg^{-1}$)	TSR ($m^2\ m^{-2}$)	Residue (%)
				THR_1 ($MJ\ m^{-2}$)	EHC_1 ($MJ\ kg^{-1}$)		THR_2 ($MJ\ m^{-2}$)	EHC_2 ($MJ\ kg^{-1}$)				
0E	1209	78	15,5	16	21	54	40	31	56	52	326.80	0.00
0E-5%L	902	84	10,7	29	24	72	22	31	51	55	296.78	1.40
0E-3LDH	1214	81	15,0	17	22	57	36	30	53	52	292.13	0.00
0E-5%L/3LDH	798	87	9,2	33	24	75	17	30	50	55	287.65	2.37
5E	980	79.5	12,3	15	18	60	37	29	52	47	557.99	0.90
5E-5%L	851	88.5	9,6	24	21	69	24	29	48	50	358.42	3.34
5E-3LDH	852	91.5	9,3	24	21	72	25	31	49	52	427.41	1.61
5E-5%L/3LDH	645	91.5	7,0	35	23	84	13	32	48	55	456.79	4.29

pHRR: maximum heat release rate value (peak heat release rate).

tpHRR: time to reach the pHRR.

THR: total heat released in the whole process (THR) or in stages 1 or 2 ($THR_{1,2}$).

EHC: effective heat of combustion in the whole process (EHC) or in stages 1 or 2 ($EHC_{1,2}$).

t_{pool}: time at which second stage of combustion (pool fire burning) begins.

TSR: total smoke release.

Residue: obtained gravimetrically after CC test.

The effective heat of combustion (EHC) is defined as the heat release per unit mass, and was calculated as the total heat evolved (THE) divided by the total mass loss (TML). For all tested materials, the EHC of the first stage of decomposition (EHC_1) was lower than the EHC of the second stage (EHC_2). 0E foams containing lignin had a slightly increased EHC_1, indicating a decomposition of the filler during the first stage.

The quotient of pHRR/tpHRR gives an idea of the material's propensity to combustion (Schartel and Hull, 2007). **Table 6.6** displays that the unfilled 0E and 5E foams had significantly higher values than filled ones. Compared to 0E series, pHRR/tpHRR decreased from 15.5 kW m^{-2} s^{-1} to 9.2 kW m^{-2} s^{-1} for 0E-5%L/3LDH and to 7.0 kW m^{-2} s^{-1} for the 5E foam containing lignin and LDH. This reduction is a result not only of the decreased pHRR, but also of the delayed tpHRR through the formation of a minor protective layer. This layer was formed mainly during the first stage of decomposition, when bubbling less intense than during the pool fire stage enabled its formation.

Figures 6.9e and **6.9f** display the CO production during combustion of the foams. It was observed that in the 0E series the CO production was constant throughout the measurement, but increased after flameout. This peak is indicative of a change from pyrolytic decomposition feeding the flame, to a thermo-oxidative decomposition of the residue called afterglow (Schartel and Hull, 2007).

The peak of CO production was significantly higher for foams containing lignin, since their residue at flameout exceeded the residue of foams without lignin, as shown in **Table 6.6**. 5E foams exhibited a different behavior. The flame inhibition reducing the EHC in the gas phase was accompanied by increasing combustion products, typical for incomplete combustion in the flame. The CO yield during the first stage of decomposition was considerably increased, while it was similar to the 0E foams during the afterglowing of the char. Minor peaks occurred after flameout, indicating the afterglow. CO production for 5E foams containing LDH was significantly decreased during the first stage of decomposition as compared to 5E foams without LDH.

Cone calorimeter investigations were performed in a vertical orientation as well, since the dripping characteristics of the materials are not taken into account in

the horizontal orientation. Vertical orientation enhances the dripping effect and the heat feedback from the pool of burning pyrolysis products, since foam collapse and pool fire do not overlap each other (Galaska et al., 2016; Schartel, 2010).

Figure 6.11 shows the melt dripping 30 s after flame application. Most of the samples exhibited severe flaming from the pool fire in the catch pan underneath the sample holder after dripped off pyrolysis products were collected. Heat feedback from the flames of the pool fire accelerated the combustion of the specimen in the cage of the sample holder. Different burning behavior was observed for 0E-5%L/3LDH and 5E-5%L/3LDH. Both foams filled with lignin and LDH showed increased viscosity of their pyrolysis products, which led to non-dripping decomposition in the vertical cone calorimeter measurement, so that no pool fire was formed. While smaller burning pieces falling off the specimen were observed for 0E-5%L/3LDH, no burning material was collected in the catch pan during the combustion of 5E-5%L/3LDH.

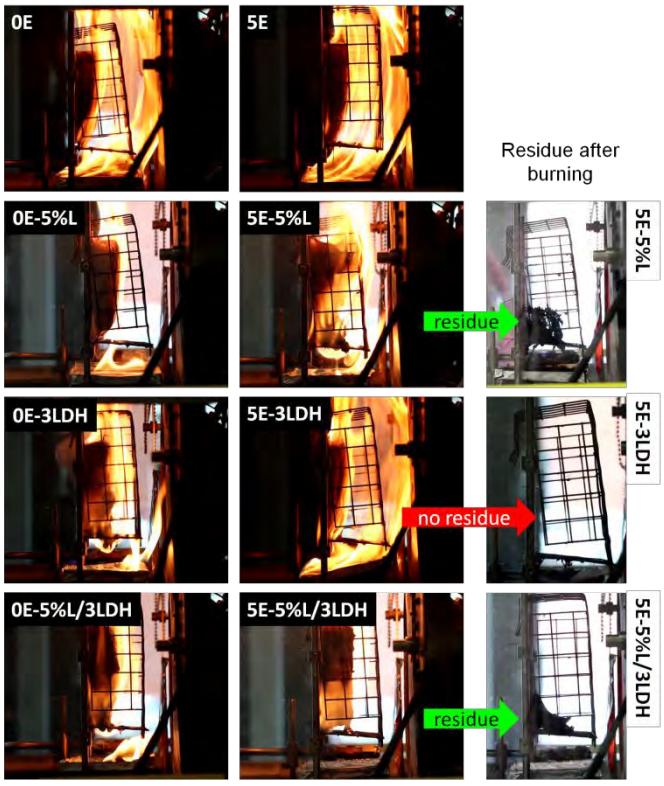

Figure 6.11. Burning cone calorimeter samples (30 s after ignition) and residues.

It is worth noting that there was no residue left in the sample cage after the burning of most samples, except in the cases of 5E-5%L and 5E-5%L/3LDH, confirming the enhanced char formation by the combination of E560 and lignin. The dripping prevention with this low filler content is a promising way to improve PUF performance under fire conditions, since almost all of the existing fire retardants for PUF are designed not to prevent dripping, but to decrease HRR and reduce flame spread and/or delay ignition (Galaska et al., 2016).

6.4. Conclusions

Flexible polyurethane foams containing lignin, LDH and a phosphorous oligomeric diol as additives were successfully prepared with a density around 40 ± 2 kg m^{-3}. The effect of these additives was to change the viscosity of the reactive mixture, which affected the urea microphase separation. This phase segregation was favored in 0E foams, due to the lower viscosity of their reactive mixtures as compared with 5E foams. This urea segregation was especially reflected in foams' mechanical properties, such as resilience, CFD, compression set, elastic modulus, compressive stress and energy absorption.

Nevertheless, the presence of such low amounts of lignin by itself did not increase the flame retardancy of PUF, but the addition of E560 increased charring efficiency, while the addition of LDH contributed to reinforcing the char layer, yielding a more cohesive protective layer that decreased the pHRR in 47% (in 5E-5%L/3LDH) as compared with the unfilled foam 0E. Apart from a lower pHRR, a delayed tpHRR and time to pool fire were obtained, which suggests a delay in the most dangerous event during a fire: the flashover phenomenon.

Additionally, the mixture of these three additives (E560, lignin and LDH) yielded an increased melt viscosity of the liquid degradation products of the PUF, preventing melt dripping during combustion. The mixture of E560 and lignin contributed to increasing char yield, while the addition of LDH reinforced the char layer.

It turned out that the amounts added were far too small to achieve interesting fire performance. Nevertheless, even these small amounts deliver significant insight into the complex flame retardant modes of action introduced by E560, LDH, and lignin. Not only did flame inhibition, charring, and a protective layer effect occur, but the crucial influence of viscosity was also demonstrated. These results could be considered a valuable preliminary approach to improve the flame retardancy of polyurethane foams, while giving added value to an industrial byproduct such as lignin and using eco-friendly alternatives like LDH towards a safer and more environmentally friendly future.

6.5. References

Alongi, J., Carosio, F., 2017. Flame retardancy of flexible polyurethane foams: traditional approaches versus layer-by-layer assemblies, in: Wang, D.-Y. (Ed.), Novel Fire Retardant Polymers and Composite Materials. Elsevier Ltd, The Netherlands, pp. 171–200.

Armistead, J.P., Wilkes, G.L., Turner, R.B., 1988. Morphology of water-blown flexible polyurethane foams. J. Appl. Polym. Sci. 35, 1988.

Cheng, K., Winter, W.T., Stipanovic, A.J., 2012. A modulated-TGA approach to the kinetics of lignocellulosic biomass pyrolysis/combustion. Polym. Degrad. Stab. 97, 1606–1615.

Danowska, M., Piszczyk, Ł., Strankowski, M., Gazda, M., 2013. Rigid polyurethane foams modified with selected layered silicate nanofillers. J. Appl. Polym. Sci. 130, 2272–2281.

Das, S., Dave, M., Wilkes, G.L., 2009. Characterization of flexible polyurethane foams based on soybean-based polyols. J. Appl. Polym. Sci. 112, 299–308.

Drysdale, D.D., 1986. Fundamentals of the fire behaviour of cellular polymers, in: Buist, J.M., Grayson, S.J., Wooley, W.D. (Eds.), Fire and Cellular Polymers. Elsevier,

Dordrecht, pp. 61–76.

Fierro, V., Torn, V., Celzard, A., 2005. Study of the decomposition of kraft lignin impregnated with orthophosphoric acid. Thermochim. Acta 433, 142–148.

Galaska, M.L., Morgan, A.B., Schenck, K.A., Stalter, J.G., 2016. Apparatus for the vertical orientation cone calorimeter testing of flexible polyurethane foams. Fire Mater. 40, 158–176.

Harikrishnan, G., Patro, T.U., Khakhar, D. V, 2006. Polyurethane foam-clay nanocomposites: nanoclays as cell openers. Ind. Eng. Chem. Res. 45, 7126–7134.

Krämer, R.H., Zammarano, M., Linteris, G.T., Gedde, U.W., Gilman, J.W., 2010. Heat release and structural collapse of flexible polyurethane foam. Polym. Degrad. Stab. 95, 1115–1122.

Liu, L., Wang, W., Hu, Y., 2015. Layered double hydroxide-decorated polyurethane foam: significantly improved toxic effluent elimination. RSC Adv. 5, 97458–97466.

Lorenzetti, A., Modesti, M., Gallo, E., Schartel, B., Besco, S., Roso, M., 2012. Synthesis of phosphinated polyurethane foams with improved fire behaviour. Polym. Degrad. Stab. 97, 2364–2369.

Mahmoud, A.A., Abdel Ader Nasr, E., Abdel Hamed Maamoun, A., 2017. Influence of polyurethane foam on the insulation characteristics of mortar pastes. J. Miner. Mater. Charact. Eng. 5, 49–61.

Schartel, B., 2010. Uses of fire tests in materials flammability development, in: Wilkie, C.A., Morgan, A.B. (Eds.), Fire Retardancy of Polymeric Materials. CRC Press, Boca Ratón, pp. 387–420.

Schartel, B., Bartholmai, M., Knoll, U., 2006. Some comments on the main fire retardancy mechanisms in polymer nanocomposites. Polym. Adv. Technol. 772–777.

Schartel, B., Dittrich, B., Wartig, K., Hofmann, D., Rolf, M., 2015. The influence of layered, spherical, and tubular carbon nanomaterials' concentration on the flame

retardancy of polypropylene. Polym. Compos. 1230–1241.

Schartel, B., Hull, T.R., 2007. Development of fire-retarded materials - Interpretation of cone calorimeter data. Fire Mater. 31, 327–354.

Sonnenschein, M.F., Prange, R., Schrock, A.K., 2007. Mechanism for compression set of TDI polyurethane foams. Polymer 48, 616–623.

Szycher, M., 2013. Catalysis of Isocyanate Reactions, in: Szycher's Handbook of Polyurethanes. CRC Press, Boca Ratón, pp. 319–344.

Tsai, K., 2009. Orientation effect on cone calorimeter test results to assess fire hazard of materials. J. Hazard. Mater. 172, 763–772.

Turner, R.B., Nichols, J.B., Kuklies, R.A., 1989. The influence of viscosity in cell opening of flexible molded foams. J. Cell. Plast. 25, 117–124.

Vanspeybroeck, R., Van Hees, P., Vandevelde, P., 1993. Combustion behaviour of polyurethane flexible foams under Cone Calorimetry test conditions. Fire Mater. 17, 155–166.

Xing, W., Yuan, H., Yang, H., 2013. Functionalized lignin for halogen-free flame retardant rigid polyurethane foam: preparation, thermal stability, fire performance and mechanical properties. J. Polym. Res. 20, 234–246.

Zammarano, M., Franceschi, M., Gilman, J.W., Meriani, S., 2005. Preparation and flame resistance properties of revolutionary self-extinguishing epoxy nanocomposites based on layered double hydroxides. Polymer 46, 9314–9328.

Zhang, L., 2008. Structure-property relationship of polyurethane foam made from natural oil polyols. PhD Dissertation. Faculty of the Graduate School of the University of Minnesota.

“You know somethin’, Utivich? I think this just might be my masterpiece!”

L. Bender (Producer) and Q. Tarantino (Director). Inglorious Basterds. United States and Germany: Universal Pictures, 2009.

Chapter 7

7

General **conclusions, future** work and **publications**

7. General conclusions, future work and publications

7.1. General conclusions

Different eco-friendly fillers have been successfully modified and introduced in flexible polyurethane foams formulated with a renewable sourced polyol, as potential halogen-free replacement for conventional flame retardants.

The replacement of carbonate anions by different inorganic and organic phosphorus containing molecules between the brucite-like layers of synthetic hydrotalcite clay (LDH) increased the interlayer spacing and determined the dispersion degree of the clay in the matrix. The dispersion degree and the chemical nature of the LDH intercalating anions affected directly the resilience and the compression force deflection values and the thermal stability of the foams, respectively.

The introduction of a phosphorus containing oligomeric diol in FPUF yielded to catalyze the polyurethane degradation owing to the presence of phosphorus, whereas the presence of the different LDHs contributed to counteract this effect owing to their laminar structure that resulted to act as a shield against heat. The presence of this phosphorus containing oligomeric diol did not affect the dispersion degree of the LDH, but affected the compression force deflection the resilience values of the foams, resulting in more viscoelastic materials.

On the other hand, the effect of kraft lignin as a potential charring agent into FPUF was studied. It was observed that lignin decreased the reactivity of the system, so its functionalization with isocyanate groups was performed. This functionalization apart of enhancing the reactivity of the system, anchored the lignin particles to the polyurethane matrix avoiding in this way particle migration during the end-use of the product. The presence of unmodified lignin resulted in more rigid foams with higher ability to absorb energy during deformation, whereas isocyanate functionalized lignin containing foams presented lower energy absorption capacity suggesting the presence of a less crosslinked structure.

Finally, the combination of the different eco-friendly fillers (LDH and lignin) with phosphorus oligomeric diol yielded to increase the char yield of the foams resulting in a decrease of the peak heat release rate of the foam. The different water

(blowing agent) content used to maintain the density of the foams constant, enhanced the urea microphase segregation especially in foams without phosphorus oligomeric diol. This phase segregation had an impact especially in mechanical properties such as resilience, compression force deflection, compression set, elastic modulus, compressive stress and energy absorption of the foams.

All these results were obtained with low filler content (3 pphp of LDH, 5% by weight of lignin) and low flame retardant polyol content (5 pphp E560), so it is expected that increasing the dosage of these additives could yield to a better improvement of the flame retardancy of the foams.

7.2. Future work

This work could be yet furtherly developed and completed by the proposals mentioned below, focusing especially in lignin in order to give added value to such an important industrial byproduct:

- Study the possibility of introducing higher amount of fillers in FPUF formulations, in order to allow them to get improved specific properties such as flame retardancy without affecting the cellular structure of the foams.

- Analyze different approaches in order to functionalize lignin with phosphorus containing moieties owing to increase its charring effect during thermal decomposition.

- Study possible combinations of phosphorus functionalized lignin and potential blowing agents such as melamine-containing compounds in order to achieve an intumescent effect during thermal decomposition that would increase considerably the volume of the formed char during decomposition acting as an effective heat and oxygen shield, protecting the underlying foam.

- Consider other ways of incorporating lignin into the foams different to its introduction as filler or in solution, such as layer-by-layer depositions that could yield to a higher lignin loading without affecting the foaming process of FPUF.

- Also, as it has been researched in this work, the combination of phosphorus-functionalized lignin with different combinations of LDH could also be performed, and a deeper study on the flame retardant properties could be carried out.

7.3. Publications and conference communications

7.3.1. List of publications

Authors: Sandra Gómez-Fernández, Martin Günther, Bernhard Schartel, Maria Angeles Corcuera, Arantxa Eceiza

Title: Impact of the combined use of layered doubles hydroxides, lignin and phosphorus containing polyol on the fire behavior of flexible polyurethane foams

Journal: Industrial Crops and Products

Year: 2018

Impact factor: 3.181 (JCR 2016)

Rank: 43/173 (Q1) in Agricultural engineering and 10/83 (Q1) in Agronomy (JCR 2016)

Authors: Sandra Gómez-Fernández, Lorena Ugarte, Tamara Calvo-Correas, Cristina Peña-Rodríguez, Maria Angeles Corcuera, Arantxa Eceiza

Title: Properties of flexible polyurethane foams containing isocyanate functionalized kraft lignin

Journal: Industrial Crops and Products

Year: 2017

Impact factor: 3.181 (JCR 2016)

Rank: 43/173 (Q1) in Agricultural engineering and 10/83 (Q1) in Agronomy (JCR 2016)

Authors: Sandra Gómez-Fernández, Lorena Ugarte, Cristina Peña-Rodríguez, Maria Angeles Corcuera, Arantxa Eceiza

Title: The effect of phosphorus containing polyol and layered double hydroxides on the properties of a castor oil based flexible polyurethane foam

Journal: Polymer Degradation and Stability

Year: 2016

Impact factor: 3.386 (JCR 2016)

Rank: 15/86 (Q1) in Polymer Science (JCR 2016)

Authors: Sandra Gómez-Fernández, Lorena Ugarte, Cristina Peña-Rodríguez, Manuela Zubitur, Maria Angeles Corcuera, Arantxa Eceiza

Title: Flexible polyurethane foam nanocomposites with modified layered double hydroxides

Journal: Applied Clay Science

Year: 2016

Impact factor: 3.101 (JCR 2016)

Rank: 43/249 (Q1) in Mineralogy, 68/275 (Q1) in Materials Science, Mutidisciplinary and 54/146 (Q2) in Chemistry, Physical

7.3.2. List of conference communications

Authors: Sandra Gómez-Fernández, Martin Günther, Lorena Ugarte, Bernhard Schartel, Maria Angeles Corcuera, Arantxa Eceiza

Title: Effect of the combined use of layered double hydroxides, lignin and phosphorus containing polyol on the fire behavior of flexible polyurethane foams

Conference: Fire Retardant Polymeric Materials (FRPM17)

Contribution: Poster

Year: 2017

City (Country): Manchester (United Kingdom)

Authors: Sandra Gómez-Fernández, Lorena Ugarte, Cristina Peña-Rodríguez, Maria Angeles Corcuera, Arantxa Eceiza

Title: Effect of isocyanate functionalized lignin on the properties of flexible polyurethane foams

Conference: 9th International Conference in Modification, Degradation and Stabilization of Polymers (MoDeSt2016)

Contribution: Oral

Year: 2016

City (Country): Krakow (Poland)

Authors: Sandra Gómez-Fernández, Lorena Ugarte, Cristina Peña-Rodríguez, Maria Angeles Corcuera, Arantxa Eceiza

Title: Effect on the properties of flexible polyurethane foam with phosphorus containing polyol and modified layered double hydroxides

Conference: COST MP1105 Training School on "Strategies to study fire behaviors and fire retardant mechanisms"

Contribution: Poster

Year: 2016

City (Country): Barcelona (Spain)

Authors: Sandra Gómez-Fernández, Manuela Zubitur, Agurtzane Mugica, Maria Angeles Corcuera, Arantxa Eceiza

Title: Effect on the properties of flexible polyurethane foam with phosphorus containing polyol and modified layered double hydroxides

Conference: 5th International Conference on Biobased and Biodegradable Polymers (BIOPOL-2015)

Contribution: Poster

Year: 2015

City (Country): San Sebastian (Spain)

Authors: Sandra Gómez-Fernández, Lorena Ugarte, Borja Fernández-d'Arlas, Maria Angeles Corcuera, Arantxa Eceiza

Title: Study of flame retardancy of flexible polyurethane foam nanocomposites with modified layered double hydroxides

Conference: Eurofillers and Polymer Blends 2015

Contribution: Poster

Year: 2015

City (Country): San Sebastian (Spain)

What feels like the end is sometimes the beginning

APPENDIX

List of **tables**, **figures** and **abbreviations**

APPENDIX: LIST OF TABLES, FIGURES AND ABBREVIATIONS

List of tables

Chapter 2: Materials and characterization techniques

Chapter 3: Flexible polyurethane foams with modified layered double hydroxides

Chapter 4: Flexible polyurethane foams with phosphorus containing oligomeric diol and layered double hydroxides

Chapter 5: Flexible polyurethane foams with isocyanate functionalized lignin

Chapter 6: Fire behavior: Combination of layered double hydroxides, phosphorus containing oligomeric diol and lignin

List of figures

Chapter 1: Introduction

Chapter 3: Flexible polyurethane foams with modified layered double hydroxides

Chapter 4: Flexible polyurethane foams with phosphorus containing oligomeric diol and layered double hydroxides

Chapter 5: Flexible polyurethane foams with isocyanate functionalized lignin

Chapter 6: Fire behavior: Combination of layered double hydroxides, phosphorus containing oligomeric diol and lignin

List of abbreviations

3R	3 layer polytype clay with rhomboedral symmetry
a	Distance between two adjacent metal ions (a cell lattice parameter)
AAS	Atomic absorption spectroscopy
AIL	Acid insoluble lignin
ALC	Alcupol® F-4811
APP	Ammonium polyphosphate
ASL	Acid soluble lignin
ASTM	American Society for Testing and Materials
ATH	Alumina trihydrate (aluminium hydroxide)
ATR	Attenuated total reflectance
CC	Cone calorimetry
CFD	Compression force deflection
CP/MAS	Cross-polarization magic angle spinning
D	Mean size of the ordered domains
d	Interplanar spacing between crystalline planes
DBTDL	Dibutyltin dilaurate
DEHP$^-$	Bis(2-ethylhexyl) phosphate
DMA	Dynamic mechanical analysis
DSC	Differential scanning calorimetry
DTG	First derivative of mass loss (from thermogravimetric analysis)
E'	Storage modulus
E''	Loss modulus
E560	Exolit® OP 560
EDX	Energy dispersive X-ray spectroscopy

EHC	Effective heat of combustion
Eq wt	Equivalent weight
f	Functionality
FPUF	Flexible polyurethane foam
FR	Flame retardant
FTIR	Fourier transform infrared spectroscopy
G	Guaiacyl unit from lignin
GPC	Gel permeation chromatography
H	p-hydroxylphenyl unit from lignin
HB	Horizontal burning
HDEHP	Bis (2-ethylhexyl) hydrogen phosphate
HDI	Hexamethylene diisocyanate
HRC	Heat release capacity
HRR	Heat release rate
HS	Hard segment
HPLC	High permeation liquid chromatography
I.I.	Isocyanate index
ICP-OES	Inductively coupled plasma optical emission spectrometry
$\mathbf{I_{OH}}$	Hydroxyl number
IPDI	Isophorone diisocyanate
ISO	International Standards Organization
K	Scherrer constant or shape factor
LB50	Lupranol Balance® 50
LDH	Layered double hydroxide
LOI	Limiting oxygen index
$\overline{\mathbf{M}}_w$	Weight average molecular weight

MDI Methylene diphenyl diisocyanate

NFPA National Fire Protection Association

NMR Nuclear magnetic resonance

OM Optical microscopy

PCFC Pyrolysis combustion flow calorimetry

PD Polydispersity

pHRR Peak heat release rate

pphp Parts per hundred of polyol

PU Polyurethane

PUF Polyurethane foam

R Resilience

RPUF Rigid polyurethane foam

pBDE Pentabromodiphenyl ether

S Syringyl unit from lignin

SEC Size exclusion chromatography

SEM Scanning electron microscopy

SS Soft segment

TEM Transmission electron microscopy

TBB 2-Ethylhexyl-2,3,4,5-tetrabromophtalate

TBPH Bis (2-ethylhexyl)-2,3,4,5-tetrabromophtalate

TCEP Tris (2-chloroethyl) phosphate

TCPP Tris (2-chloro-1-methylethyl) phosphate

TDI Toluene diisocyanate

T_g Glass transition temperature

TGA Thermogravimetric analysis

TGA-MS Mass spectrometry coupled thermogravimetric analysis

TGA-FTIR	Fourier transform infrared spectroscopy coupled thermogravimetric analysis
THE	Total heat evolved
THF	Tetrahydrofuran
THR	Total heat released
THRR	Temperature of the peak heat release rate
T_m	Melting temperature
TML	Total mass loss
T_{max}	Maximum degradation rate temperature
T_{onset}	Temperature at 5% mass loss
t_{pool}	Time at which the second stage of combustion (pool fire) begins
TPU	Thermoplastic polyurethane
TSPU	Thermoset polyurethane
TSR	Total smoke released
TTI	Time to ignition
UL 94	Underwriter Laboratories test for flammability of plastic materials for parts in devices and appliances
UV-vis	Ultraviolet-visible spectroscopy
XRD	X-ray diffraction
β	Peak width at half maximum intensity
ΔH_m	Melting enthalpy
θ	X-ray diffraction angle
λ	Wavelength